Hydrodynamic studies on Hull-Propeller-Rudder Interaction

Svilen Ivanov

Master Thesis

presented in partial fulfillment
of the requirements for the double degree:
“Advanced Master in Naval Architecture” conferred by University of Liege
"Master of Sciences in Applied Mechanics, specialization in Hydrodynamics, Energetics and Propulsion” conferred by Ecole Centrale de Nantes

developed at "Dunarea de Jos" University of Galati
in the framework of the

“EMSHIP”
Erasmus Mundus Master Course
in “Integrated Advanced Ship Design”

Ref. 159652-1-2009-1-BE-ERA MUNDUS-EMMC

Supervisor: Prof. Adrian Lungu, “Dunarea de Jos” University of Galati

Reviewer: Prof. Pierre Ferrant, Ecole Central De Nantes

Galati, January 2013

Contents

Declaration of Authorship

I declare that this thesis and the work presented in it are my own and have been generated by me as the result of my own original research.

Where I have consulted the published work of others, this is always clearly attributed.

Where I have quoted from the work of others, the source is always given. With the exception of such quotations, this thesis is entirely my own work.

I have acknowledged all main sources of help.

Where the thesis is based on work done by myself jointly with others, I have made clear exactly what was done by others and what I have contributed myself.

This thesis contains no material that has been submitted previously, in whole or in part, for the award of any other academic degree or diploma.

I cede copyright of the thesis in favour of the University of Galati.

Date: 21.01.2013 *Signature*

ABSTRACT

Description of the topic – Each of the components investigated in this study (hull , propeller, rudder) are disturbing the flow in a specific way, depending on their geometrical characteristics. The interactions that appear between hull, propeller and rudder are complicated and difficult to determine. The flow developed around these parts is governed by some challenging physical phenomena. Investigating the interaction between the hull , propeller and rudder – is the aim of the present work.

The Objectives are: To perform a gird convergence study in order to choose the most suitable grid for the present research. To validate the numerical methodology which will be used in order to determine ship resistance and flow features for the bare hull case. To validate the lifting line numerical methodology used for propeller computation. To use propeller open water and self-propulsion computational results in order to determine the propulsion coefficients (ITTC'78 procedure). To determine the hydrodynamic forces and moments developed on the hull equiped with propeller and rudder during static rudder motion.

A simplified potential theory method and a boundary layer theory based method, both implemented in the SHIPFLOW code, are used in order to obtain the wave resistance and the frictional resistance of the 1:67 model scale KCS ship. The results are compared with experimental reference results and the error is estimated. Also, the Reynolds Averaged Navier Stokes equation (RANS) are used in order to compute the viscous resistance, axial velocities, and pressure coefficient for the bare hull, the hull with propeller and the hull with rudder and propeller. The results are also compared with reference results.
The potential flow computation shows good agreement between numerical and experimental results. The wave pattern, computed with the potential flow solver is almost 100% similar with EFD results.
The RANS solution for bare hull shows much more real picture about the resistance, which means bigger error in the low speeds and even less than 1 % error in the speed of interest.

Using potential and viscous CFD methods the present study offers an image of the flow pattern developed around the abovementioned configurations, bare hull ship resistance, propulsion coefficients and hydrodynamic forces and moments developed on the fully equiped hull being determined.

INTRODUCTION

The objective of this study is to provide the specific knowledge to simulate and analyze numerically the viscous interaction that appears and develops between hull, propeller and/or rudder. The influence of each configuration can be effectively understood if each individual action is studied separately. That is, numerical simulations have to be performed for the flow around the bare hull at first, then around the hull with propeller/or rudder to define the influence of the latter, and finally around the whole ensemble, so taking into consideration the effect of propeller – rudder as a whole.

As long as each one (hull, propeller, rudder) with their different configurations, will provide different performance, the purpose of this study must be also finding the combined optimal configuration of hull propeller and rudder. For this purpose I suggest optimization software to be used in order to have optimal solution of the problem. But since the time is short, this suggestion will be taken into account for further investigation of the problem.

Study of the influence exerted by rudder and/or propeller on the hydrodynamic characteristics of the given ship – will be the **main purpose** of this thesis.

Particularly at the initial phase many alternatives have to be evaluated in a short period of time. In this research time will be saved by using the efficient potential flow panel methods, which predict important quantities like waves and wave resistance rapidly, yet with enough accuracy for hull ranking.

All the viscous flow computation, for the present work, will be made by means of the XCHAP module of the SHIPFLOW CFD code, which is a finite volume Reynolds-Averaged Navier-Stokes solver. The solution of the RANS equations gives the time averaged velocity and pressure.

The Ship Geometry is described in separated file called offset file. List of coordinate values of points lying on the hull surface is used for the purpose. The section of the rudder is given as a set of points specified in an offset file as well.

The propeller is modeled by a lifting line method that is coupled to the RANS solver by a body force approach.

The propeller and/or rudder are fitted to the ship in an attempt to achieve the objective of this study: to explore and understand the physics of the interactions that originate between hull, propeller and/or rudder.

The reported research is focused on the influences that the abovementioned ensemble and each individual component have on the propulsion and resistance characteristics.

The numerical solution of the viscous flow around the ship equipped with rudder and propeller will, also, provide some precious information about the ship stern flow characteristics as well as about the influences that a rudder and a propeller may have on this fully three dimensional viscous flow.

The computational results will be accurately compared with available experimental data in order to have a measure of the validity of the method.

JUSTIFICATION

Ship design is in many ways a compromise, the naval architect having the obligation to make the best choices so that the final product of his design - the vessel, to answer to most of the input data issued by the ship owner in a higher percentage. Numerical simulation is one of the tools widely used by ship designers in their continuous attempts to get the best results, one of the main objectives of this modern technique being that of getting accurate information for the propulsion and steering unit design. Using a CFD solver, the present research aims to investigate the hydrodynamic interaction between the hull-Propeller and Rudder of single screw Container ship KCS.

One of the main issues of the naval hydrodynamics worldwide is to understand the phenomena which occur in the three-dimensional viscous flow which defines the operating space of the vessel, when the ship follows a straight route or performs a maneuver. Calculating the hydrodynamic forces and moments developed on the hull and rudder as well as determination of the drag and the propulsion characteristics of the advancing ship has always been the main objective of the naval architect. On the turbulent flow which is developed around the stern of the ship due to the hydrodynamic interaction between the hull, propeller and rudder, has to be paid special attention. The International Maritime Organization is paying more and more attention at the same area of investigation mentioned above. In terms of maritime safety and marine environment IMO is constantly demanding

very strict rules and the concepts like “safety at sea” or “environmental friendly ships” are the newest product which is working mainly on improving marine environment and the live at sea.

Lately the Computational fluid dynamics – the numerical approach of fluid dynamics is the method which increasingly exceed the theoretical and experimental methodologies, with consuming less time and money to simulate and investigate for instance the flow developed around the ship on a straight course or while maneuvering.

Using the CFD techniques with the main idea to study the propulsive performances developed by the operating propeller , for a given rudder angle, the present research offers a detailed insight of the complicated phenomena which are defining the non uniform turbulent flow developed around the following configurations: Propeller in Open Water, Hull-Propeller and Hull-Propeller-Rudder. The accomplishment of the present study is based on the numerical integration of the incompressible Reynolds Averaged Navier – Stokes equations. The complex character of the flow imposes to the fundamental laws of fluid motion to be Reynolds-averaged. The equations for continuity and momentum are solved in such a manner that the primitive variables will describe the steady flow which surrounds the three-dimensional ensembles. The closure equation is obtained through the EASM turbulence model, the Reynolds stress components being explicitly determined from the tensor functions of the velocity gradients, turbulent kinetic energy, and turbulent length scale.

STRATEGY

The strategy described below by points is used to give an idea about the sequence followed due to the computations.

1. Resistance
    - Bare hull case
    - Five speeds

A) Potential flow
    - Compute the wave resistance
    - Compute the frictional resistance

B) Viscous flow
    - Compute the viscous resistance

C) Compare CFD with EFD

2. Propeller Open Water (POW)
3. Self propulsion test
   A) Hull with propeller
4. Hull with rudder
   A) Five speeds
5. Hull with rudder and propeller
   A) One speed

1. STATE OF THE ART OF THE HULL-PROPELLER-RUDDER INTERACTION

The KCS (Kriso container ship – Figure 1) was conceived to provide data for both explication of flow physics and CFD validation for a modern container ship with bulbous bow and stern (i.e., ca. 1997). No full-scale ship exists.

Figure 1 – KCS Hull shape - [http://www.simman2008.dk/KCS/kcs_geometry.htm]

Towing tank tests are usually used to determine the resistance components of a new hull forms. There is significant change of the flow field around the hull if there are also propeller and rudder. To perform such a model test in towing tank will be usually very expensive, that's why there is increasing need to assess the resistance components and the influence of the propeller and rudder to the flow around the ship hull, by using the **numerical** approach.

The computational cost of fully resolving the flow around a propeller geometry and hull inhibits the use of numerical simulations for commercial use. Anyway there are simplified body force propeller models which accurately induce the accelerations produced by a propeller in to the fluid. It is intended to use a similar body force propeller model to investigate its impact on resistance and the free surface around the stern of a self propelled ship.

Initially it is essential to use a numerical method for evaluating the resistance components on a towed hull. This requires a free surface model that will allow the wave pattern and therefore

wave resistance to be assessed. The accurate modeling of the boundary layer growth is required to capture the frictional resistance and the form drag.

For ship resistance and powering, CFD has become increasingly important and is now an indispensable part of the design process. Typically inviscid free-surface methods based on the boundary element approach are used to analyse the forebody, especially the interaction of bulbous bow and forward shoulder. Viscous flow codes often neglect wave making and focus on the aftbody or appendages. Flow codes modelling both viscosity and the wavemaking are at the threshold of practical applicability. CFD is still considered by industry as too inaccurate for resistance or power predictions. Instead, it is used to gain insight into local flow details and derive recommendation on how to improve a given design or select a most promising candidate design for model testing.

A commonly used method to predict the turning and steering of a ship is to use equations of motions with experimentally determined coefficients. Once these coefficients are determined for a specific ship design – by model tests or estimated from similar ships or by empirically enhanced strip methods – the equations of motions are used to simulate the dynamic behaviour of the ship. The form of the equations of motions is fairly standard for most hull designs. The predictions can be used, e.g., to select rudder size and steering control systems, or to predict the turning characteristics of ships. As viscous CFD codes become more robust and efficient to use, the reliance on experimentally derived coefficients in the equations of motions may be reduced. In an intermediate stage, CFD may help in reducing the scaling errors between model tests and full scale.

Usually unless the new ship design is similar to some known ship or close to an experimental series – the design process require lots of model tests and sometimes with many models with slight differences. This is no longer necessary thanks to CFD developments. Combining CAD (computer-aided design) to generate new hull shapes in concert with CFD to analyse these hull shapes allows for rapid design explorations without model testing. CFD allows the preselection of the most promising design. Then often only one or two models are actually tested to validate the intended performance features in the design and to get a power prediction accepted in practice as highly accurate.

As long as the CFD tool are developing nonstop they are increasingly becoming more reliable and the naval architects are using them in the early design stage, and this is not only to

simulate the straight ahead course conditions but also to simulate the maneuvering conditions. Using the numerical tools like CFD to study the turbulent flow which is developed due to the hydrodynamic interaction between the hull-rudder and propeller and the physical process which describes this flow, has actually its drawbacks. In general, numerical computations were used to model one or two of the components: hull-rudder (Hideki et al., 2001), hull-propeller (Han et al., 2006 and Larsson et al., 2006) or propeller-rudder in open water (Turnock, 1996 and Han et al., 2007) or behind ship hull (Moryiama, 1981 and Li, 1994). The study of hull-propeller-rudder interaction, by the use of CFD, was made by Simonsen and Stern, 2006. Combining all the components they focused on maneuvering performances.

2. NUMERICAL METHODOLOGY

In the most common approach, simplifications of the equations are used. These are usually based on combinations of approximations and dimensional analysis. To obtain an approximate solution numerically, we have to use discretization method which approximates the differential equation by a system of algebraic equations, which can then be solved on a computer. The approximation are applied to small domain in space and/or time so the numerical solution provides results at discrete locations in space and time. Much as the accuracy of experimental data depends on the quality of the tools used, while the accuracy of the numerical solution is dependent on the quality of the discretization used.

If it is not possible to obtain accurate solution for all flows, we have to determine what we can produce and learn to analyze and judge the results. The fact that the numerical results are always approximate must be kept in mind. There are reasons for the differences between the computed result and the reality. The errors come from each part of the process which produces the numerical solution.

When for example the Navier Stokes equation for incompressible Newtonian fluids is governed accurately, a solution of any desired accuracy can be achieved in principle. However for phenomena like turbulence, combustion, and multiphase flow – the exact equations are either not available or numerical solution is not feasible. This makes introduction of models a necessity. Even if the equation is solved exactly, the solution will not be a correct representation of the reality. In order to validate the models it is necessary to make a comparison with experimental data.

By using more accurate interpolation or approximation or by applying the approximation to smaller regions – the discretization error could be reduced, but this usually increases the time and cost of obtaining the solution. Compromise is usually needed.

Visualisation of the numerical solutions using vector, contour or other kinds of plots or even videos of unsteady flows is important for the interpretation of the results. There is the possibility that a wrong solution may look good but may not correspond to the actual boundary conditions, fluid properties etc. The industrial users of commercial CFD must be very careful as the optimism of the salesman is legendary. Results must be examined very carefully before they are believed.

2.1. Mathematical Model Potential Flow

The potential flow solver is used in order to simplify the computations by computing the free surface elevation and the frictional coefficient. The mathematical model is described in this chapter as well as the assumption on which the method is based.

a. Assumptions
   - Inviscid fluid
   - Irrotational flow
   - Steady state
   - Incomprasible flow

b. Governing equations

Velocity potential ϕ,
$$u = \frac{\partial \phi}{\partial x}, \qquad v = \frac{\partial \phi}{\partial y}, \qquad w = \frac{\partial \phi}{\partial z} \tag{1}$$

Laplace equation:
$$\frac{\partial^2 \phi}{\partial x^2} + \frac{\partial^2 \phi}{\partial y^2} + \frac{\partial^2 \phi}{\partial z^2} = 0 \tag{2}$$

Total velocity potential:
$$\phi = U_{\infty x} * x + U_{\infty y} * y + U_{\infty z} * z + \phi \tag{3}$$

c. Boundary conditions for the Hull surface
   - The total velocity in the body surface normal direction must have a known value, F.

$$\frac{\partial \phi}{\partial n} = F \qquad \text{F=0} \quad \text{or} \tag{4}$$

$$\frac{\partial \phi'}{\partial n} = \bar{\bar{U}}_{\infty} * \bar{n}_i + F \tag{5}$$

- The disturbance velocity due to the body goes to zero as the distance r from the body approaches infinity – Figure 2

$$\lim_{r \to \infty} \left| \nabla \phi' \right| = 0 \tag{6}$$

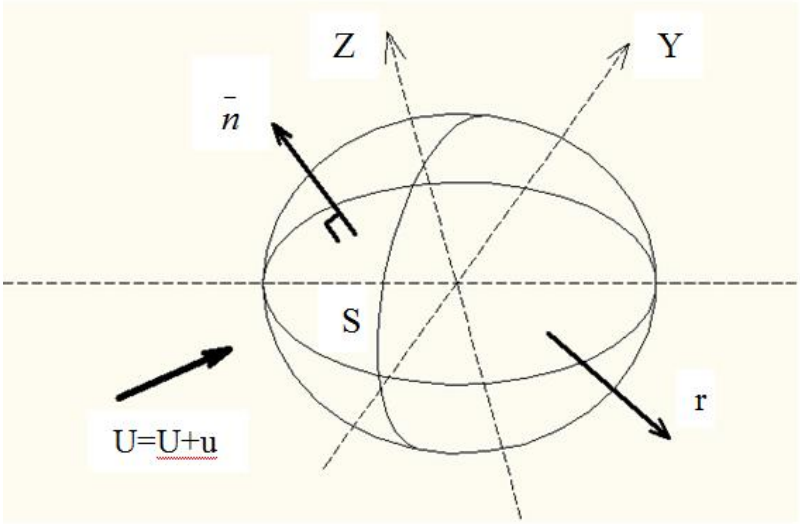

Figure 2 – Boundary conditions

d. Boundary conditions for the Free surface

- The flow must be tangent to the free-surface:

$$\frac{\partial \phi}{\partial x}\frac{\partial h}{\partial x} + \frac{\partial \phi}{\partial y}\frac{\partial h}{\partial y} - \frac{\partial \phi}{\partial z} = 0 \qquad \text{Kinematic condition} \tag{7}$$

- The static pressure on the free surface must be constant:

$$gh + 0.5\left(\left(\frac{\partial \phi^2}{\partial x} \right)^2 + \left(\frac{\partial \phi^2}{\partial y} \right)^2 + \left(\frac{\partial \phi^2}{\partial z} \right)^2 - U_{\infty}^2 \right) = 0 \qquad \text{Dynamic condition} \tag{8}$$

- Radiation condition (no upstream waves) – Figure 3

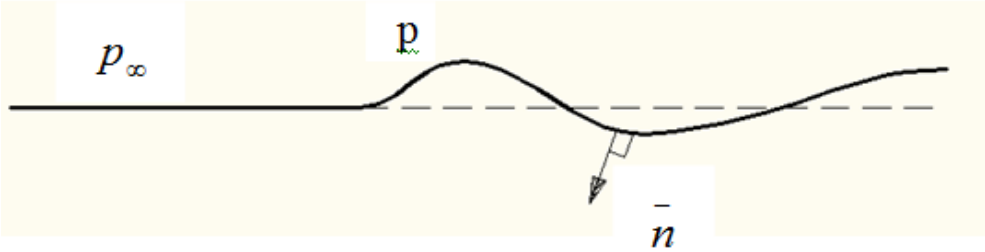

Figure 3 – Radiation Condition

e. Linearization of the free surface boundary condition

- Introduce a known Basic solution and a disturbance

$$\phi = \Phi + \phi', \tag{9}$$

$$h = H + h' \tag{10}$$

- Kinematic free surface boundary condition:

$$\frac{\partial\phi}{\partial x}\frac{\partial H}{\partial x} + \frac{\partial\phi}{\partial y}\frac{\partial H}{\partial y} - \frac{\partial\phi}{\partial z} + \frac{\partial\Phi}{\partial x}\frac{\partial h'}{\partial x} + \frac{\partial\Phi}{\partial y}\frac{\partial h'}{\partial y} = 0 \tag{11}$$

- Dynamic free surface boundary condition:

$$h' = \left(\frac{1}{g}\right)\left[\left(\frac{\partial\Phi}{\partial x}\right)^2 + \left(\frac{\partial\Phi}{\partial y}\right)^2 + \left(\frac{\partial\Phi}{\partial z}\right)^2 - \left(\frac{\partial\Phi}{\partial x}\frac{\partial\phi}{\partial x} + \frac{\partial\Phi}{\partial y}\frac{\partial\phi}{\partial y} + \frac{\partial\Phi}{\partial z}\frac{\partial\phi}{\partial z}\right)\right] \tag{12}$$

The wave height:

$$h = \left(\frac{1}{2g}\right)\left[U_\infty^2 + \left(\frac{\partial\Phi}{\partial x}\right)^2 + \left(\frac{\partial\Phi}{\partial y}\right)^2 + \left(\frac{\partial\Phi}{\partial z}\right)^2 - 2\left(\frac{\partial\Phi}{\partial x}\frac{\partial\phi}{\partial x} + \frac{\partial\Phi}{\partial y}\frac{\partial\phi}{\partial y} + \frac{\partial\Phi}{\partial z}\frac{\partial\phi}{\partial z}\right)\right] \tag{13}$$

f. Three basic-model solutions:

- Neuman-Kelvin

$$\phi = U_\infty * x + \phi', \qquad h = 0 + h' \tag{14}$$

- Double model solution

Mirror image of the hull – Figure 11

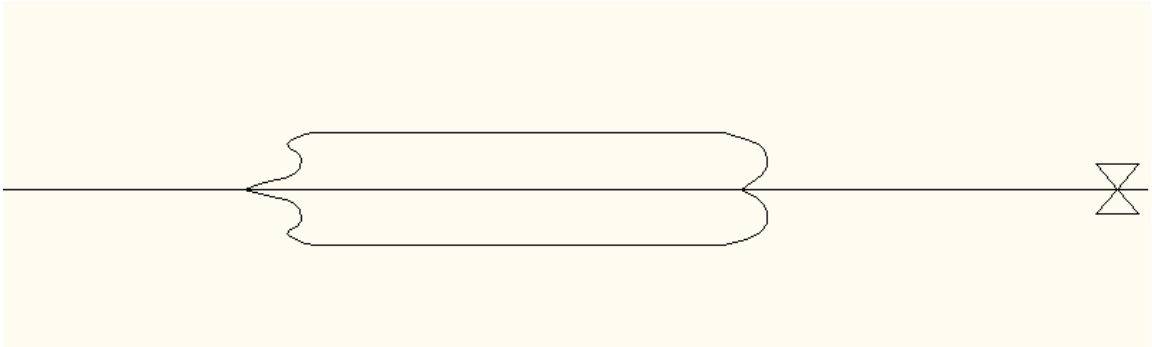

Figure 4 – Double model

- Single-model solution – Neuman on the free surface

2.2 Mathematical Model Viscous Flow

In the beginning of any numerical method is the mathematical Model, which means the set of partial differential or integro-differential equations and boundary conditions. So in the very beginning must be very clear what the physical problem is and which is the object of the current investigation. Also depending on the physical problem and the object of the investigation, must be decided if any simplifications are necessary. A solution method is usually designed for a particular set of equations. Trying to produce a general purpose solution method, i.e. one which is applicable to all flows, is impractical, if not impossible and, as with most general purpose tools, they are usually not optimum for any application.

2.3. Discretization Method

The next step after setting up the mathematical model is choosing the discretization method. There are many approaches but the most important are: Finite difference (FD); Finite volume (FV) and Finite element (FE) methods.

As long as **Finite Differences** method is dealing only with simple geometries, it cannot be used for ships unless it uses a body-and-boundary fitted coordinate system.

The main advantage as well as the main disadvantage of **Finite Elements** is that it is difficult to put any physical significance on the terms in the algebraic equations. In the finite volume method, we are always dealing with fluxes - not so with finite elements.

So the most suitable method for CFD around the ship hull is **Finite Volume** and that's why ShipFlow is dealing only with Finite Volume method.

2.3.1 Equations

Two-dimensional case an infinitely small control volume is considered, **u** and v are the velocity components in **x** and **y** respectively direction. Subscripts denote partial derivatives, e.g. **ux = ∂u/∂x**. Positive mass flux leaves the control volume, negative mass flux enters the control volume. The total mass flux has to fulfil:

$$-\rho dyu + \rho dy(u + u_x dx) - \rho dx v + \rho dx(v + v_y dy) = 0 \tag{15}$$

$$u_x + v_y = 0 \tag{16}$$

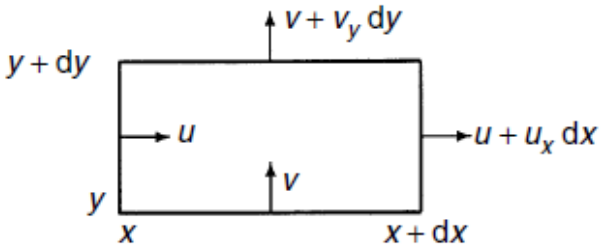

Figure 5 - Control volume to derive continuity equation in two dimensions

The continuity equation in three dimensions can be derived correspondingly to:

$$ux + vy + wz = 0 \tag{17}$$

Velocities and pressure may be divided into a time average and a fluctuation part to bring the Navier–Stokes equations closer to a form where a numerical solution is possible. Time averaging yields the Reynolds-averaged Navier–Stokes equations (RANS). u, v, w and p are from now on time averages. u0, v0, w0 denote the fluctuation parts. For unsteady flows (e.g. manoeuvring), high-frequency fluctuations are averaged over a chosen time interval (assembly average). This time interval is small compared to the global motions, but large compared to the turbulent fluctuations. Most computations for ship flows are limited to steady flows where the terms ut, vt, and wt vanish.

The RANS have a similar form to the Navier–Stokes equations:

$$\rho(u_1 + uu_x vu_y + wu_z) = \rho f_1 - p_x + \mu(u_{xx} + u_{yy} + u_{zz}) - \rho((\bar{u'}\bar{u'})_x + (\bar{u'}\bar{v'})_y + (\bar{u'}\bar{w'})_z) \tag{18}$$

$$\rho(v_t + u v_x v v_y + w v_z) = \rho f_2 - p_y + \mu(v_{xx} + v_{yy} + v_{zz}) - \rho((\bar{u}'\bar{v}')_x + (\bar{v}'\bar{v}')_y + (\bar{v}'\bar{w}')_z) \quad (19)$$

$$\rho(w_t + u w_x v w_y + w w_z) = \rho f_3 - p_z + \mu(w_{xx} + w_{yy} + w_{zz}) - \rho((\bar{u}'\bar{w}')_x + (\bar{v}'\bar{w}')_y + (\bar{w}'\bar{w}')_z) \quad (20)$$

They contain as additional terms the derivatives of the Reynolds stresses:

$$-\rho\bar{u}'\bar{u}' - \rho\bar{u}'\bar{v}' - \rho\bar{u}'\bar{w}' \quad (21)$$

$$-\rho\bar{u}'\bar{v}' - \rho\bar{v}'\bar{v}' - \rho\bar{v}'\bar{w}' \quad (22)$$

$$-\rho\bar{u}'\bar{w}' - \rho\bar{v}'\bar{w}' - \rho\bar{w}'\bar{w}' \quad (23)$$

The time averaging eliminated the turbulent fluctuations in all terms except for the Reynolds stresses. The RANS require a turbulence model that couples the Reynolds stresses to the average velocities.

[1]

2.4. Turbulence Model

The flows which are usually encountered in the engineering practice are mostly Turbulent. This kind of flows are characterised by some properties:

- They are highly unsteady;
- They are three dimensional;
- They contain a great deal of virtuosity due to the higher flow speed and lower pressure;
- Turbulence increase the rate of the process in which parcels of fluid with different concentration of at least one of the conserved properties are brought in to contact. This process is called “stirring process”. The name “Turbulent Diffusion” is also used often;
- Turbulence brings fluids of different momentum content into contact. This mixing is a dissipative process;
- Turbulent flow contains repeatable and essentially deterministic events that are responsible for large parts of mixing;

- Turbulent flow fluctuates on a wide range of length and time scales;

Intensive mixing is useful when chemical mixing or heat transfer is needed; both of these may be increased by orders of magnitude because of Turbulence. On the other hand, increased mixing of momentum is increasing the frictional forces, and as a consequence the power required to pump the fluid or to propel a vehicle is increased. Engineers need to understand these effects and to be able to predict them in order to achieve a good design. In some cases it is possible to control the turbulence partially.

Optimizing the design it is usually necessary to understand the source of the undesired effects; this requires detailed measurements which are costly and time consuming. Some types of measurement for example, the fluctuation pressure within the flow are almost impossible to make at the present time. Others cannot be made with the required precision. That's why the numerical methods have an important role to play.

There are several approaches to predict the Turbulent flow. According to Bardina et al. (1980) there are six categories of approaches:

- The first one involves the use of correlations;
- The second uses integral equations which can be derived from the equations of motions by integrating over one or more coordinates;
- The third one is called "on-point closure" and leads to a set of partial differential equations called Reynolds-averaged Navier-Stokes equation (RANS);
- The fourth is called "two point closure" ;
- The fifth is "Large eddy simulation" (LES) – It is used for largest scale motions of the flow;
- And the sixth is called "Direct Numerical Simulation" (DNS) – This method is probably more accurate but also more costly;

Most widely used approach is "one point closure" which uses RANS equation. This method is based on equations obtained by averaging the equations of motion over time (if the flow is statistically steady), over a coordinate in which the mean flow does not vary, or over ensemble of realizations. These equations do not form a closed set, so this method requires the introduction of approximations (**Turbulent Models**).

One of the most common turbulence models in practice is standard k-ε model. This model is based on the following two equations:

$$\frac{\partial(\rho k)}{\partial t}+\frac{\partial(\rho \bar{u}_j k)}{\partial x_j}=\frac{\partial}{\partial x_j}\left(\mu\frac{\partial k}{\partial x_j}\right)-\frac{\partial}{\partial x_j}\left(\frac{\rho}{2}\overline{u'_j u'_i u'_i}+\overline{p'u'_j}\right)-p\overline{u'_i u'_j}\frac{\partial \bar{u}_i}{\partial x_j}-\mu\frac{\partial \bar{u}_i'}{\partial x_k}\frac{\partial \bar{u}_i'}{\partial x_k} \quad (24)$$

$$\frac{\partial(\rho\varepsilon)}{\partial t}+\frac{\partial(\rho u_j \varepsilon)}{\partial x_j}=C_{\varepsilon 1}P_k\frac{\varepsilon}{k}-\rho C_{\varepsilon 2}\frac{\varepsilon^2}{k}+\frac{\partial}{\partial x_j}\left(\frac{\mu_t}{\sigma_\varepsilon}\frac{\partial \varepsilon}{\partial x_j}\right) \quad (25)$$

Equation “23” – The equation for the turbulent kinetic energy, is the most used equation for determining the velocity scale.

Equation “B” – Is an exact equation for the dissipation “ε”, derived from the Navier-Stokes equations.

Also k-ω models are proposed for ship flows. These models are like the k-ε models two-equation models and can be seen as a further evolution of them. ω is proportional to ε/k and can be interpreted as a ‘turbulence frequency’. k-ω models yield better agreement with experiments in many cases; however, they react more sensitively to grid quality. Reynolds stress models calculate the individual Reynolds stresses from their modelled transport equations without recourse to an eddy viscosity hypothesis. These models require more computational effort than, e.g., the two-equation k-ε model, but showed in several ship flow applications superior results. However, it is not yet decided if similarly good results can be obtained by simple turbulence models with properly adjusted coefficients. Probably the most widely used turbulence model in engineering applications is the (standard) k-ε model, (Launder and Spalding (1974)). k is the kinetic energy of the turbulence, ε the dissipation rate of k. The k-ε model expresses the eddy viscosity _t as a simple function of k and ε:

$$\mu_t = 0.09\rho k^2/\varepsilon \quad (26)$$

Where 0.09 is an empirical constant. k and ε are expressed by two partial differential equations.

Closure to turbulence in “ShipFlow” is achieved by means of the algebraic EASM model, the Reynolds stress components being explicitly determined from the tensor functions of the velocity gradients, turbulent kinetic energy, and turbulent length scale. Starting from a Reynolds stress closure model, Gatski and Speziale developed the algebraic EASM model by

using a three term tensor basis and the Galerkin method to determine the coefficients of the model. The resulting model is relatively complex but has the unique advantage that the explicit solution of the Reynolds stresses is given at each computational iteration.

Turbulence actually is not fully understood. All turbulence models used for fluid flows are semi-empirical. They use some theories about the physics of turbulence and supply the missing information by empirical constants. None of the turbulence models used so far for ship flows has been investigated for its suitability at the free surface.

[2]

2.5. Boundary Conditions

Each control volume provides one algebraic equation. Volume integrals are calculated in the same way for every Control Volume, but fluxes through -faces coinciding with the domain boundary require special treatment. These boundary fluxes must either be known, or be expressed as a combination of interior values and boundary data. Since they do not give additional equations, they should not introduce additional unknowns. Since there are no nodes outside the boundary, these approximations must be based on one-sided differences or extrapolations.

Usually, convective fluxes are prescribed at the inflow boundary. Convective fluxes are zero at impermeable walls and symmetry planes, and are usually assumed to be independent of the coordinate normal to an outflow boundary; in this case, upwind approximations can be used. Diffusive fluxes are sometimes specified at a wall e.g. specified heat flux or boundary values of variables are prescribed. In such a case the diffusive fluxes are evaluated using one-side approximations for normal gradients. If the gradient itself is specified, it is used to calculate the flux, and an approximation for the flux in terms of nodal values can be used to calculate the boundary value of the variable. This is demonstrated in the example below (Figure 2)

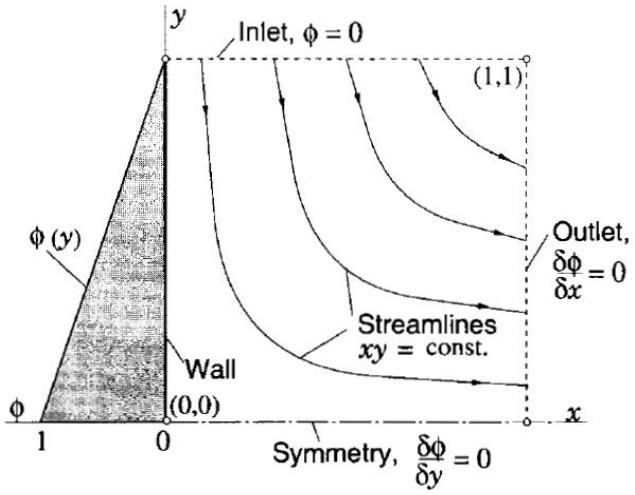

Figure 6 - Geometry and boundary conditions for the scalar transport in a stagnation point flow.

Unfortunately the computational grid cannot cover the entire fluid domain because it will be very costly and time consuming. That is why artificial boundary conditions are necessary to be defined. Very often the wave making at the free surface is neglected and it is treated as a rigid plane of symmetry.

The outer boundaries have a relative velocity to the ship. Usually, the physical boundaries would be too far away to be considered. Then the side and bottom boundaries should be sufficiently removed from the ship. Often the side and bottom boundary forms (quarter for double-body flow with symmetry in y), as a cylinder leads usually to better grids (for single-block grids) than block-type grid. A typical cylinder radius would be between 0.5 and 1 ship length. The boundary condition on the hull is a no-slip condition (zero relative speed) which is either enforced directly or via a wall function depending on the turbulence model employed. At the inlet all unknowns are specified. If the inlet is chosen sufficiently upstream of the ship, uniform flow with corresponding hydrostatic pressure can be assumed. If the k-ε model is employed, the distribution of k and ε at the inlet also have to be specified. The influence of the specified values for k and ε decays rapidly downstream, such that errors have decayed by some orders of magnitude after several cells.

At the inlet all unknowns are specified. If the inlet is chosen sufficiently upstream of the ship, uniform flow with corresponding hydrostatic pressure can be assumed.

At the outlet usually the derivatives in longitudinal direction are set for all unknowns to zero and the flow leaving the domain is determined such that continuity is preserved for the whole fluid domain. The longitudinal derivatives are actually not really zero, but this boundary

condition prevents upstream propagation of any reflections of disturbances created by the numerical method. Numerical experiments show that these boundary conditions affect results only in a small local region near the outlet.

At symmetry planes normal velocity and all derivatives in the normal direction are set zero. Since the normal derivatives of the tangential velocities vanish, the shear stresses are zero. The outer boundary of the computational domain (side and bottom) may be treated as 'symmetry plane', i.e. on each outer cell face normal velocity and all normal derivatives are set zero. In this case, the outer boundary must be far away from the ship such that virtually uniform flow is encountered.

[1, 2]

3. SHIP, PROPELLER AND RUDDER CHARACTERISTICS

The following tables are describing all the geometrical characteristics of the hull rudder and the propeller, including the test conditions for the model.

Table 1 – Geometrical characteristics of the ship (full scale and model scale)

Characteristics	Simbol	Full Scale	Model Scale
Length Overal	L_{OA}	243.840 [m]	3.713 [m]
Length Water Line	L_{WL}	232.50 [m]	3.540 [m]
Length Between perpendiculars	L_{PP}	230.0 [m]	3.502 [m]
Breadth	B	32.20 [m]	0.490 [m]
Average Draft	T_M	10.80 [m]	0.164 [m]
Height	D	19.0 [m]	0.289 [m]
Longitudinal centre of buoyancy	LCB	111.596 [m]	1.699 [m]
Volume Displacement	∇	52030.0 [m^3]	0.1837 [m^3]
Wetted surface area	S	9424.0 [m^2]	2.185 [m^2]
Temperatura	t	15.0 [deg]	24.0 [deg]
Density	ρ	1.025 [t/m^3]	997.2 [kg/m^3]
Cinematic viscosity	υ	1.18831E-06 [m^2 /s]	0.9134E-06 [m^2 /s]
Gravitational acceleration	g	9.810 [m/s^2]	9.810 [m/s^2]
Bloc coefficient	C_B	0.6505	0.6505
Prismatic coefficient	C_P	0.660	0.660
Coeficientul secţiunii maestre	C_M	0.985	0.985
Velocity	v_s	24 [Nd]	1.523 [m/s]
Froude Number	Fn	0.26	0.26

Table 2 – Model speed, Froude number and Reynolds number used for the experiments.

Test No.	v_m [m/s]	Fn	Rn
1	0,889	0,1516	2,66E+06
2	1,142	0,1949	3,42E+06
3	1,333	0,2274	3,99E+06
4	1,523	0,2599	4,56E+06
5	1,651	0,2816	4,94E+06

The rudder model used in this research is scaled, based on NACA0018 semi/balanced rudder of the KCS model M1213 built in SVA with the following dimensions Table 3.

Table 3 – Rudder dimensions

Characteristics	Symbol	Units	**Semi-Balanced Horn Rudder**
Profile type			NACA 0018
Rudder area	A_R	[m^2]	54.45
Percentage of lateral area	A_R/LT	[%]	2.21
Movable rudder area	A_M	[m^2]	45.30
Percentage of lateral area	A_M/LT	[%]	1.83
Balancing rudder area	A_B	[m^2]	13.62
Rudder height	b	[m]	9.90
Mean chord length	c_m	[m]	5.50
Mean thickness	t_m	[m]	0.99
Aspect ratio, geometric	□	[-]	1.80
Thickness ratio	t_m/c_m	[-]	0.18
Degree of twist	α	[°]	0

Table 4 – Geometrical characteristics for the propeller

Propeller	
type	FP
No. of Blades	5
D (m)	0,105

P/D (0,7R)	0,997
Ae/A0	0,8
Rotation	Right hand
Hub Ratio	0,18
Appendages	
Bilge keels	None

4. GRID GENERATION

"Numerical grid generation can be thought of as a procedure for the orderly distribution of observers, or sampling stations, over a physical field in such a way that efficient communication among the observers is possible and that all physical phenomena on the entire continuous field may be represented with sufficient accuracy by this finite collection of observations."- J.E. Thompson/"Numerical Grid Generation".[6]

Of most importance in getting accurate results for complex flow problems is the way of generating the computational grid which must describe the changes in the geometries of hull and free surface and all the modifications that interfere in the flow field. Being the structure that supports all flow solutions must be treated with major attention especially if we deal with a fully appended ship. The Chimera-type schemes, which allow grid blocks to overlap in arbitrary manner and structured grid schemes, can be used for flow computations over such complicated domains.

In our case two SHIPFLOW modules were used for grid generation: XMESH that is a panel generator for the potential flow and XGRID which generates the grid for the viscous computations.
XMESH was at first executed as a separate program to check the panelization of the hull (Figure 7) and free-surface (Figure 8) before non-linear potential flow computations were performed.

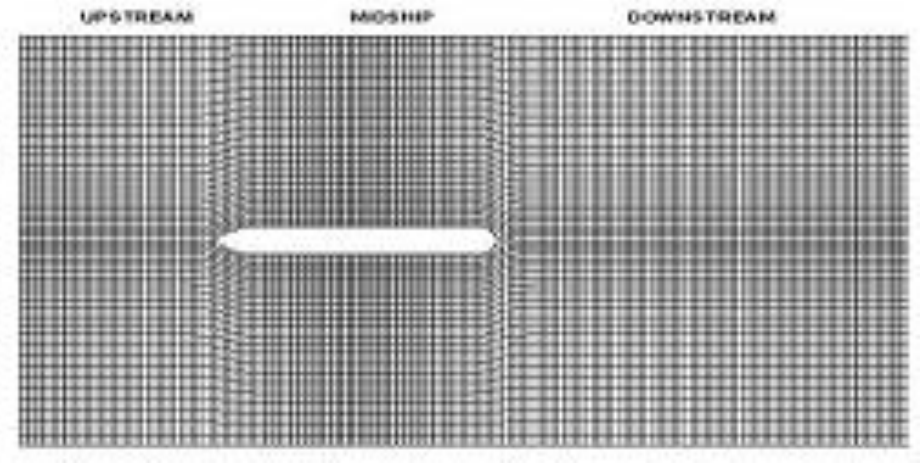

Figure 7. Free surface panelization [16]

The surface of the ship was divided in four groups (hull, bulb, stern and bulb stern) each group being defined by a number of stations and points.

During the non-linear computation, the grid on the ship hull, extended with two panels above the free surface, changes with iteration, following the wave height.

The water free-surface (Figure 8) was decomposed in three main parts: one upstream of the ship, one along the ship and one downstream of the ship every part being divided by a number of stations (in longitudinal direction) and points (in transverse direction).

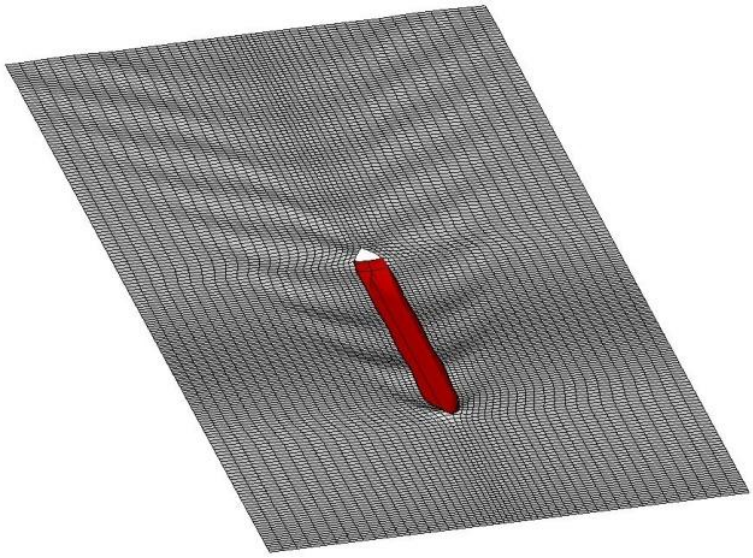

Figure 8. Free-surface panelization [16]

The number of stations on the free-surface, in the longitudinal direction, was determined by the Froude number, F_n, knowing that is recommended to have around 30 panels in the grid of the free surface per wave length, λ.

$$F_n = \frac{v}{\sqrt{gL}} = 0.22 \tag{27}$$

$$\lambda = 2\pi L F_n^2 = 24\,[\text{m}] \tag{28}$$

In the present case, three wave-lengths along the hull were chosen, one wave-length and a half ahead of the ship, where the recommendations ask for half the number of stations that are along the ship, and three waves-lengths after the ship.

In the transverse direction the panels were stretched towards the hull, the beam being divided in 25 segments.

Offset File

Offset file is used from ShipFlow to represent the ship model. It is a separate file which describes in details point by point the entire hull shape.

There are two ways to create the offset file:

a. Hull --> Tribon (lines plan) --> Lines --> Export dxf --> Rhino --> Generate the points on each station
b. Surface --> Rhino --> Generate sections (stations) --> Generate the points on each station

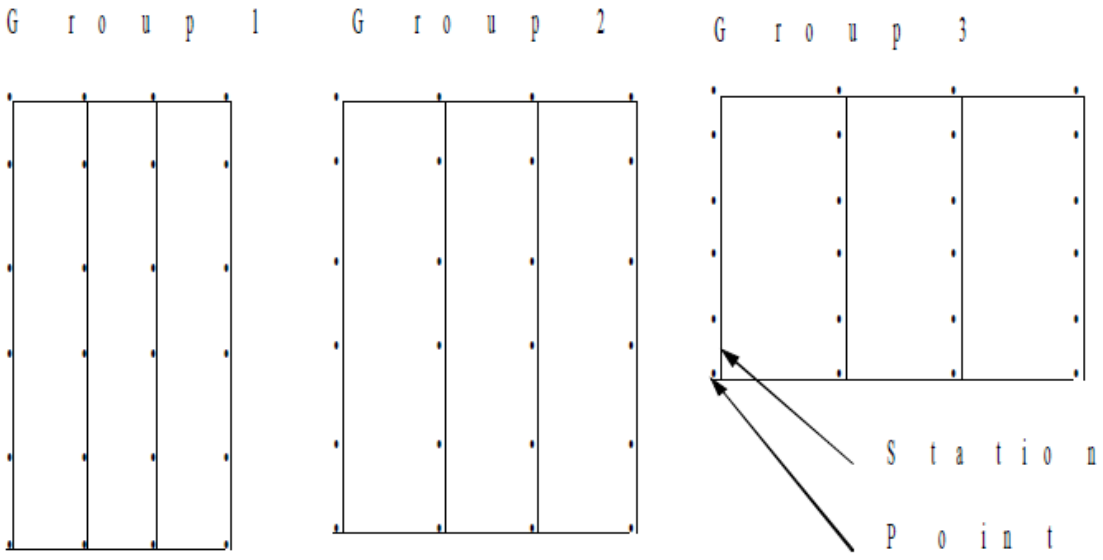

Figure 9 – Label name of an offset group used to identify the group. [3]

The ship is divided in 4 groups. Overhang, Hub, Hull, Bow (Figure 10).

Figure 10 – Hull divisions

Each group is divided by sections and each section is defined by points – starting from the keel and finishing to the Main Deck. Ship Flow manual. [3]

Standard Case

Standard case is the case which doesn't need any additional set - it is running by default properties In Ship Flow.

In this part attention will be paid on the panelization.

As long as in potential flow there is no fluid domain – the discretization is on the free surface and the hull, by using singularities (Panel method)

On Figure 11 is shown the grid from different views.

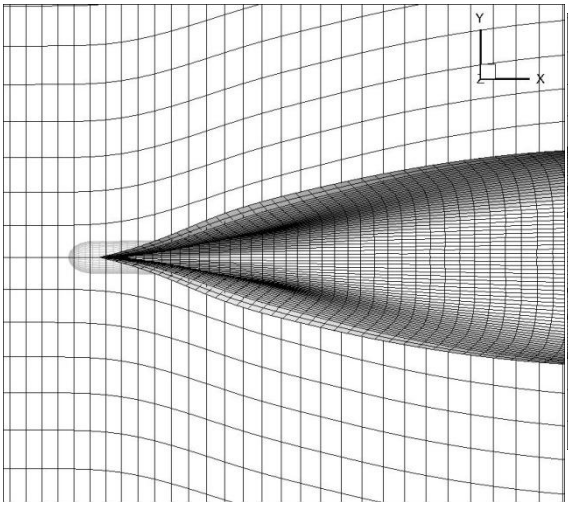

Figure 11a - Fore part

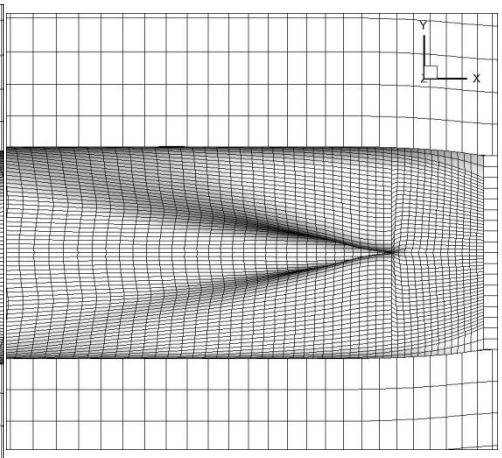

Figure 141 - Aft Part

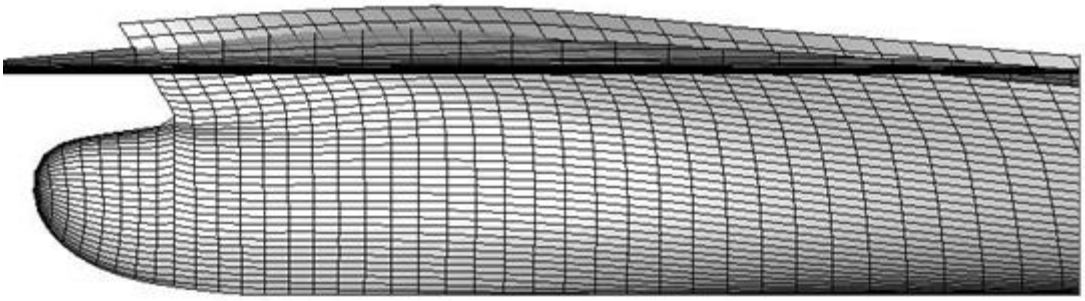

Figure 11c – Fore part (Side view)

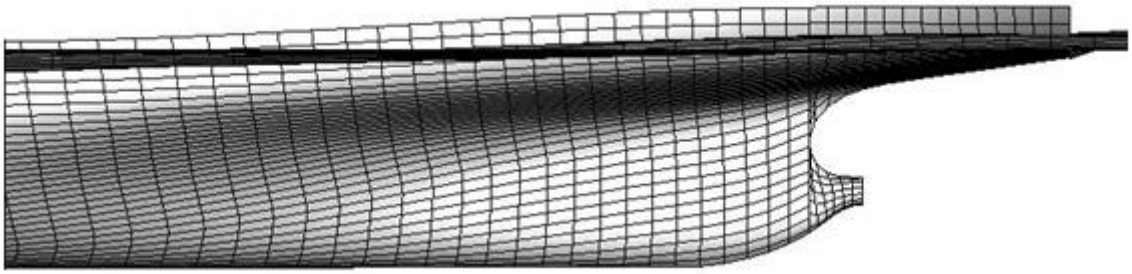

Figure 11d – Aft Part (Side view)

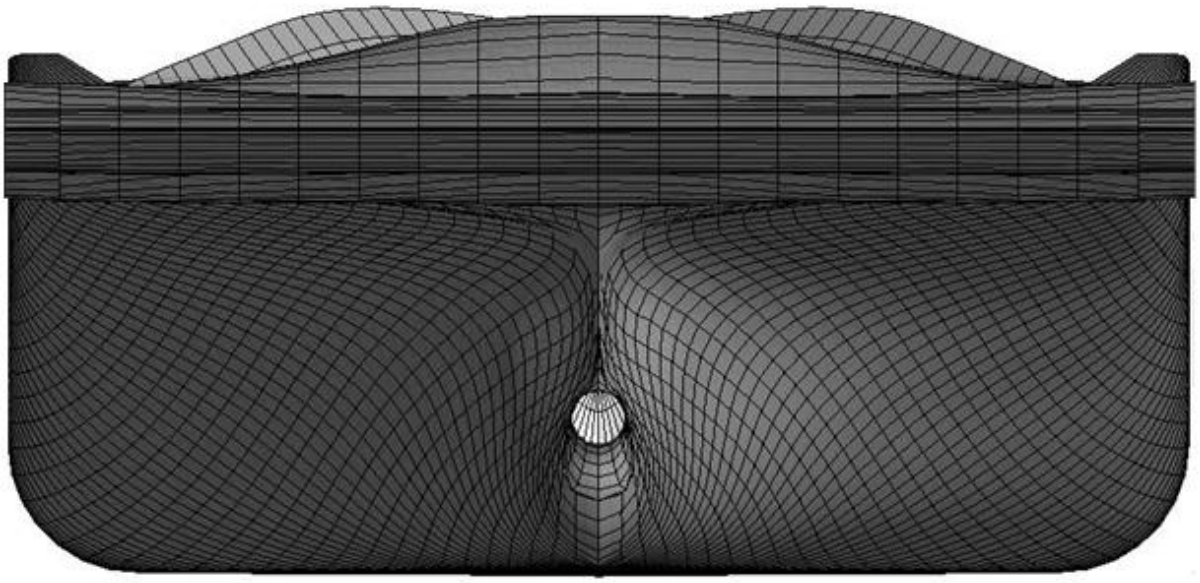

Figure 11e – Front view

Panelization

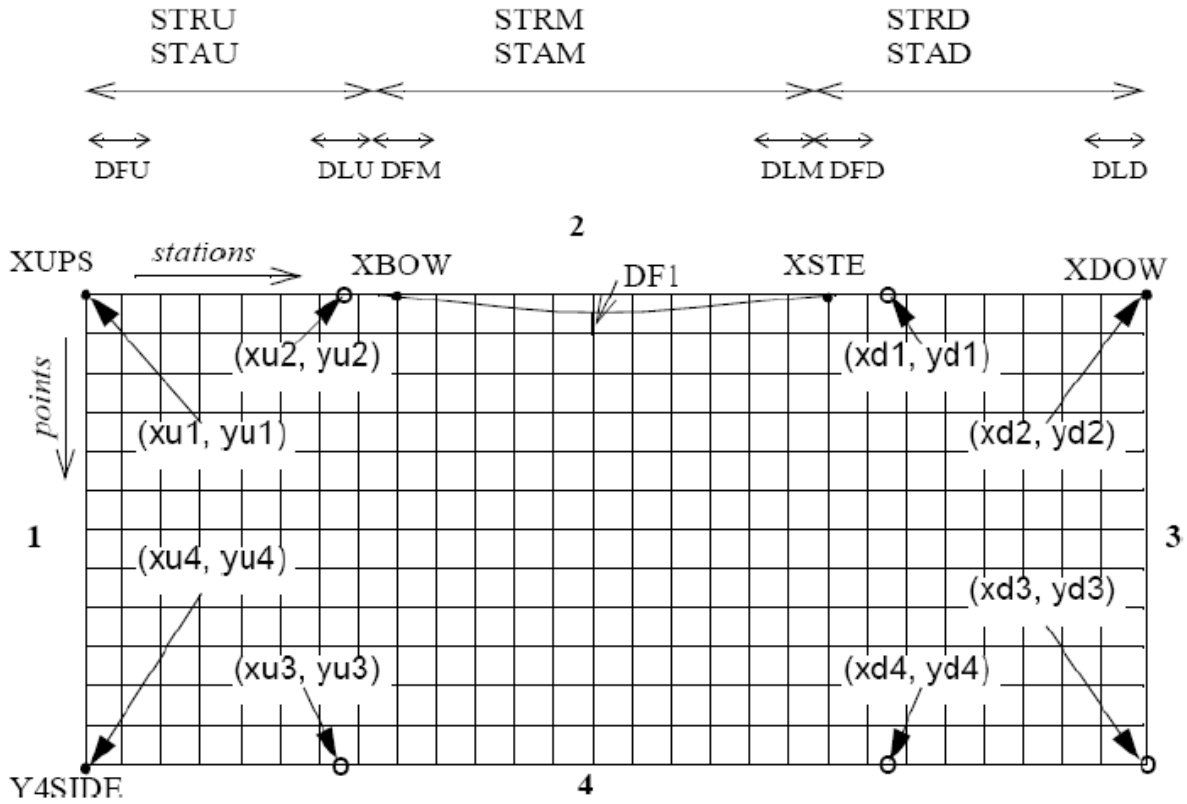

Figure 12 – Panel Distribution on the hull and the free surface. Ship Flow manual. [3]

Using formula 1 the wave length is calculated using given Froude number. Dividing the model length with the wave length the exact number of waves developed beside the hull is calculated.

Computations were performed with the following number of panels per wave length: 15; 20; 25; 30; 35; 40, in order to see which case will be more suitable for the physical problem. The case with 30 panels – recommended by the ShipFlow developers was chosen considering also the computational time and the accuracy of the solution.

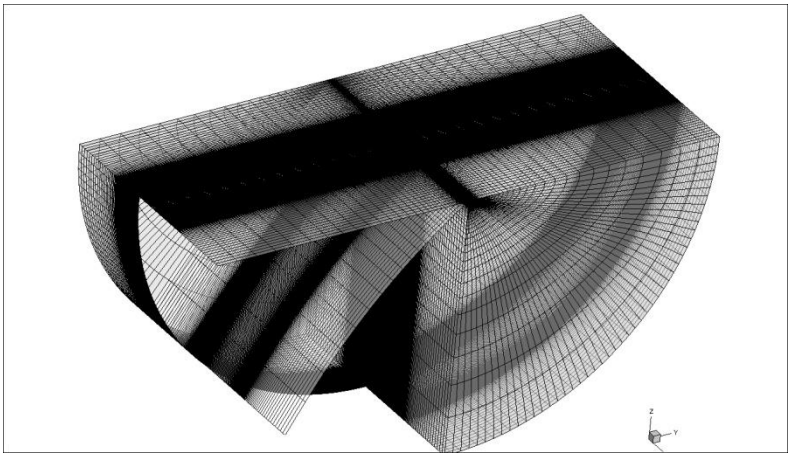

Figure 13 - Computational grid

In the viscous computation, a mono-block structured grid of 2020200 cells has been generated using the XGRID module to cover the entire computational domain around the bare hull (Figure 13 and Figure 14. The grid was clustered in longitudinal direction near bow and stern and near the solid body of the ship – useful for obtaining good pressure and velocity gradients.

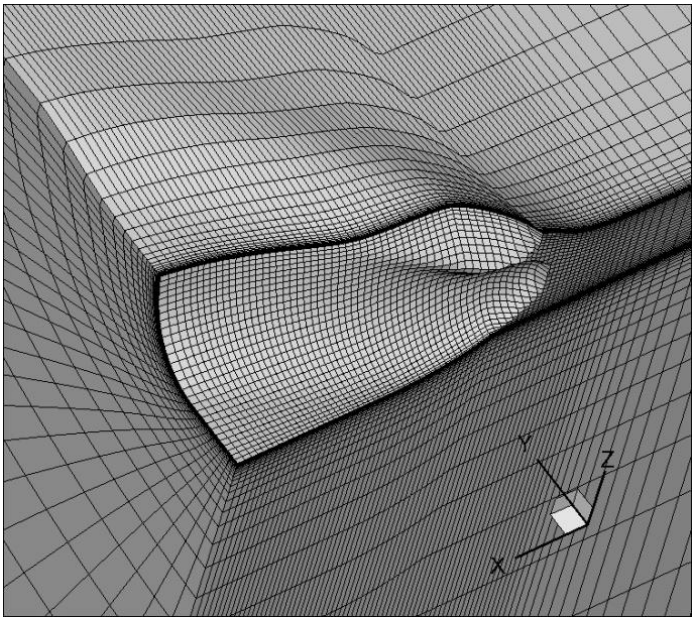

Figure 14. Computational grid detail [16]

The XCHAP solver, used for the viscous computation, can handle overlapping grids. Several parametric models of appendages such as propeller, rudders, brackets or shafts are available in the computational code. Once the problem of the computational grid for the bare hull was solved using the XGRID module, a set of boundary fitted structured component grids have been generated around the propeller and the rudder resulting a composite grid of two additional overleaping grids as it can be seen in Figure 15. For simplifying the generation of the grid and the computation, the propeller is modeled by an actuator disk, which accelerates the flow in axial direction and determines a pressure jump in the propeller plane. The free-surface, normally treated as a slip plane, was fitted to the computational domain by means of the free-surface computed by the potential flow solver.

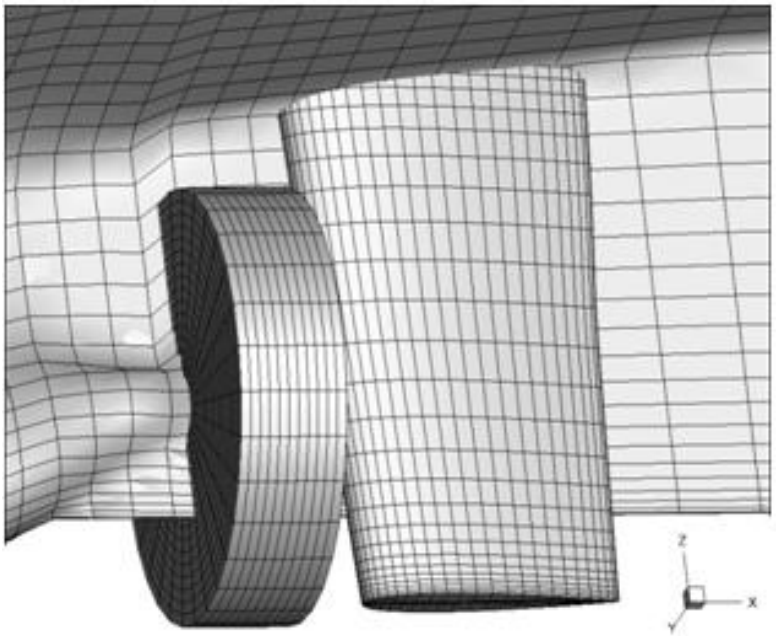

Figure 15 – Overleaping grids

5. BARE HULL

Every ship hull has its own resistance and flow pattern. Therefore each hull has a unique propeller which is designed only for it, the propeller disc being forced to work in a particular wake. In order to have a well designed ship hull and propeller and even rudder the naval architect has to pay special attention to the hydrodynamic characteristics of the given elements as well as to the flow pattern. The interactions that appear between the mentioned components are of most importance, the optimum design of the vessel being strongly influenced by these.

In this regard, the present work considers the hydrodynamic study of the flow developed around the bare hull, the hull with propeller, the hull with rudder and the hull with rudder and propeller, the influence exerted by each of them being determined and explained. Also, the accurate determination of ship resistance, propulsion coefficients and hydrodynamic forces and moments developed on the hull and rudder is considered for the bare hull case, the hull with propeller case and the hull with rudder case.

KCS is a ship that has a significant wave fact that sustains the application of the potential flow theory which can be used in order to numerically determine the wave pattern and the wave resistance. Also of major importance the viscous resistance of the ship as well as the three-dimensional flow developed around all considered configurations will be calculated by the use of a viscous solver. Both potential and viscous flow theories are implemented in

SHIPFLOW. Also, the lifting line theory considered for propeller computation is implemented in the program.

Of major importance the flow around the bare hull is first studied, the ship resistance, the wave pattern, the axial velocity distribution and the pressure distribution on the hull being thoroughly determined.

[1]

5.1. Ship Resistance

"The total resistance of the ship R_T is the projection of the resultant of the hydro-aerodynamics forces that are acting on the ship, in the direction of advance and is opposite to the motion of the ship" (Obreja, 2005). [18]

It is obviously necessary to determine this force even from the first stages of ship design, theoretical, experimental or computational methods being considered in this regard. Limited by a number of restrictive conditions that are related to the type of the vessel or to the shape of the hull the theoretical methods cannot be widely applied. Also, even though the most accurate the experimental methodologies which are often used in the preliminary design stage have the disadvantages given by the high costs and the time that are required in order to achieve a full set of tests. In these circumstances CFD methods which due to the latest technical developments are easy to use, less time consuming and can be applied for any kind of ship hull are gaining more and more field becoming a widely used tool even in the preliminary design stages.

The present study considers this type of numerical methodologies the ship resistance of the KCS container ship being accurately calculated. Of most importance the validation of the numerical methodology is achieved, the experimental results of the resistance tests that were conducted in the 45 x 4 x 3 meters towing tank of the Faculty of Naval Architecture from the "Dunarea de jos" University of Galati (Figure 16) being used in this concern.

Figure 16 – Towing Tank – University of Galati

Done in complete accordance with the ITTC 7.5-02-02-01 procedures [2-http://ittc.sname.org/2002_recomm_proc/7.5-02-02-01.pdf], the experimental tests were performed at 14^{o} C water temperature. A specialized carriage was used in order to tow with five different speeds the KCS experimental model (Fig 34) which was built based on the ITTC 7.5-01-01-01 [1-http://ittc.sname.org/2002_recomm_proc/7.5-01-01-01.pdf] recommendations. There was no rudder or other appendage fitted to the KCS scale model, two degrees of freedom which allowed trimming and sinking being considered.

Potential Flow

As a first step the simplified potential theory and the boundary layer theory were used in order to determine ship resistance. The wave resistance and the frictional resistance were calculated for the entire range of speeds considered during the experiment (0.889 m/s; 1.142 m/s; 1.333 m/s; 1.523 m/s; 1.651 m/s).

In this regard, Figure 17 depicts the frictional resistance which was computed based on the abovementioned computational method all the values being compared with the empirical results that were obtained by the ITTC' 57 formula (29).

$$Cf = 0.075/(\log Rn - 2)^2 \quad (29)$$

The estimated comparison errors for the frictional resistance are shown in Table 5. The depicted errors show very good agreement between the numerical and theoretical results the accuracy of the method being revealed.

Table 5 – Numerical error estimated comparing with ITTC 57

Fn	Error Rf %
0,1516	-8,426
0,1949	-9,024
0,2274	-9,507
0,2599	-9,777
0,2816	-9,647

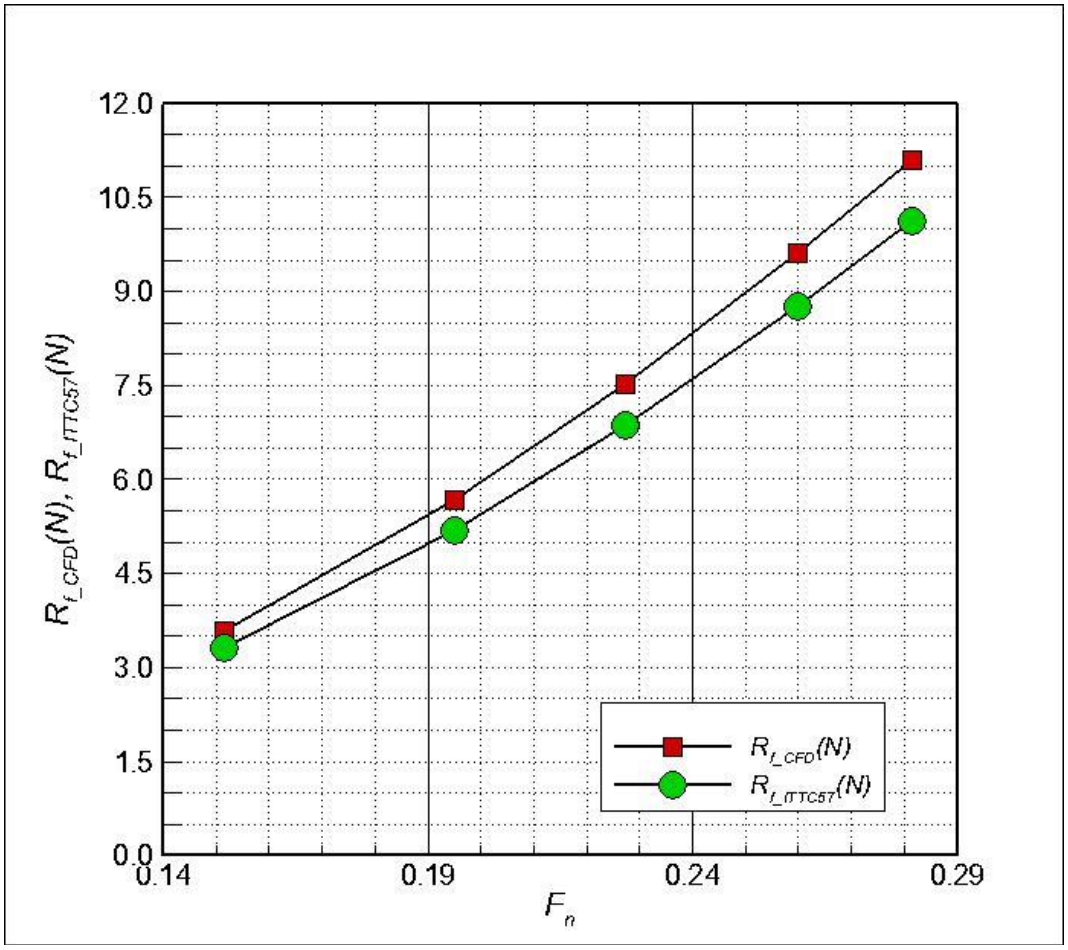

Figure 17 - Comparison between CFD and ITTC for Frictional resistance.

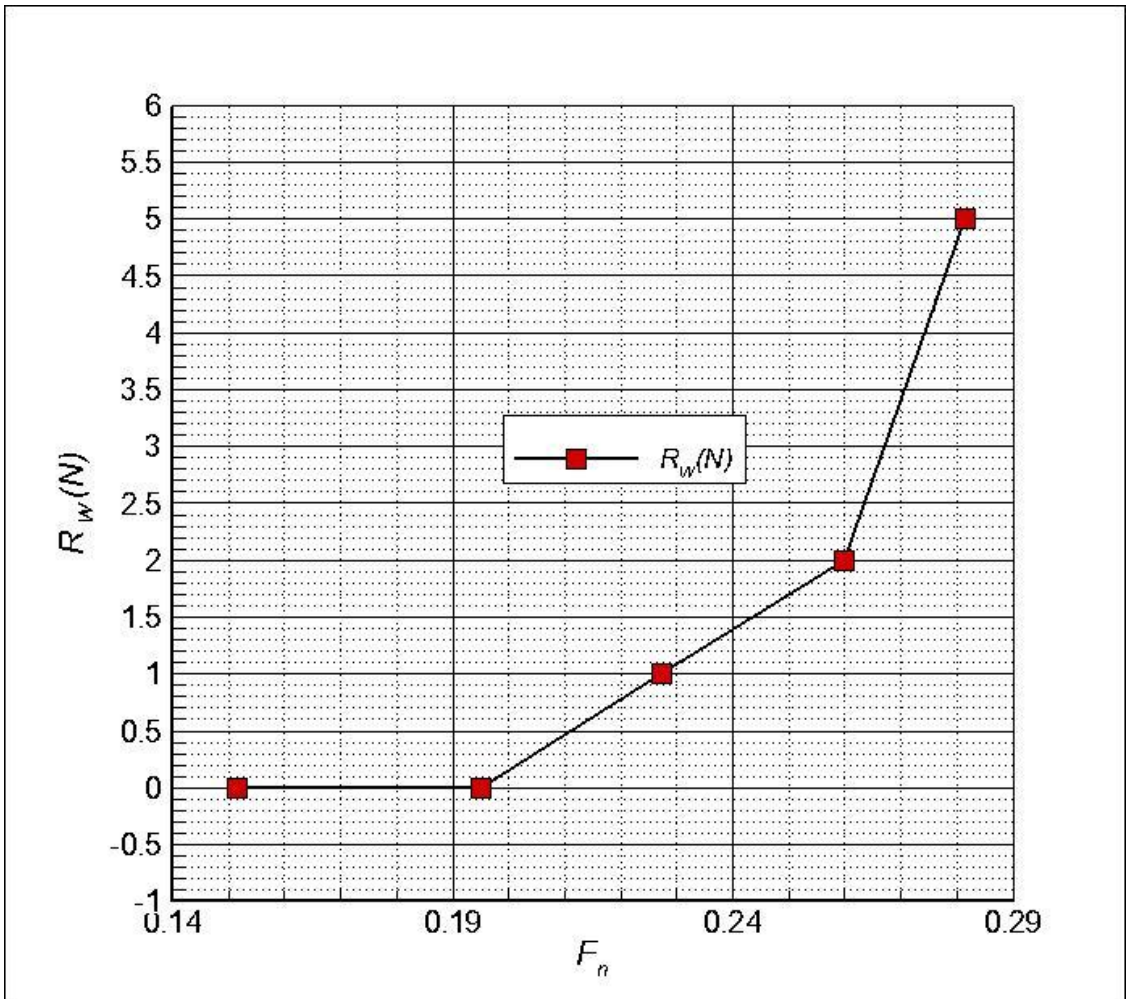

Figure 18 - Wave Resistance computed by the Potential flow.

Viscous Flow

In order to have a much more realistic picture of the problem viscous flow computations are used. Viscous flow means more physics included in the computations and particularly viscosity. Therefore a different mathematical model is needed in order to find the solutions of fluid motion. But the more physics is included more complications arise. If the ensemble (hull-propeller-rudder) is broken down on pieces and each part is investigated separately the process becomes a simplified one. This kind of investigation is of course important the user being able to see in what manner each component is changing the flow in a very specific way. One of my Professors Armin Troesch (University of Michigan) was giving us a perfect example as follows:"We have to look first at the threes and then we will be able to see and to assimilate how big and powerful is the forest". In the present study "the threes" are the hull, the propeller and the rudder and the forest is the entire ensemble.

In this particular study the viscous flow solver was use in order to determine as a first step the viscous resistance of the ship, component that being strongly dependent on the shape of the hull is not so good captured by the simplified theories. Considering the Froude and the Reynolds numbers which were determined based on the experimental data the total resistance of the KCS experimental model was computed. Figure 19 depicts the numerical results as well as the experimental results obtained in the towing tank of the Faculty of Naval Architecture from the "Dunarea de jos" University of Galati.

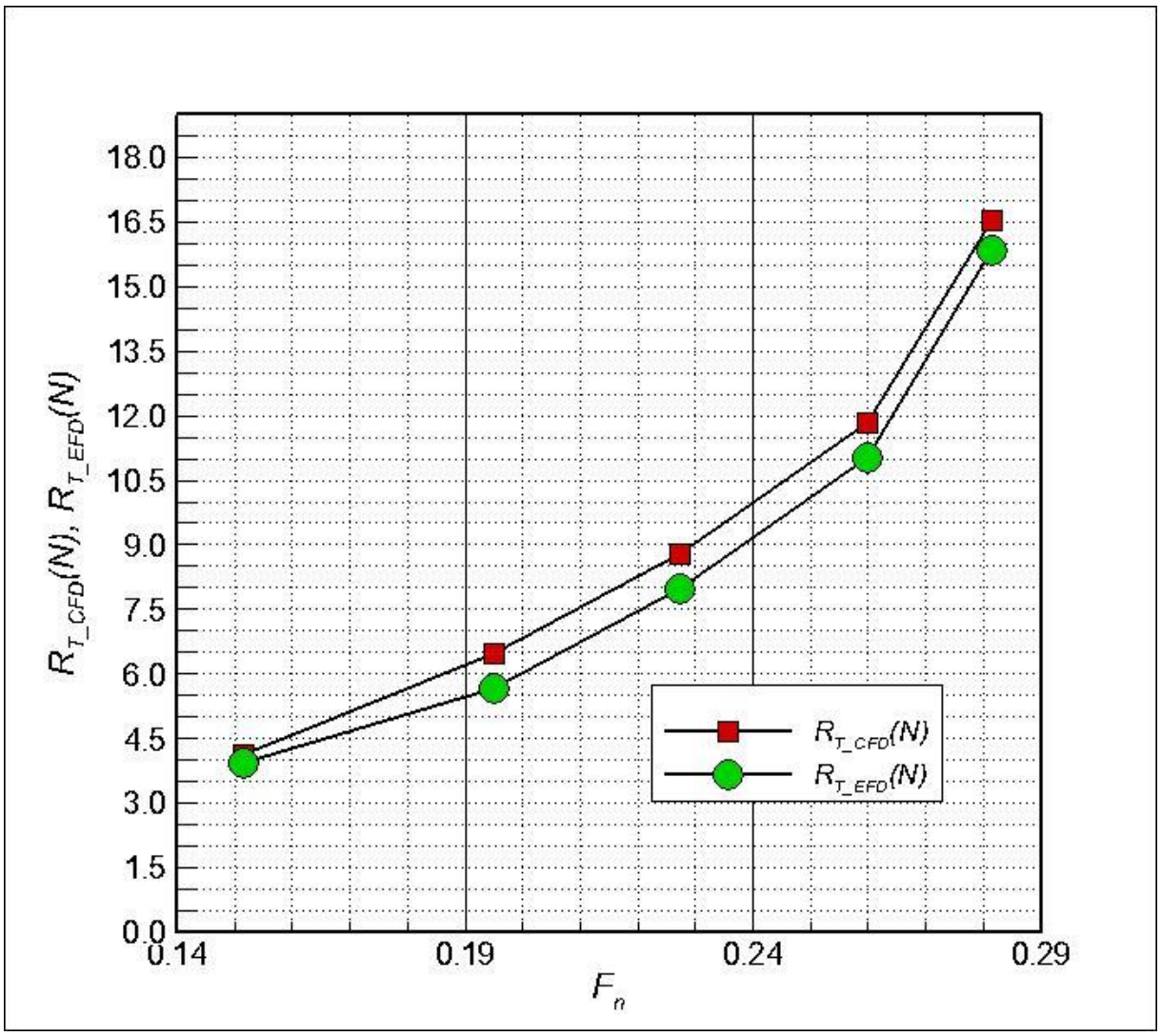

Figure 19 – Resistance comparison between CFD and EFD

The comparison error is shown on table 6. The percentages show that the differences are satisfactory.

Table 6 – Numerical error estimated in comparison with the reference results

Fn	Error %
0,1516	-4,364
0,1949	-14,75
0,2274	-10,066
0,2599	-7,35
0,2816	-4,382

5.2. Validation of the Computational Methodology Used for Study of the Flow.

For validating the numerical methodology that was used for the hydrodynamic study of the flow around bare hull, hull with propeller, hull with rudder and hull with rudder and propeller the experimental results published by [Reference 4] were used. Therefore in complete accordance with [Reference 4] a 1/31.6 virtual model was considered, the Froude and the Reynolds numbers that are governing the flow being set at 0.26 and $1.4x10^7$ respectively. Both potential and viscous flow methodologies are considered in the validation process.

5.2.1 Potential flow wave pattern

Based on the abovementioned specifications a potential flow computation was done for the scaled model taking into consideration the defined flow features. This simplified numerical methodology was validated by comparing the two sets of results: the numerical and the experimental results. The comparison is shown on Figure 20.

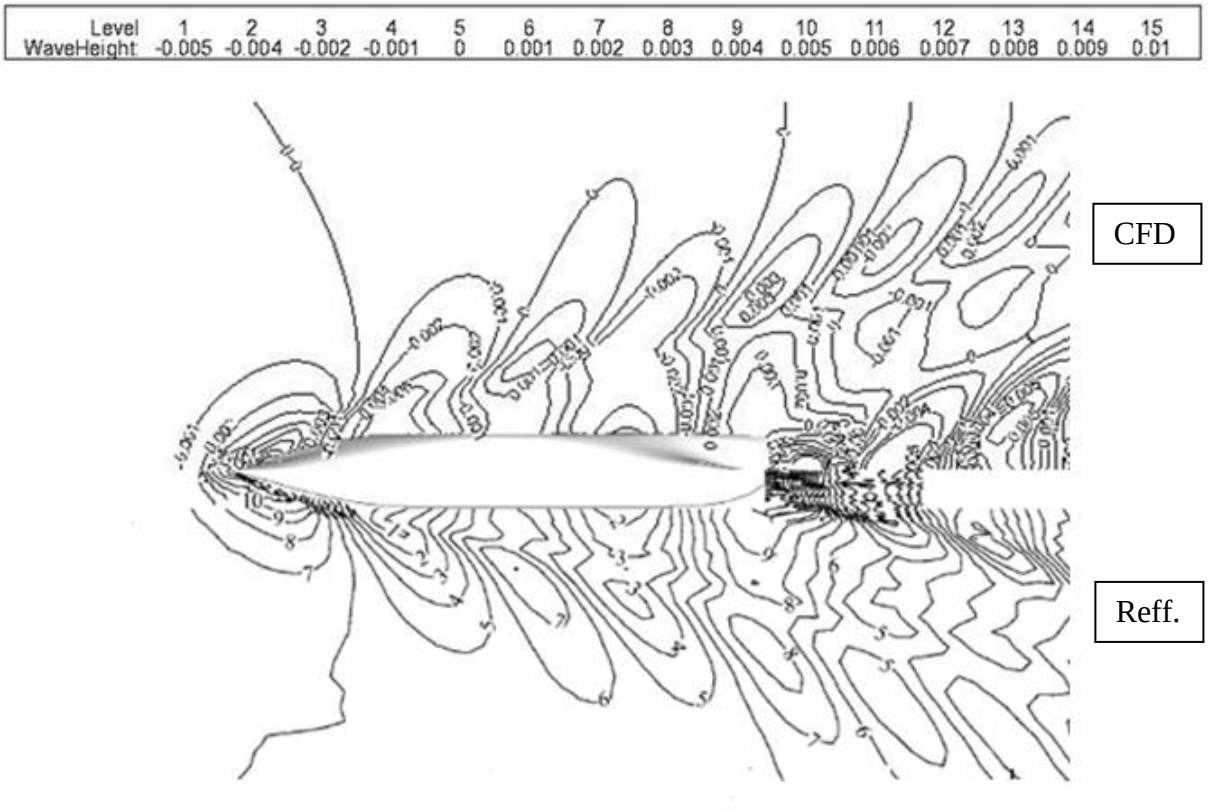

Figure 20

Is obvious that the CFD result shows very good agreement with the experimental reference result, the position and the magnitude of the contour lines being almost 100% similar.

5.2.2 Viscous flow – Axial velocity distribution

Viscous CFD computations were, also, done for the NMRI [reference 4] KCS ship model, the numerical results being compared with experimental results in order to have a validation of the numerical methodology. Five transversal planes situated at 0.9Lpp, 0.95Lpp, 0.9825Lpp, 1.0288Lpp and 1.1Lpp measured from the fore perpendicular were considered for the axial velocity distribution validation. Chosen from the reference these planes are situated upstream, in and downstream of the propeller plane. Figure 21 presents the abovementioned comparisons.

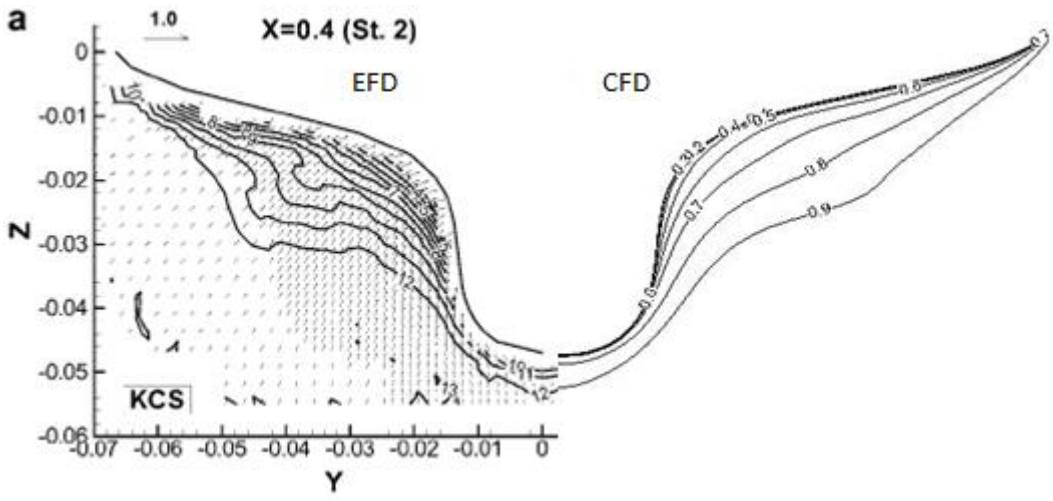

Figure 21a – Slice 0.9

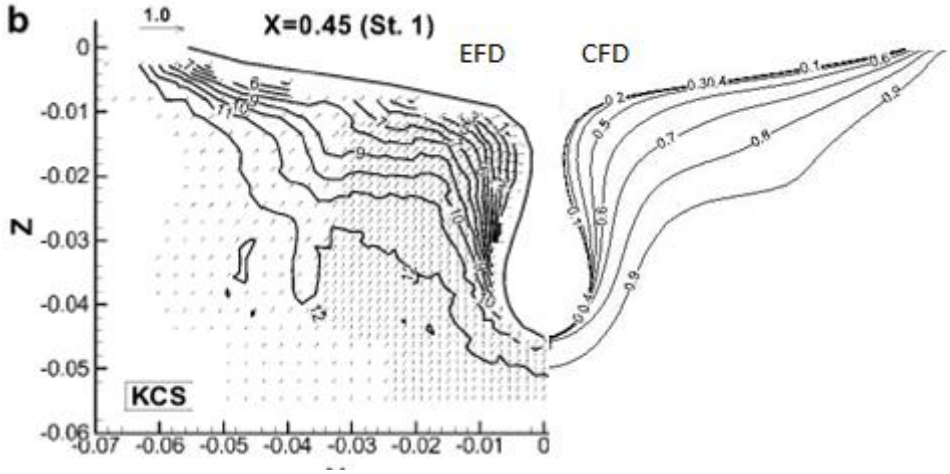

Figure 21b – Slice 0.95

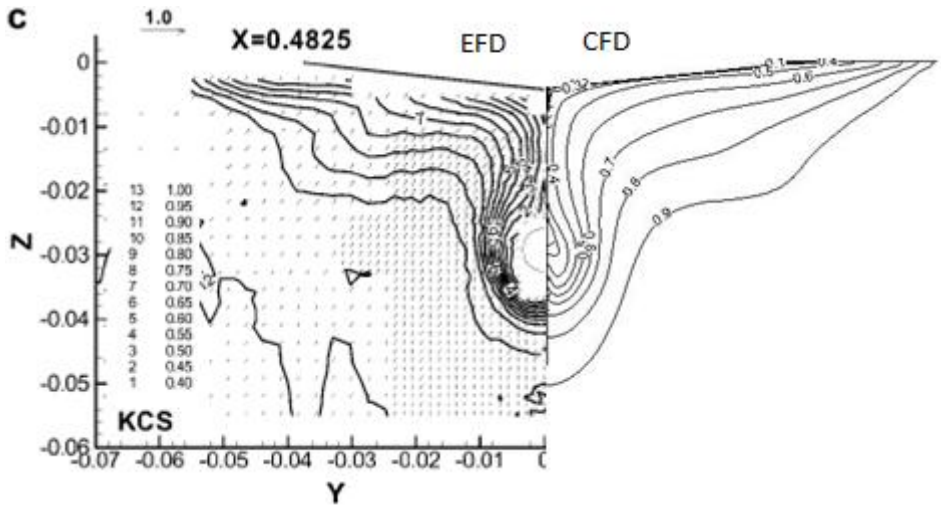

Figure 21b – Slice 0.9825

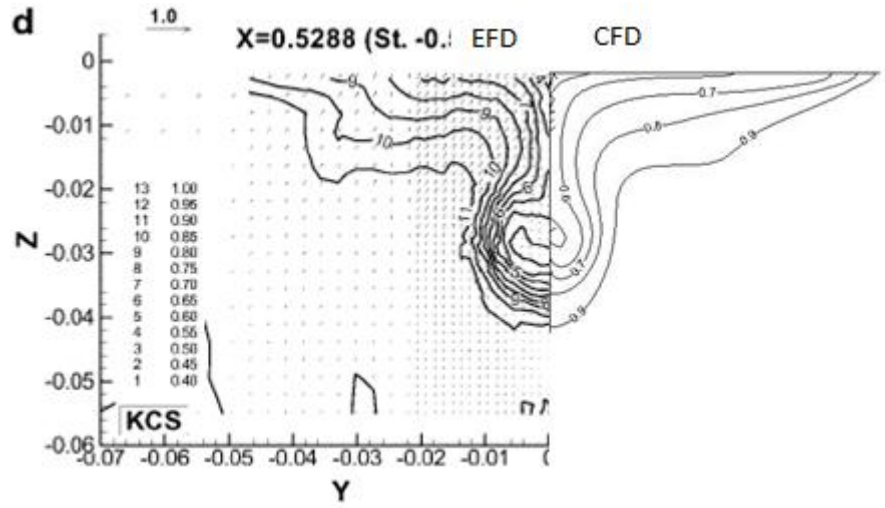

Figure 21c – Slice 1.0288

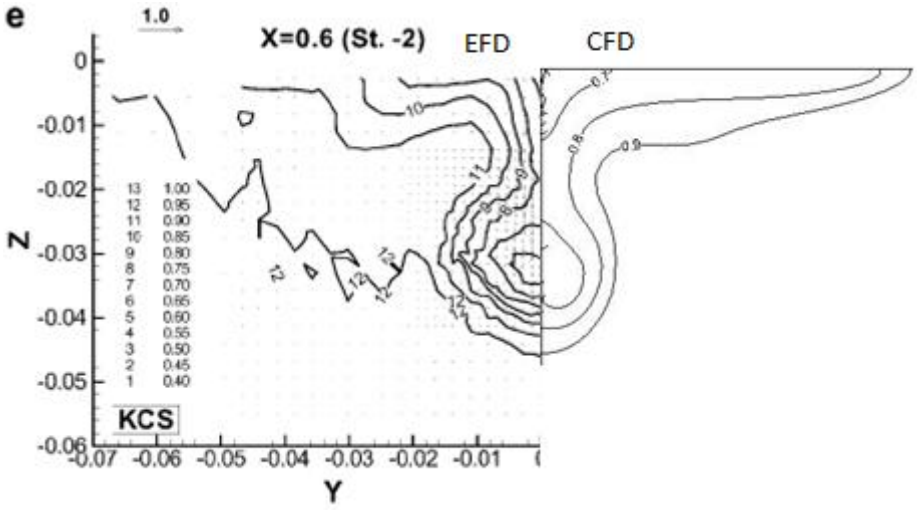

Figure 21d – Slice 1.1

Figure 21 a and b shows very good agreement between the experimental and the numerical results a minor overestimation of the axial velocity being observed in the lateral part of the contour lines where the experiments captures with higher accuracy a slight vertical movement that originates in the bilge area.

In propeller plane, Figure 21 c shows that EFD and CFD results are similar. The same overestimation of the axial velocity that was observed earlier is noticed again.

With the same observation Figures 21 d and e return the compliance that exists between the two type of results.

5.3. Study of the flow developed around the bare hull

This study was performed to show all the physics like wave pattern, axial velocity and pressure distribution around the hull without appendages. The outcome from this

computations will give us later the idea where could be the most signifficant interaction with the appendages like propeller and rudder.

5.3.1 Wave Pattern

By the use of the potential flow method the wave pattern was computed for all five speeds of interest (Figure 22).

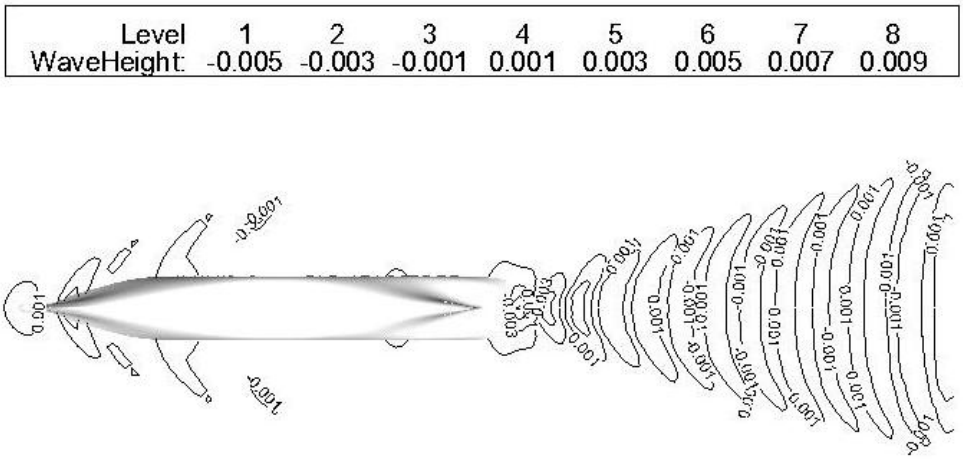

Figure 22a - Froude – 0.1516

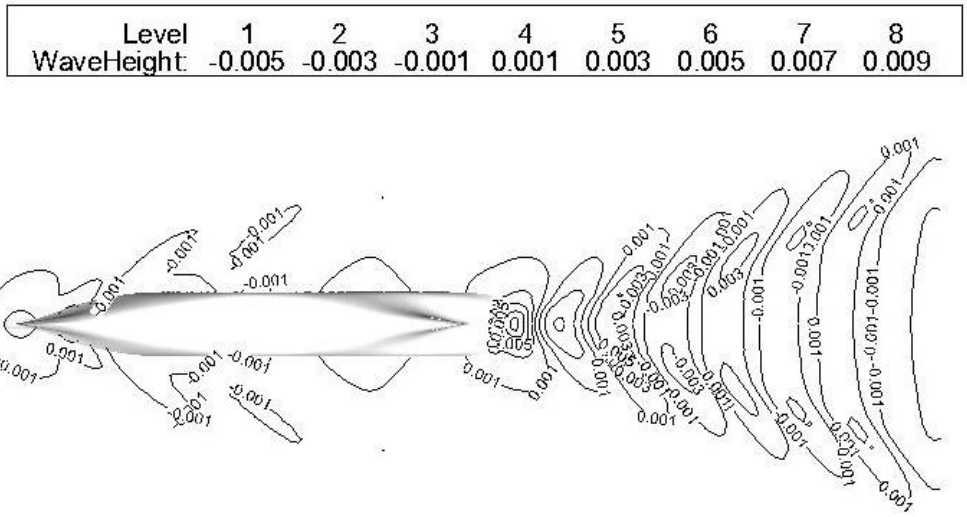

Figure 22b - Froude – 0.1949

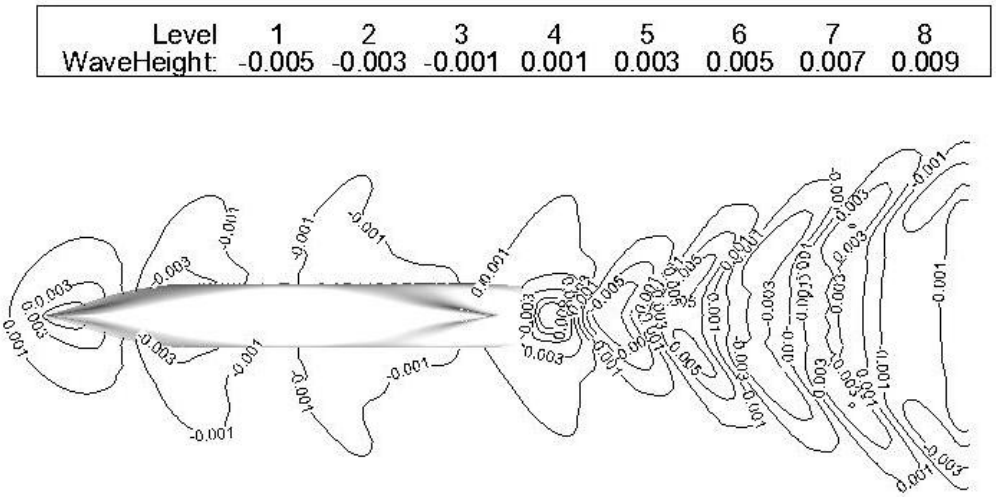

Figure 22c - Froude – 0.2274

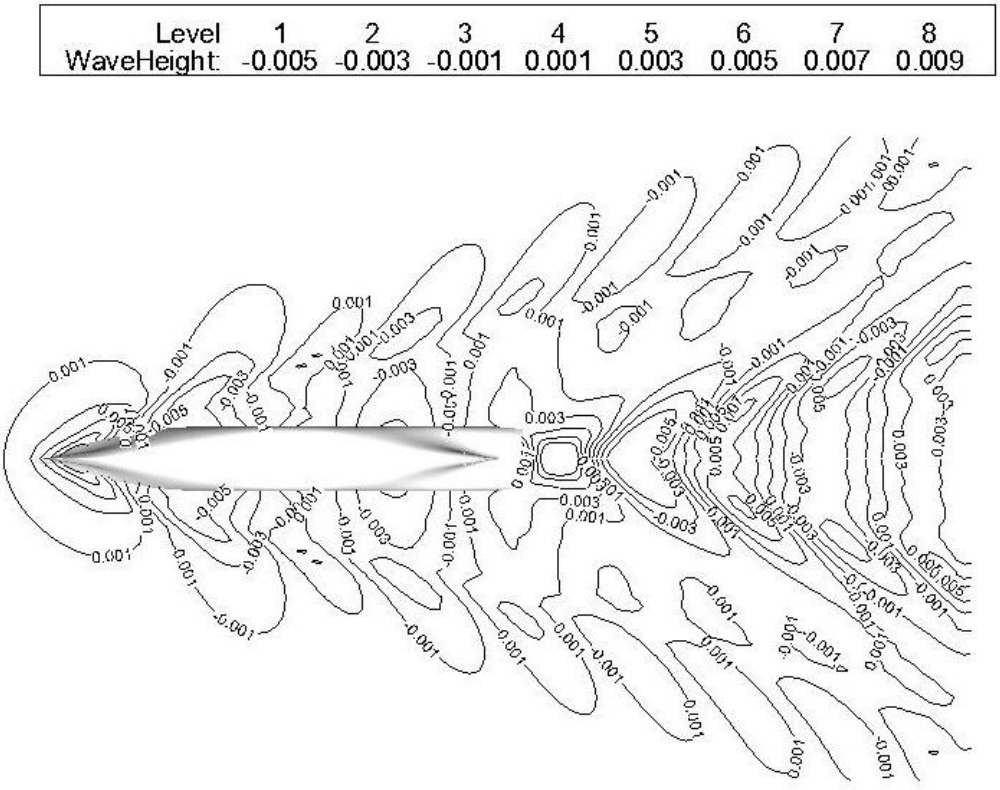

Figure 22d - Froude – 0.2599

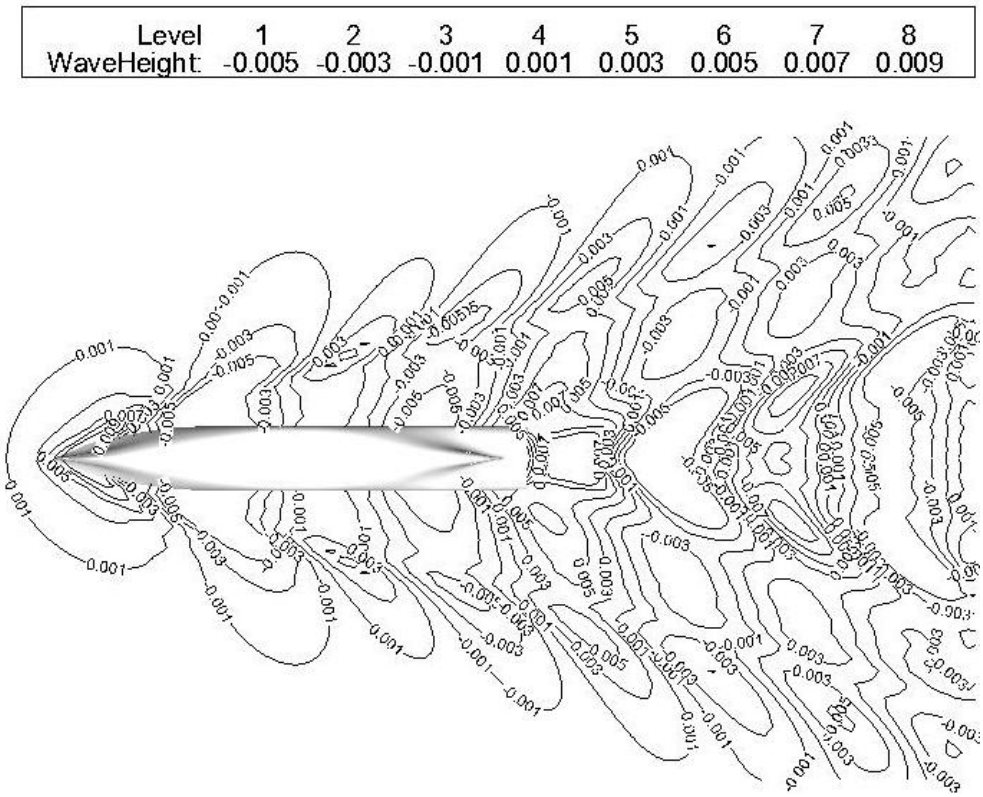

Figure 22e - Froude – 0.2816

The figures show that with increasing the Froude number the wave pattern increases as well, a significant wave being observed at 0.26 Fn. It is also revealed the fact that even at low Froude numbers the transom wave has a significant pattern the shape of the hull contributing in this respect.

5.3.2 Axial Velocity Distribution

In the attempt to reach an optimum design of the propeller is important to study the wake structure. The axial velocity distribution in the plane of the disk gives valuable information about the interactions that occur between rudder and propeller during maneuvering. Figure 23 bears out the axial velocity contours in the upstream of the propeller plane, in the propeller plane and downstream from the propeller plane, five different positions along the "x" axis being considered in this respect. The axial velocities are dimensionless quantities divided by the ship speed. The axial velocity was measured in five different planes measured in percentage of the length of the ship from the fore perpendicular.

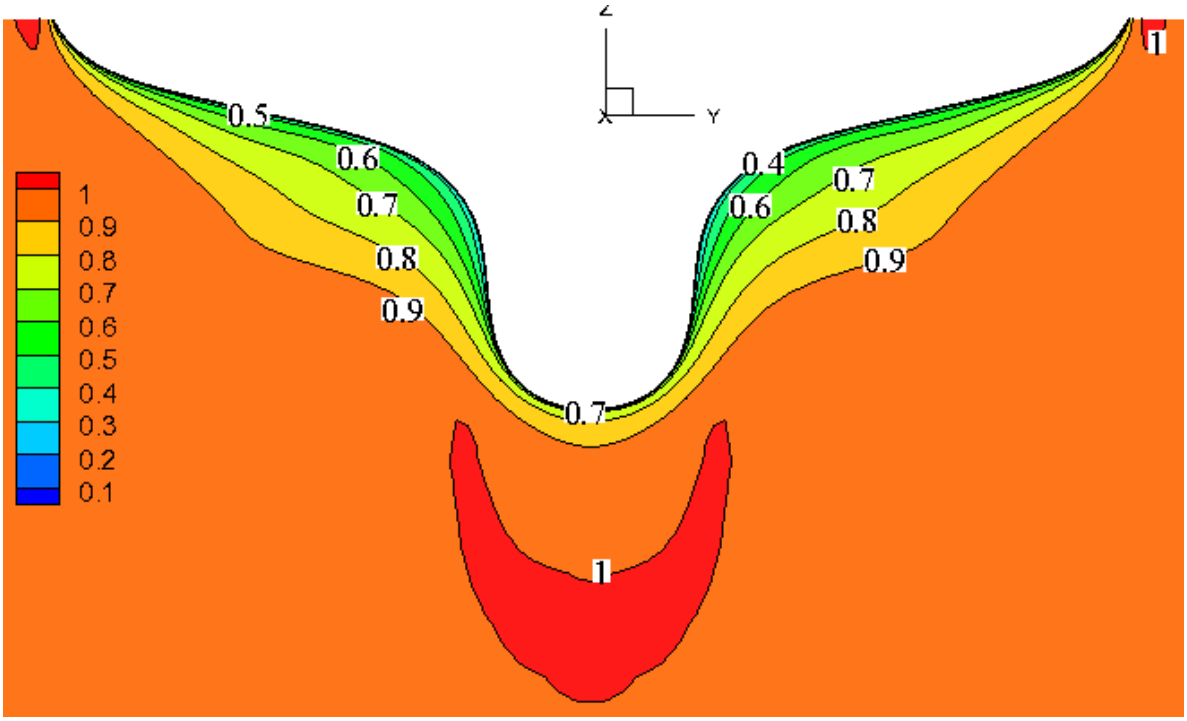

Figure 23a – Slice 0.9

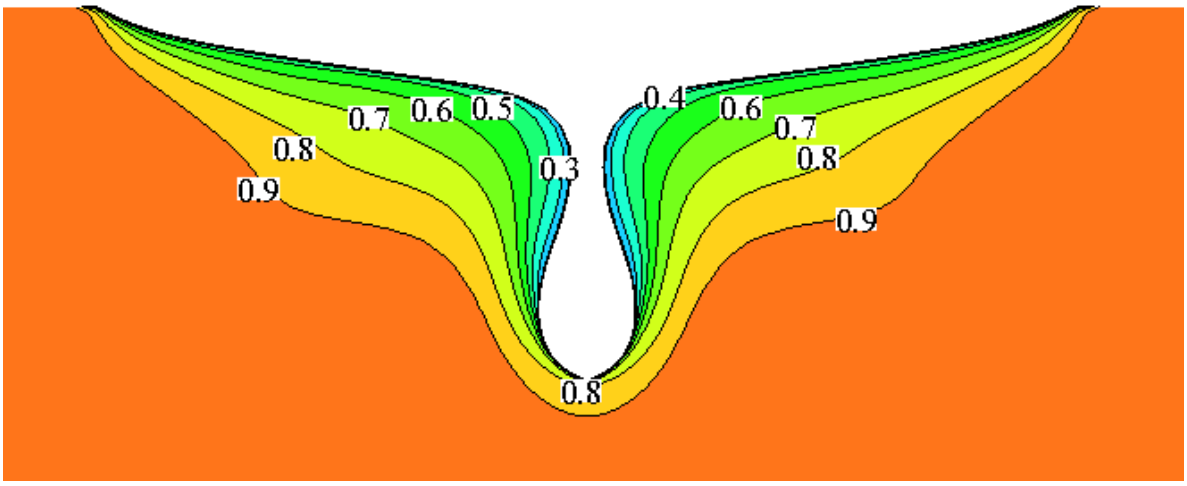

Figure 23b – Slice 0.95

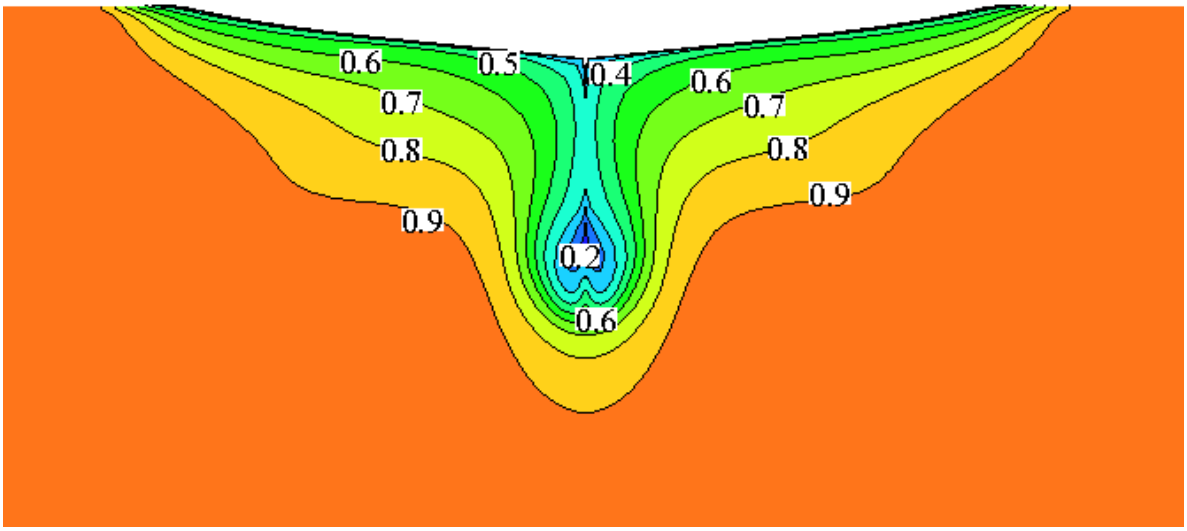

Figure 23c – Slice 0.9825

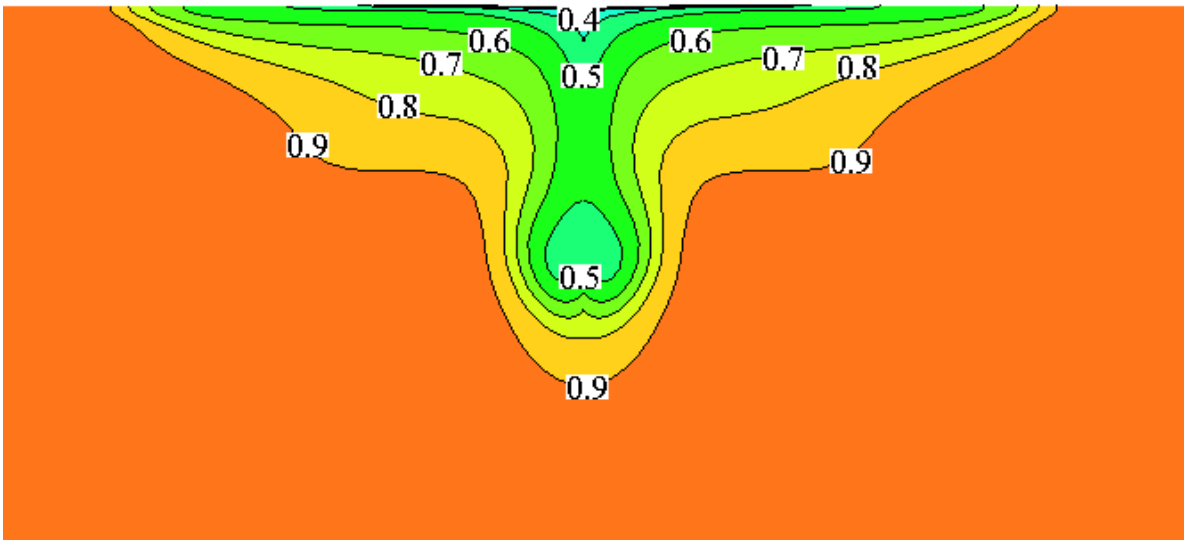

Figure 23d – Slice 1.0228

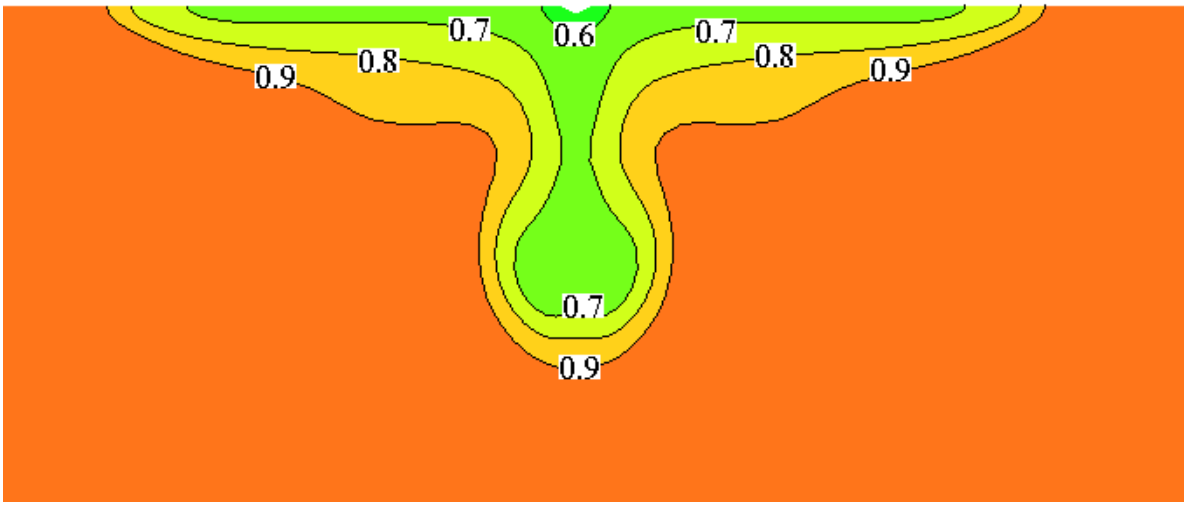

Figure 23e – Slice 1.1

Comparing the slice in Figure 23b with Figure 23a, there is a sudden change of the shape of the hull to more narrowed one, which leads to lower velocities near the shell, where the outer velocities are actually kind of hitting the shell and due to the lowered velocities there will be higher pressure. Figure 23c shows the developed picture of the lowered velocities, as long as at the next two slices Figure 23d and Figure 23e one can see that the velocities are recovering again.

5.3.3 Pressure Distribution

Figure 24 show the pressure distribution obtained in potential flow. The pressure distribution is absolutely normal – There is high pressure at the Bow due to the lower speed of the flow, which is due to the "crash" of the ship with the incoming flow. Then the speed of the flow is recovering and along the ship hull the pressure is lowering. After reaching the stern area the flow speed is lowering again and the pressure is a bit higher.

Figure 25 shows the skin friction distribution, obtained in potential flow as well. The Skin friction is obtained by the following formula 30:

$$C_f = \frac{0.075}{(\lg Fn - 2)^2} \quad - \quad \text{ITTC 57} \tag{30}$$

Figure 26 shows the pressure distribution on the same model –obtained with viscous flow computation.

Figure 27 shows the pressure distribution on the scaled model described above.

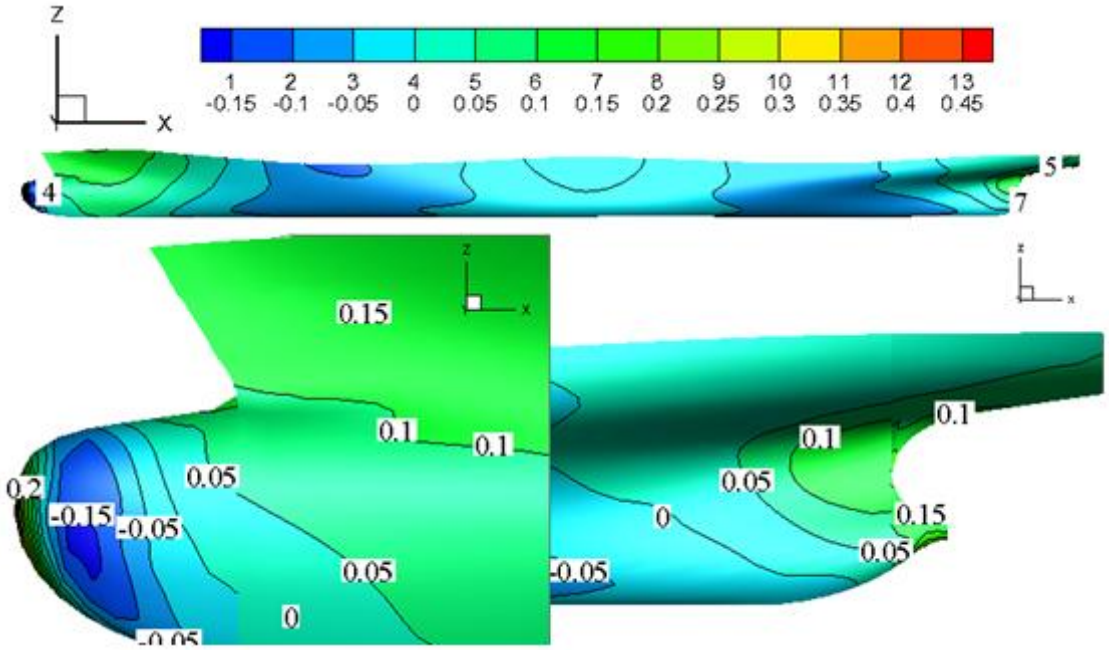

Figure 24 – Pressure distribution

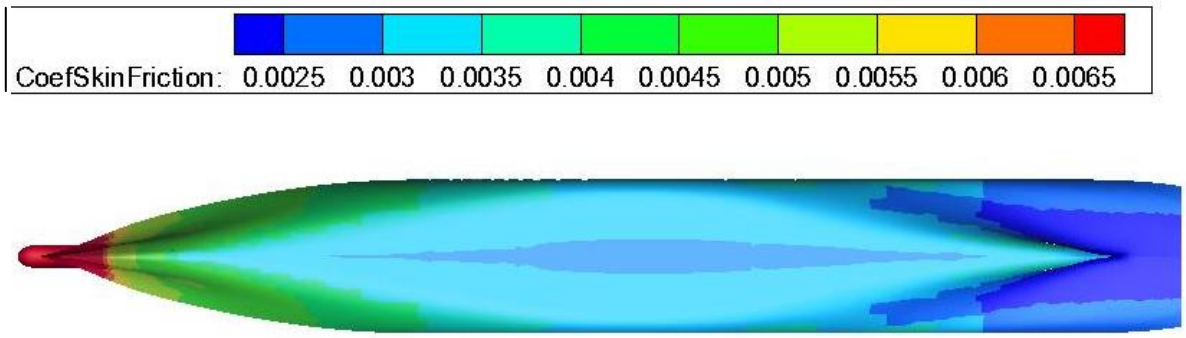

Figure 25 – Skin Friction

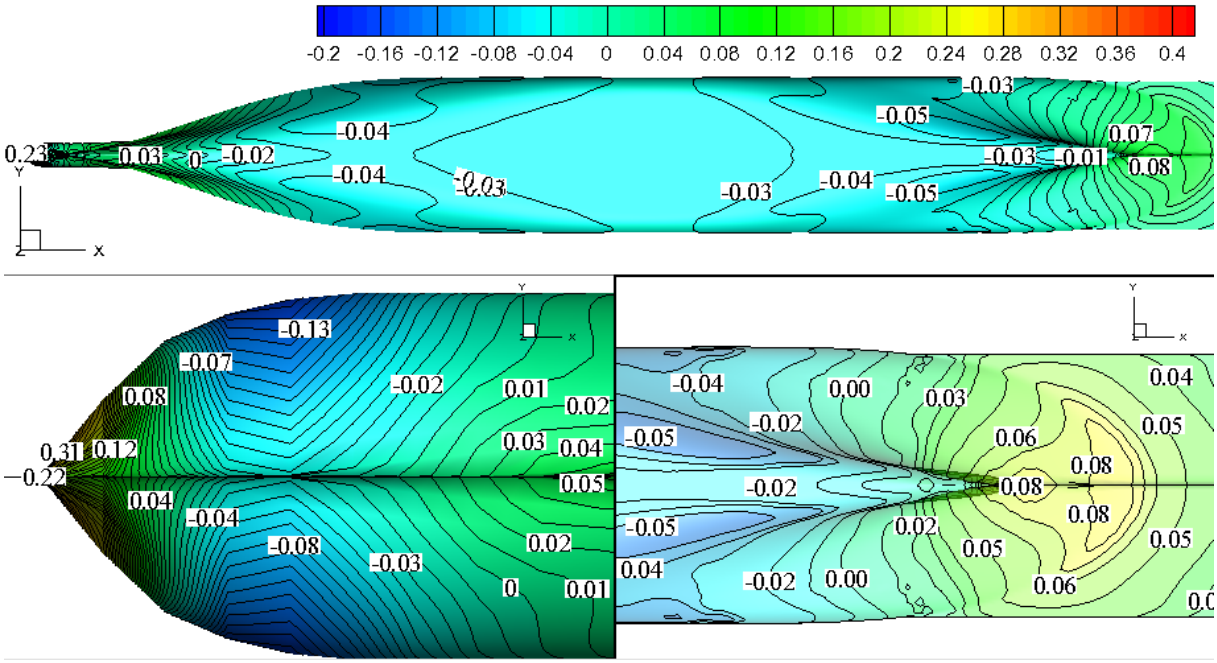

Figure 26a – Bottom view

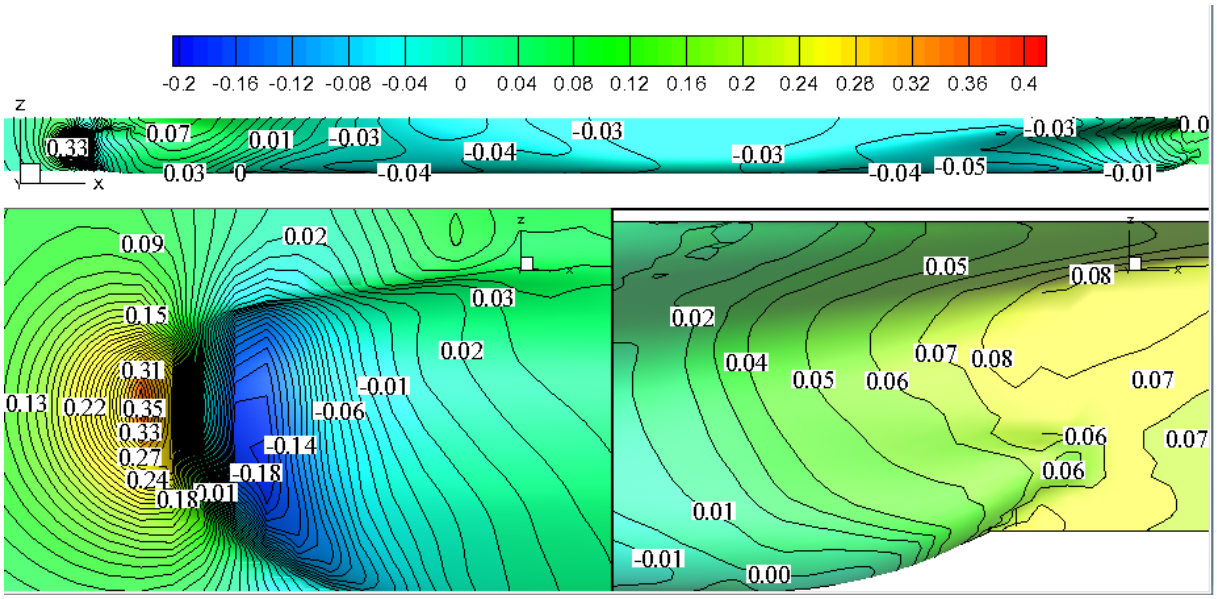

Figure 26b – Side view

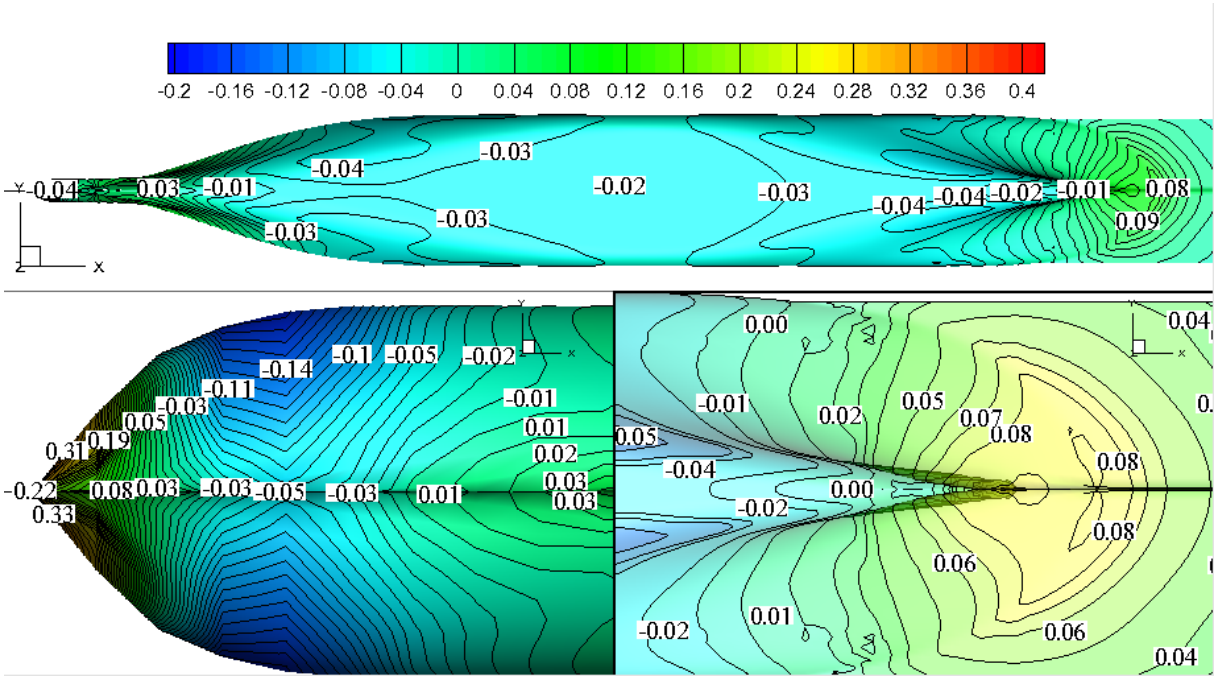

Figure 27 – Top view Scaled model – Pressure distribution

6. HULL WITH PROPELLER

As mentioned above the flow filed on and around the propeller disc is significantly changed by the hull located in front of it (upstream). All the propulsion systems interact with the ship hull. The propulsion unit accelerates the flow and depending on how the flow is changed by the hull, that acceleration creates different forces (with different magnitude and direction). Naval architects usually consider the ship hull and the propeller separately and they introduce special coefficients that can be used in order to account for the effects of this interaction. This approach is seen by many designers as really well working in solving the complex problems of ship hydrodynamics, but it could also confuse as much as it can helps. Since it is still the backbone of the experimental procedures and is strongly ingrained by generations of naval architects, the most important concepts and quantities are covered here. The hope is, however, that CFD will in future allow a more comprehensive optimization of the ship interacting with the propeller as a whole system.

The general definition ‘power = force . speed’ yields the effective power.

$$PE = RT * Vs \quad (31)$$

RT is the total calm-water resistance of the ship excluding resistance of appendages related to the propulsive organs. Sometimes the rudder is also excluded and treated as part of the propulsion system. (This gives a glimpse of the conceptual confusion likely to follow from different conventions concerning the decomposition. Remember that in the end the installed power is to be minimized. Then 'accounting' conventions for individual factors do not matter. What is lost in one factor will be gained in another.) Vs is the ship speed. PE is the power we would have to use to tow the ship without propulsive system.

Following the same general definition of power, we can also define a power formed by the propeller thrust and the speed of advance of the propeller, the so-called thrust power:

$$PT = T * VA \tag{32}$$

The thrust T measured in a propulsion test is higher than the resistance RT measured in a resistance test (without propeller). It is well known that the propeller induces an additional resistance which is determined by the fact that due to its action the pressure on the aft part of the ship is decreased. The thrust deduction fraction t couples thrust and resistance:

$$t = 1 - \frac{R_T}{T} \tag{33}$$

$$\text{or} \quad T(1-t)=R_T \tag{34}$$

t is usually assumed to be the same for model and ship, although the friction component introduces a certain scale effect. Empirical formulae for t can be found in Schneekluth and Bertram (1998), but are all plagued by large margins of uncertainty.

For usual single-screw ships, the frictional wake dominates. Wave wake is only significant for Fn > 0.3. The measured wake fraction in model tests is larger than in full scale as boundary layer and flow separation are relatively larger in model scale. Traditionally, correction formulae try to consider this overprediction, but the influence of separation can only be estimated and this introduces a significant error margin. So far CFD also largely failed to reproduce the wake even in model scale probably due to insufficient turbulence modelling. The errors in predicting the required power remain nevertheless small, as the energy loss due to the wake is partially recovered by the propeller. However, the errors in predicting the wake propagate completely when computing optimum propeller rpm and pitch.

The wake behind the ship without propeller is called the nominal wake. The propeller action accelerates the flow field by typically 5–20%. The wake behind the ship with operating propeller is called the effective wake. The wake distribution is either measured by laser-Doppler velocimetry or computed by CFD. While CFD is not yet capable of reproducing the wake with sufficient accuracy, the integral of the wake over the propeller plane, the wake fraction w, is predicted well. The wake fraction is defined as:

$$w = 1 - \frac{V_A}{V_s} \qquad (35)$$

[1]

During the present computation the propeller is modeled by a lifting line method that is coupled to the RANS solver by a body force approach. Each blade of the propeller is represented by a lifting line extended from the hub to the tip of the blade; the strength of the attached vortices varies with the propeller radius, free vortices being shed. The effect of the propeller is obtained by means of the body forces which are imposed on the grid, at the location of the blades, in axial and tangential direction, in order to compute an effective wake. The propeller load, determined by means of the effective wake, is used for solving the flow around the hull and/or rudder, solution which is transferred back to the RANS solver. In order to have an image of the accuracy of the lifting line methodology the propeller open water CFD results were considered.

6.1 POW (Propeller Open Water)

The numerical solution presented in this paper provides valuable information about the propeller features developed in non-uniform viscous flow, for all the studied configurations, covering an important area of interest in the field of naval hydrodynamics. The reported results will stand for a better understanding of the propulsion efficiency.

The propeller computation was validated based on the propeller open water NMRI [5] experimental results. The POW experimental tests are accurately following a well established methodology which gives, as a result, function of the speed of advance J, the hydrodynamic features of one particular propeller (thrust coefficient Kt, torque coefficient Kq and propeller open water efficiency η_0). During these kinds of tests the propeller model is fitted to a

propeller dynamometer (Figure 28) and advances through the undisturbed water with a known speed of advance (Figures 29 and 30). Usually the speed of advance is varied the propeller revolution being kept constant in order to achieve an entire range of advance ratios (from 0 to 1.0). Propeller thrust and torque are measured.

Figure 28 – Propeller dynamometer

Figure 29 – Open water test

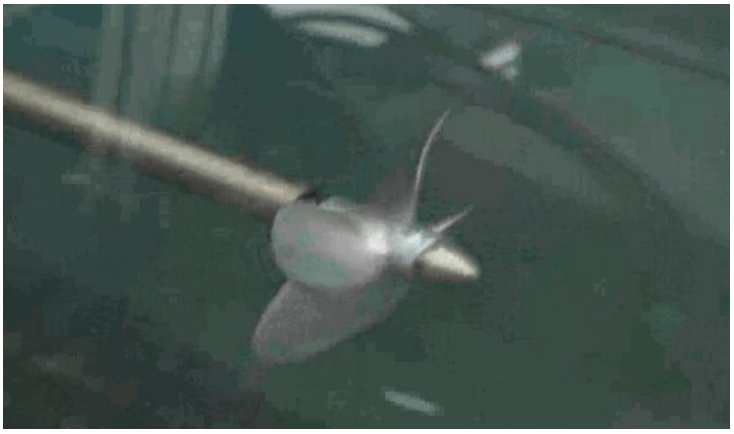

Figure 30 – Open water test

Figures 31, 32 and 33 (eta o figure cfd-efd) highlight the good agreement between the two types of approaches. The minor inconsistencies that appear in the figures can be explained by the fact that the method doesn't consider the surface of blade.

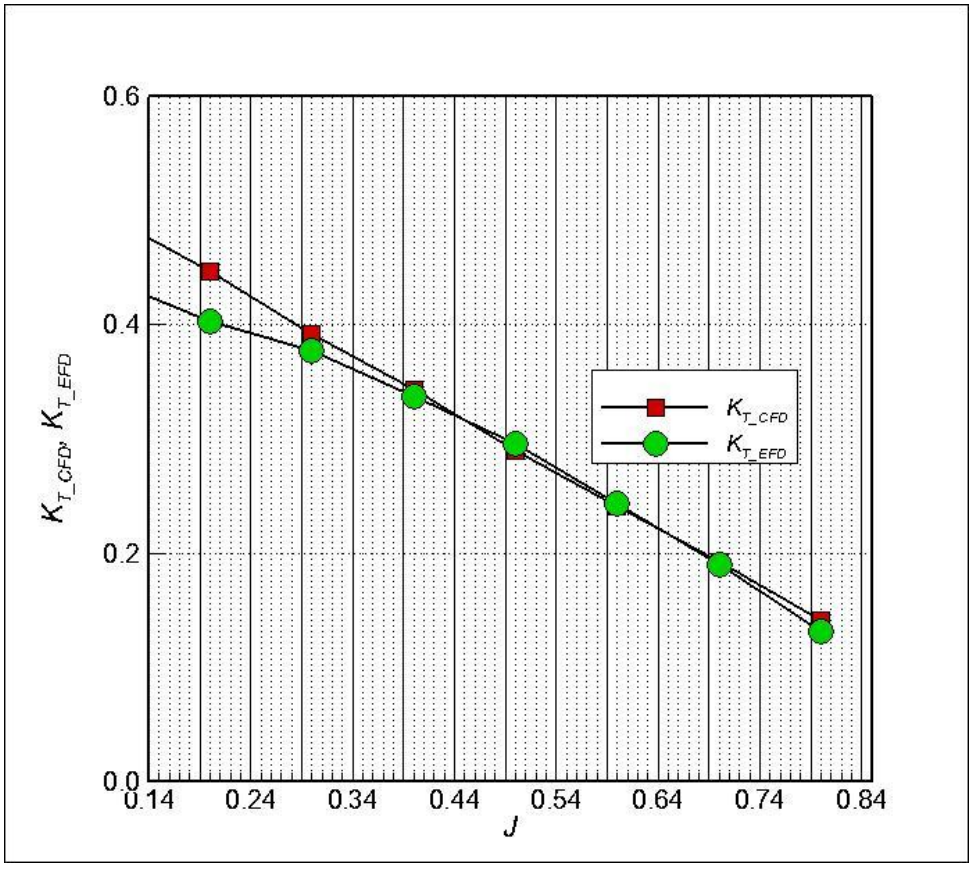

Figure 31 – Kt comparison between CFD and EFD

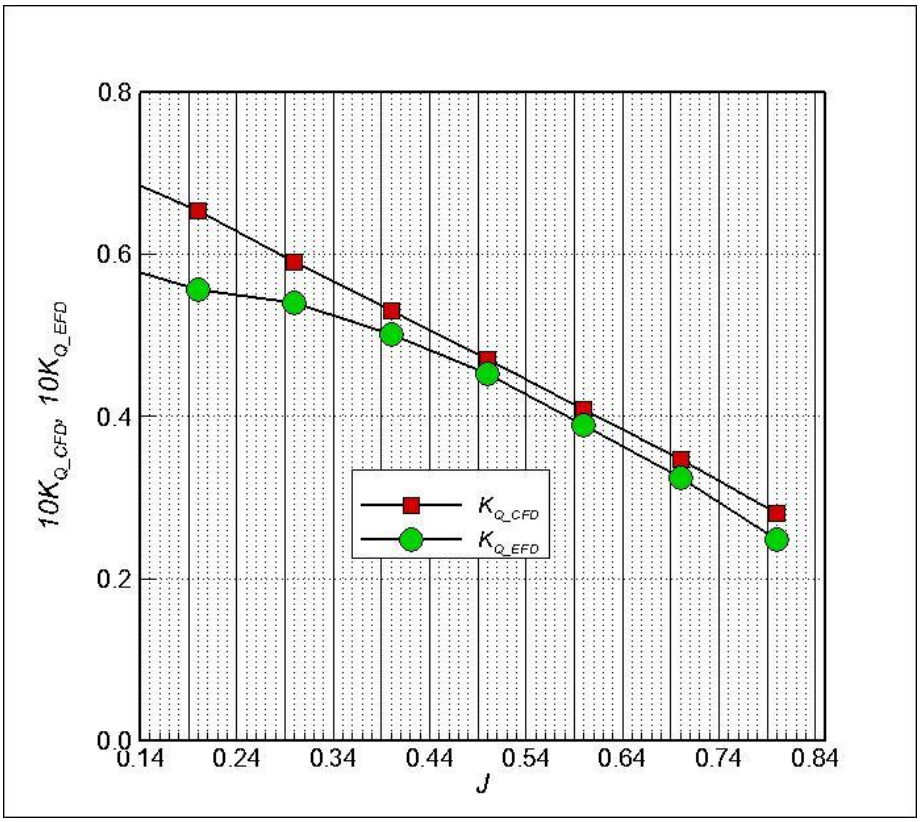

Figure 32 - Kq comparison between CFD and EFD

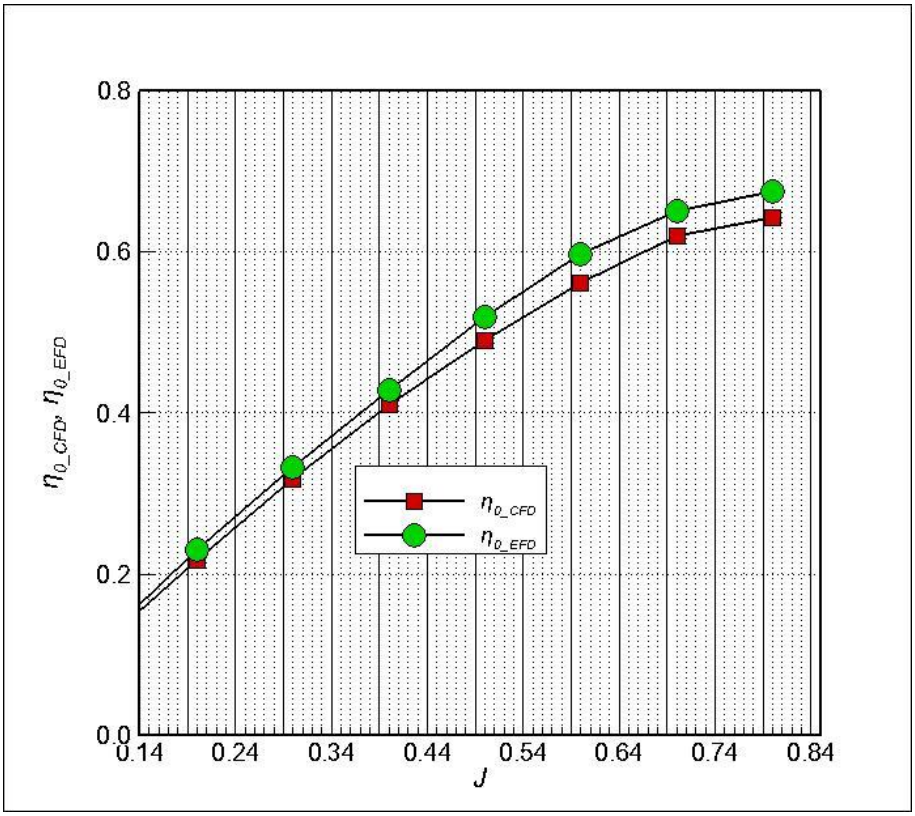

Figure 33 – η_0 comparison between CFD and EFD

Table 7 depicts for all the variables the comparison error sustaining the validation process. One may see that in the range of practical advance ratios the error is satisfactory the numerical methodology giving a good prediction.

Table 7 – Errors estimated with comparison with the reference result.

Error efd_cfd %			
J	KT	10*KQ	Eta_o
0,1	-12,555	-19,143	5,53
0,2	-10,89	-17,579	5,689
0,3	-4,116	-9,101	4,569
0,4	-1,634	-6,132	4,238
0,5	2,147	-3,726	5,662
0,6	0,939	-5,215	5,85
0,7	-1,835	-7,229	5,031
0,8	-6,922	-12,454	4,919

Once the accuracy of the propeller numerical methodology was demonstrated the propulsion coefficients can be determined based on the propeller open water, resistance and self propulsion CFD results the ITTC' 78 method being used in this regard.

6.2. Self Propulsion

The self propulsion tests are performed in order to predict the propulsive performance of a given ship. The delivered power and the propulsion coefficients are determined by means of this kind of experiments.

Usually the self propulsion tests are based on an experimental ship model which is fitted with an operating propeller (Figure 34).

Figure 34 – Wageningen B propeller

The experimental equipment (Figure 35) consists of a self propulsion dynamometer and a dummy propeller dynamometer which are conected to a standard distribution gearbox and a drive motor.

Figure 35 – Components of the experimental equipment for self propulsion tests.

In propeller design it is necessary to estimate the values of effective wake fraction, thrust fraction and relative rotative efficiency. The self propulsion is performed to predict these values of the hull-propeller interaction coefficients.

The self propulsion experimental methodology has to be in complete accordance with the ITTC Recommended Procedure 7.5-02-03-01.1, free sinkage and trim conditions being imposed to the ship model which is fitted with the same appendages that were considered during resistance experimental tests. The propulsion dynamometer measures the following

physical quantities: propeller thrust, T_m, propeller torque, Q_m and propeller revolution, n_m whereas the resistance dynamometer measures the external tow force, F_m.

The propulsion tests can be performed at different propeller revolutions and different considered speeds, the propulsion data being plotted against n_m. Using the diagrams and imposing the condition given by relation (36) the rate of revolution corresponding to the model scale self propulsion point, n_{m_A}, is determined.

$$F_m = F_D \tag{36}$$

F_D is the skin friction correction force defined by the following expression:

$$F_D = c_{F_D} \cdot \frac{1}{2} \cdot \rho_m \cdot v_m^2 \cdot S_m \tag{37}$$

where c_{F_D} is the skin friction correction force coefficient, ρ_m is the density of the water, at the measured temperature, v_m is the speed of the carriage and S_m is the wetted surface of the experimental model. The skin friction correction force coefficient is calculated with:

$$c_{F_D} = c_{F_m} - c_{F_s} - \Delta c_F \tag{38}$$

c_{F_m} and c_{F_D} - the frictional resistance coefficients of the model and of the ship, obtained with ITTC'57.

The thrust, T_{m_A} and the torque Q_{m_A} corresponding to the model scale self propulsion point are determined by interpolation, from the $T_m = f(n_m)$ and $Q_m = f(n_m)$ diagrams, using the n_{m_A} value. Applying the subsequent formulas, the value of the thrust coefficient, k_{T_A} and the torque coefficient, k_{Q_A}, defining the model scale self propulsion point, are found.

$$k_{T_{m_A}} = \frac{T_{m_A}}{\rho_m \cdot n_{m_A}^2 \cdot D_m^4} \tag{39}$$

$$k_{Q_{m_A}} = \frac{Q_{m_A}}{\rho_m \cdot n_{m_A}^2 \cdot D_m^5} \tag{40}$$

Having the results of the propulsion tests, as well as the outcome of the resistance test and the propeller open water curves, the next quantities can be calculated: the model and full scale thrust deduction factor (41), the model and full scale relative rotative efficiency (42), the

model and full scale wake fraction (44), respectively (45) and the full scale hull efficiency (46).

$$t = 1 - \frac{R_C - F_D}{T_{m_A}} \tag{41}$$

where R_C is a function of the total resistance of the model, R_{T_m}, being equal with this one if the resistance and the propulsion tests are done at the same temperature.

$$\eta_R = \frac{k_{Q0m_A}}{k_{Q_{m_A}}} \tag{42}$$

$k_{Q_{0m_A}}$ is determined by applying the thrust identity analysis, method which involves the condition that:

$$k_{T_{m_A}} = k_{T_{0m}} \tag{43}$$

$$w_m = 1 - \frac{v_{A_m}}{v_m} \tag{44}$$

v_{A_m} is the speed of advance.

$$w_s = (t + 0.04) + (w_m - t - 0.04) \cdot \cdot \frac{\left[(1+k)\cdot c_{F_s} + \Delta c_F\right]}{\left[(1+k)\cdot c_{F_m}\right]} \tag{45}$$

$$\eta_H = \frac{1-t}{1-w_s} \tag{46}$$

In order to achieve the final objective of the propulsion tests – the determination of the propulsion efficiency, η_D - the subsequent stages must be completed: extrapolation of propeller open water characteristics, determination of the full scale thrust and torque coefficients, corrected for the self propulsion condition, k_{T_s}, k_{Q_s} respectively, determination of full scale propeller revolution, n_s, determination of propeller thrust and torque appropriate for the self propulsion condition, T_s, Q_s.

Propulsion efficiency is computed in two different ways, applying:

$$\eta_{D_1} = \frac{P_E}{P_D} \tag{47}$$

$$\eta_{D_2} = \eta_{0_S} \cdot \eta_R \cdot \eta_{H_s} \tag{48}$$

For the effective power, P_E, relation (49) is considered, whereas the delivered power , P_D, is calculated with (50).

$$P_E = R_{T_s} \cdot v_s \tag{49}$$

$$P_D = 2 \cdot \pi \cdot n_s \cdot Q_S \tag{50}$$

Where R_{T_s} is the total resistance of the ship and v_s is the speed of the ship.

An accurate computation leads to:

$$\eta_{D_1} \approx \eta_{D_2} \tag{51}$$

[17]

Following the presented steps propulsion efficiency of the KCS was correctly determined.

Table 8 presents the values of the propulsion coefficients that were determined based on the abovementioned methodology applied for resistance, propeller open water and self propulsion CFD results.

Table 8 – Propulsion coefficients

wm	0,338
tm	0,251
eta0m	0,641
etahm	1,131
etarm	1,022
etadm	0,741

6.3. Hydrodynamic study of the flow developed around the hull with propeller

6.3.1 *Axial velocity distribution*

Predicting the flow behind of the propeller is important because usually the rudders are situated on the propeller slip stream, so study at the axial velocity in this case is very reasonable. Figure 40 bears out the flow development in five different planes at the aft part of the ship. Starting from the first two planes we can see the non disturbed flow around the ship, which is with slightly increased axial velocity due the presence of the propeller. The increase of the axial velocity at 0.9Lpp is not too high fact that can be explained by the fact that the influence of the propulsion unit is locally. This means that at the first touch of the flow with the propeller there are large local angles of attack which leads to high propeller loading. Moving to the next plane the flow is accelerated which explains the high axial velocities. These high axial velocities actually are decreasing the pressure and as a consequence the propeller loading is decreased as well. In that moment the inflow field starts to play a role. Using a right handed propeller in this case the blades are moving towards the surface of the port side. And at that point they are meeting the flow field (the bilge vortices) which is moving at the same direction as the propeller blades. But the picture is the opposite at the starboard side. As a result there is decreased angle of attack at the port side as long as on the starboard side the angle of attack is increased. As a consequence the local propeller loading becomes asymmetric. After all there is less accelerated flow at the port side as long as at the starboard side is exactly the opposite (Figure 36d).

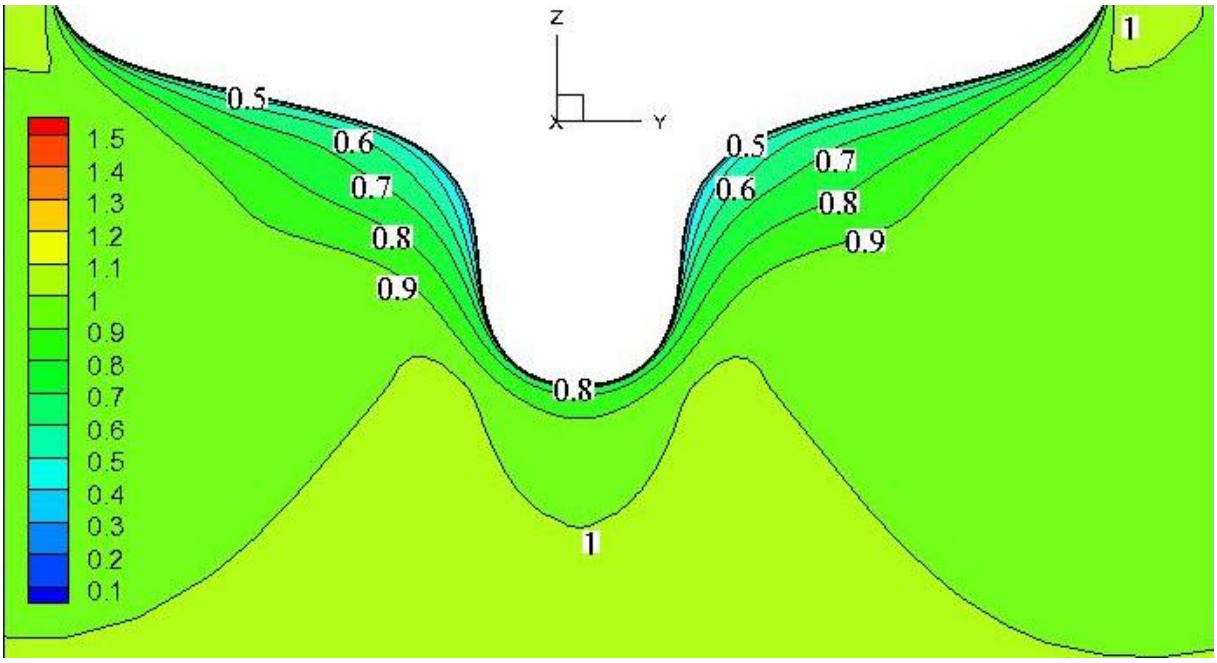

Figure 36a – Slice at 0.9

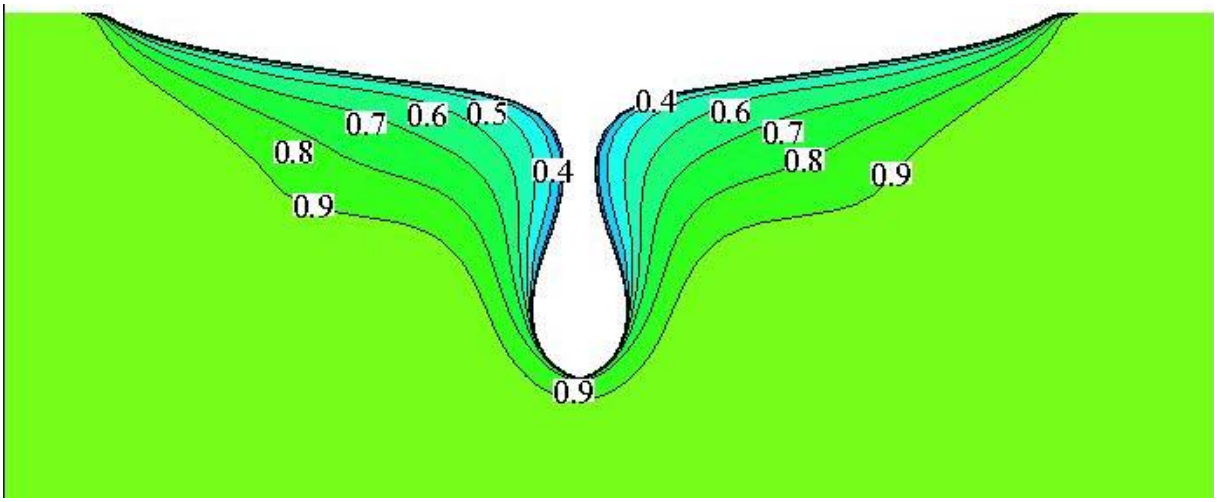

Figure 36b – Slice at 0.95

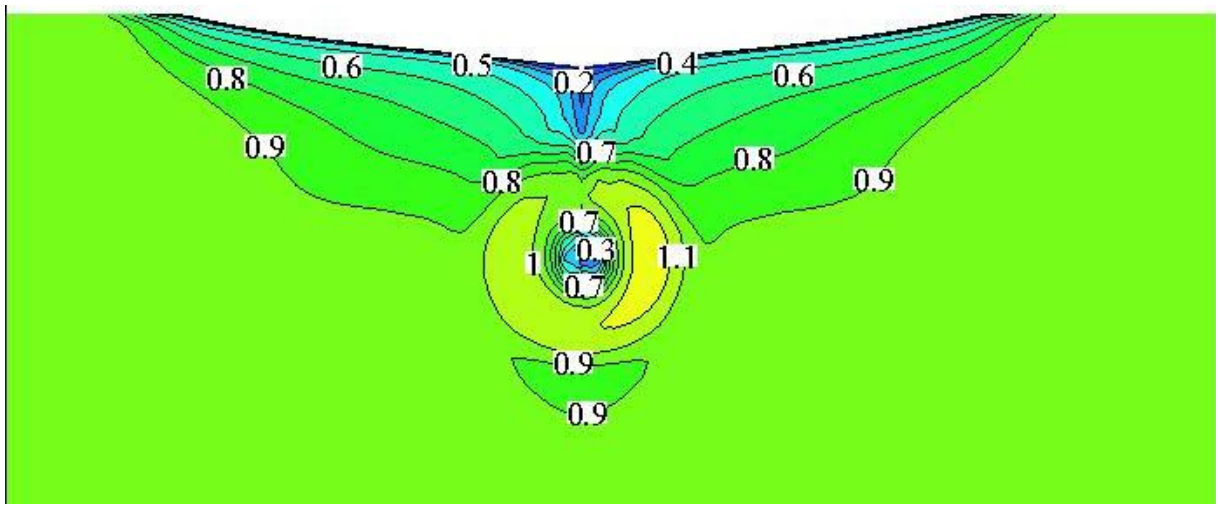

Figure 36c – Slice at 0.9825

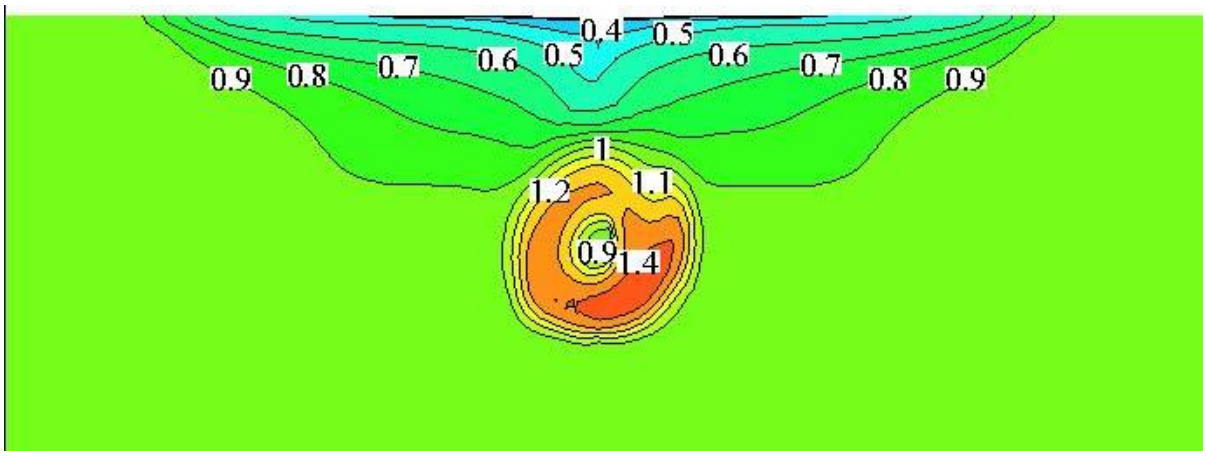

Figure 36d – Slice at 1.0288

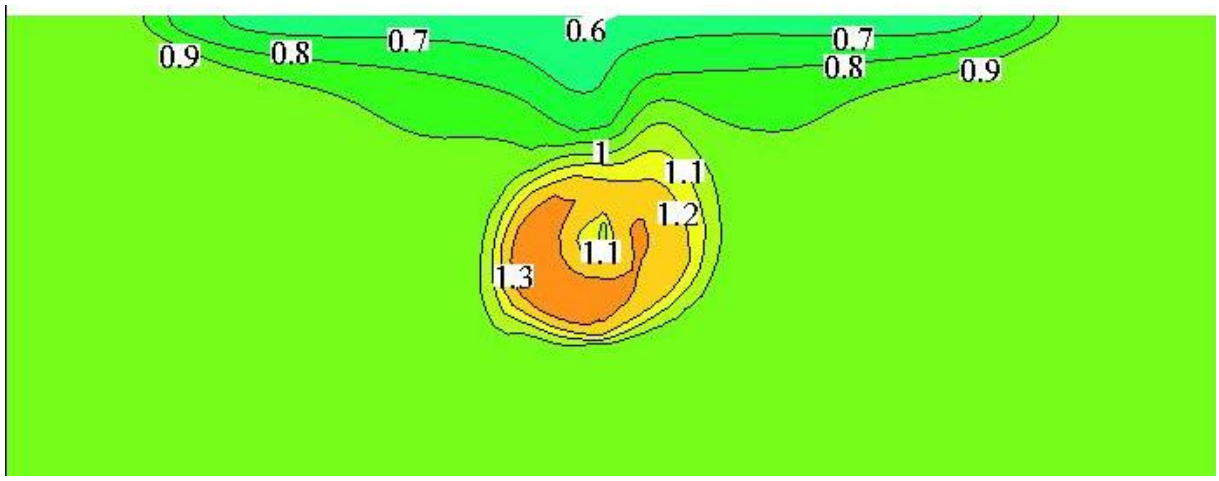

Figure 36e – Slice at 1.1

Having in mind that the validation of the axial velocities made for the bare hull case (Figure 21) shows quite good agreement between the numerical results and the reference results, and that the validation of the propeller open water numerical methodology (Figure 31, 32 and 33) shows also very reasonable results, and having in mind all the physics explained by the use of Figure 36, I can conclude that the computations made for hull with propeller are quite reliable.

6.3.2 Pressure Distribution

Figure 37, Figure 38 and Figure 39 also reveals the propeller influence. Comparing the pressure distribution for the bare hull with this case one can see that a negative pressure upstream from the propeller plane is occurring, which means that there is the suction area. This suction is due to the presence of the propeller.

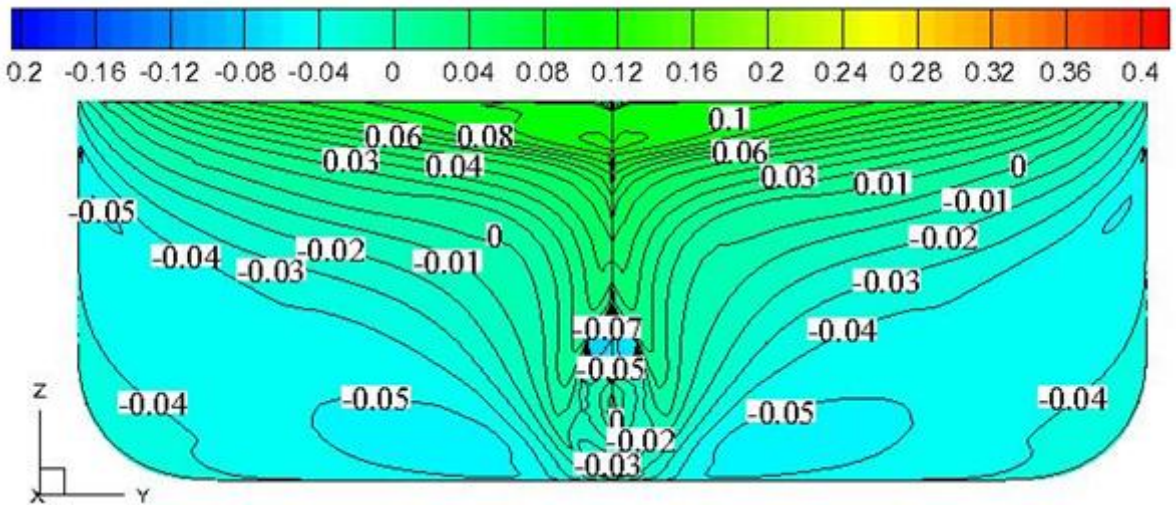

Figure 37 – Pressure distribution on the aft body

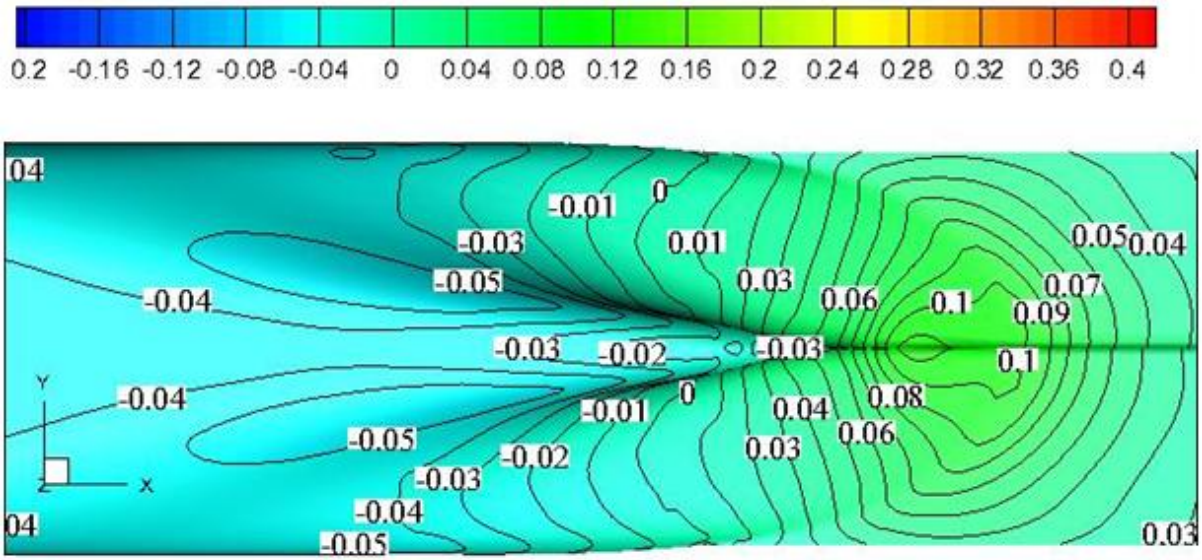

Figure 38 – Pressure distribution on the aft body – bottom view

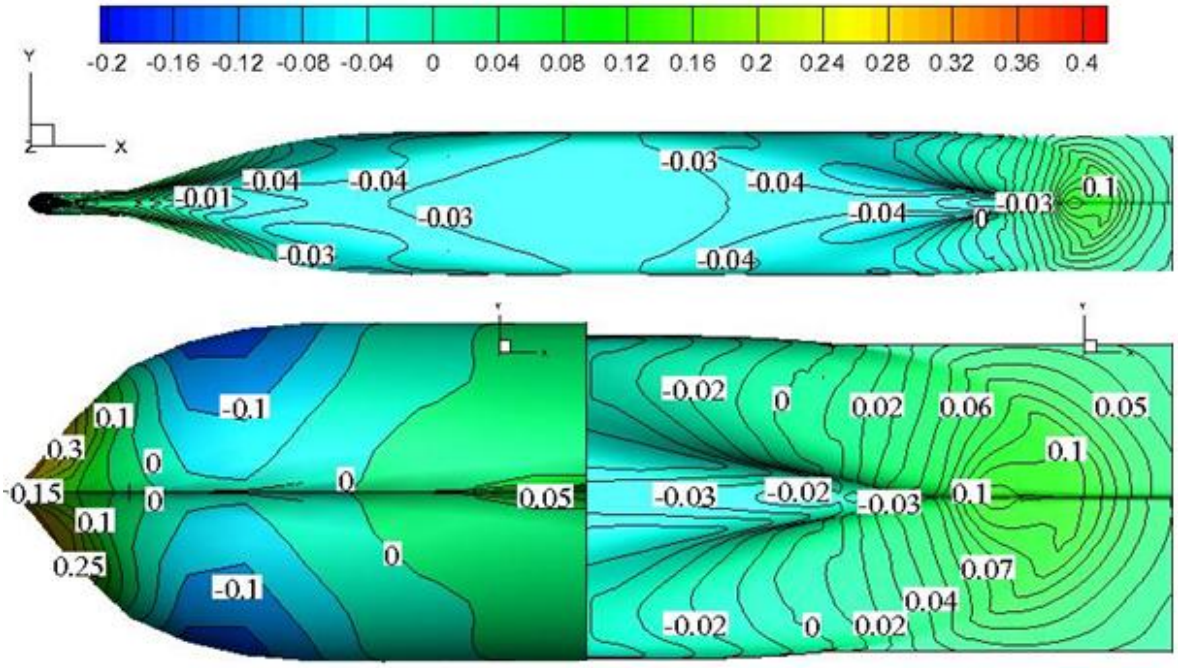

Figure 39 – Pressure distribution on the entire hull

7. HULL WITH RUDDER

The ship designer is limited in designing the rudder by the following main constraints:

- rudder dimensions depend by the shape of the stern, the draft, the propeller(s) location and the docking restrictions;
- rudder must have a minimum influence on the speed loss, in maintaining a straight course;
- undesirable effects of the rudder such as rudder-induced vibration should be kept to a tolerable level;
- the rudder system and the steering engine should be of minimum size, weight and costs.

The rudder located in the propeller slipstream can recover some of the rotating energy, in order to increase the hydrodynamic efficiency of the rudder. However there is also negative effect from that: rudder induced ship vibrations. This negative effect could be avoided by choosing the optimum clearance between the rudder and the propeller, the classification societies rules can be used in this respect. Usually, the shape of a ship's hull is developed without particular regard to the rudder design. The rudder location has to conform to the shape of the hull. A suitable rudder area for a given hull can be determined in order to satisfy the desired manoeuvrability performance. Since full form ships are generally less stable, relatively more rudder area may be adopted for the fulfilment of the stability requirements. The rudder height is limited by the stern shape and draft. This dimension should be increased as much as possible in order to obtain a very efficient aspect ratio. The bottom of the rudder is kept above the bottom of the keel for protection. The rudder will be fully immersed in order to avoid the negative effects of the free surface and the ventilation of the rudder which decrease the hydrodynamic efficiency.

The effective aspect ratio could be increased by immersing the hull above the rudder because in this way the hull suppresses the flow from the pressure side to the suction side near the upper edge of the rudder. The effects of the immersed hull are:

- it decreases the induced drag.
- it increases the slope of the lift curve versus angle of attack α.
- it hardly influences the maximum lift at the stall angle α_s.

The magnitude of this effect depends on the size of the gap between the upper edge of the rudder and the hull. For very small gaps, the aspect ratio Λeff is theoretically twice the nominal value, in practice Λeff $\approx 1{,}6 = \Lambda$geom. To close the gap between hull and rudder at least for small rudder angles υ – and thus increasing the rudder effectiveness – a fixed fin above the rudder is advantageous for small–rudder angles. If the hull above the rudder is not

immersed or if the rudder intersects the water surface, the free surface may also increase somewhat the effective aspect ratio Λeff. However, this effect decreases with increasing ship speed and may turn to the opposite at higher speed by rudder ventilation drawn from the surface along the suction side of the rudder. To decrease rudder ventilation, a broad stern shape sufficiently immersed into the water especially above the front part of the rudder is advantageous.

The wake of the hull decreases the inflow velocity to the rudder and increases the propeller load. Differences in wake and propeller load between model and ship are the main cause of scale effects in model manoeuvring experiments.Whereas the wake due to hull surface friction will be similar at the rudder and at the propeller, the potential wake – at least for small Froude numbers, i.e. without influence of the free surface – is nearly zero at the rudder, but typically amounts to 10% to 25% of the ship's speed at the propeller of usual singlescrew ships. It amounts nearly to the thrust deduction fraction t. Thus the flow outside of the propeller slipstream is accelerated between the propeller and the rudder by about t = V. This causes a pressure drop which also accelerates the propeller slipstream.

[1]

7.1 Validation of the Numerical Methodology Used for Hull With Rudder Computation

Model experiment of hull with rudder was done in the towing tank in the University of Galati. During this experiment the resistance was measured for the same five speeds which were used for bare hull.

CFD computations were done for the same hull and rudder models, in order to make validation of the numerical solution – Figure 40.

As one can see from the figure, for the first two speeds CFD result is slightly detached from the reference result, and for the third speed there is much smaller resistance measured on the experiment, which could be explained with the effect of the hydrodynamic shoulders of the ship, which are leading of the pressure drop and as a consequence there is resistance drop as well. On the higher speeds (where is also the speed of interest) the pressure is recovered and Figure 40 reveals how CFD result is in very good agreement with the reference result.

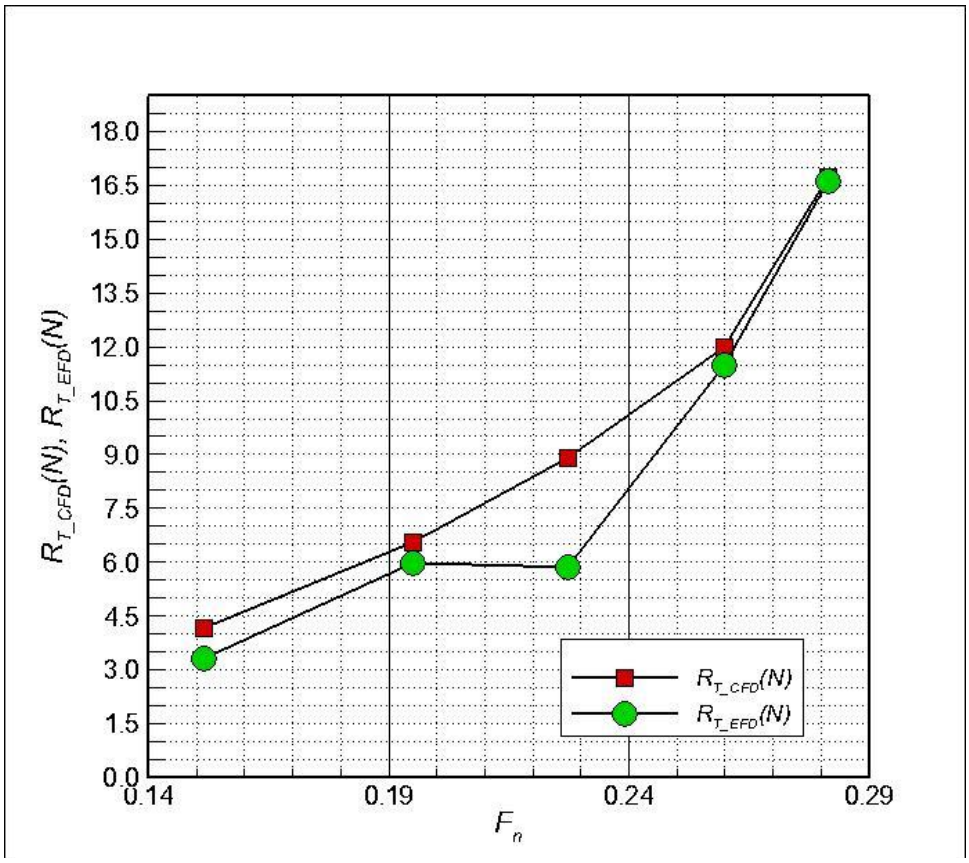

Figure 40 – Resistance comparison between CFD and EFD

7.2. Hydrodynamic Study of the Flow Developed Around the Hull With Rudder

7.2.1 Axial Velocity Distribution

Figure 41 shows that with no icdidence angle of the rudder there is no big change of the axial velocities comparing with the bare hull. The only change is the slightly increased velocity at the centre line (where the rudder is placed) at the traling edge of the rudder – Figure 41d and 41 e.

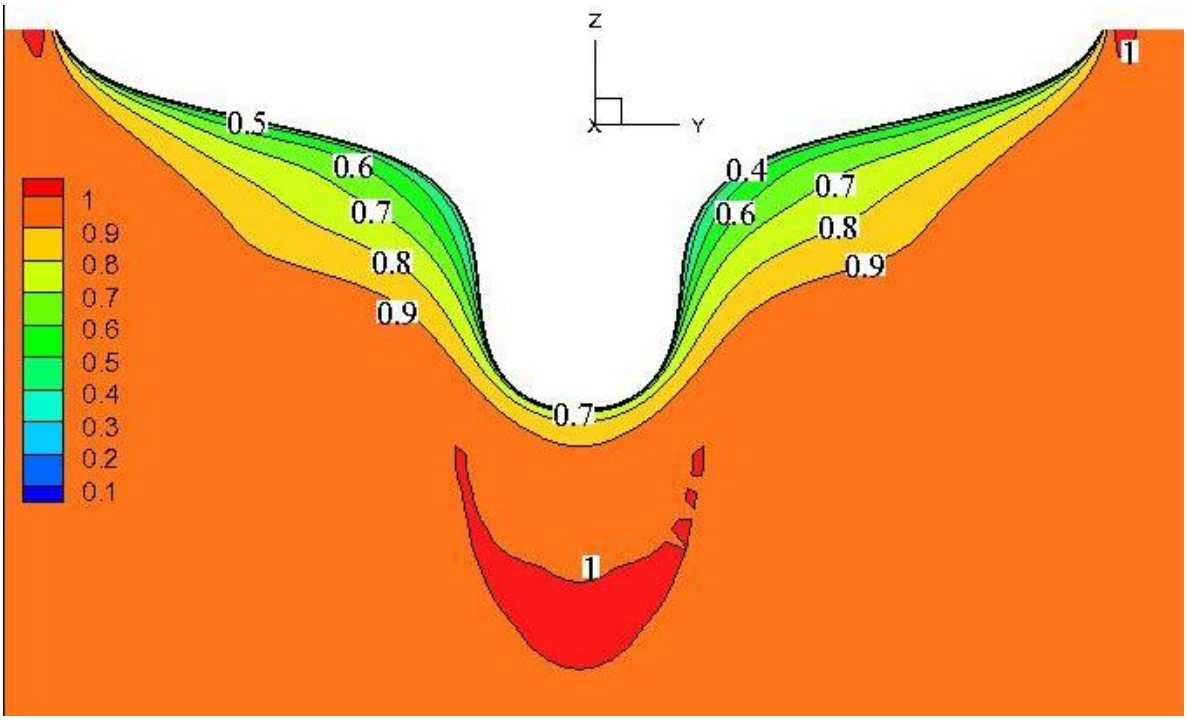

Figure 41a – Slice at 0.9

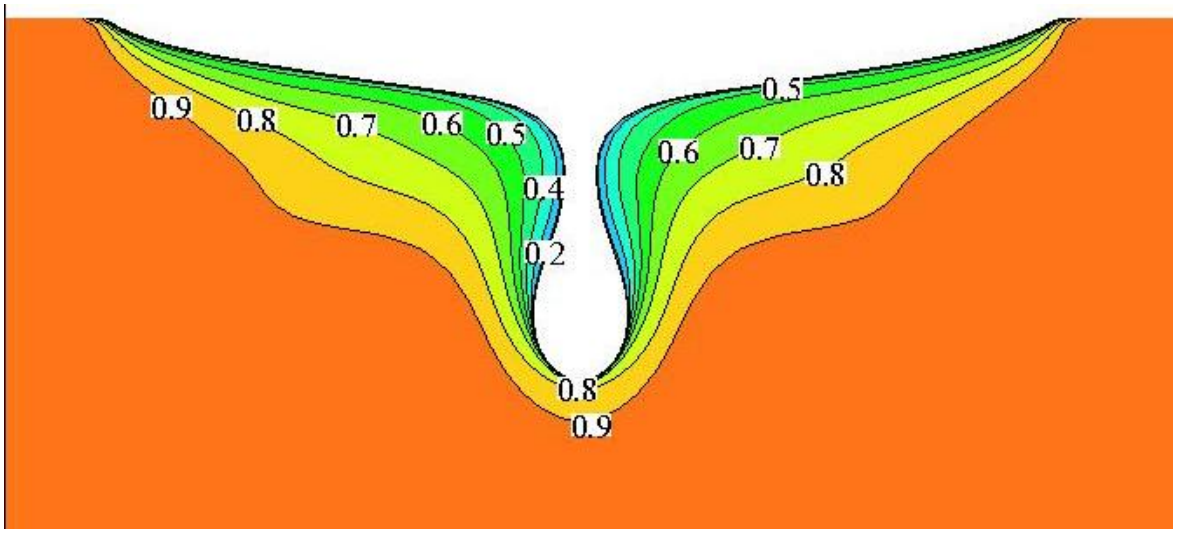

Figure 41b – Slice at 0.95

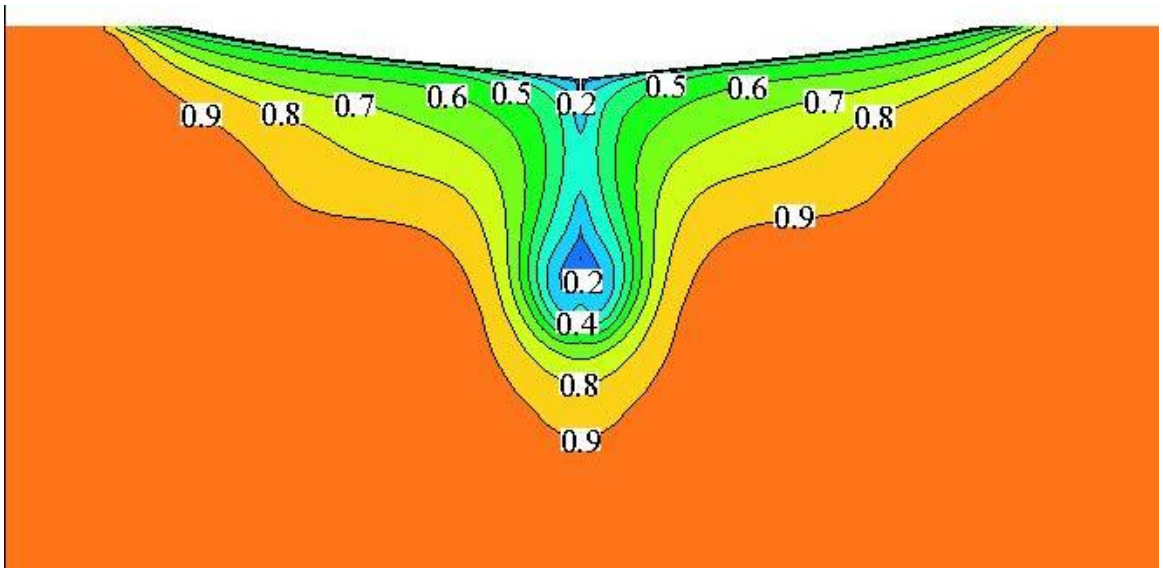

Figure 41c – Slice at 0.9825

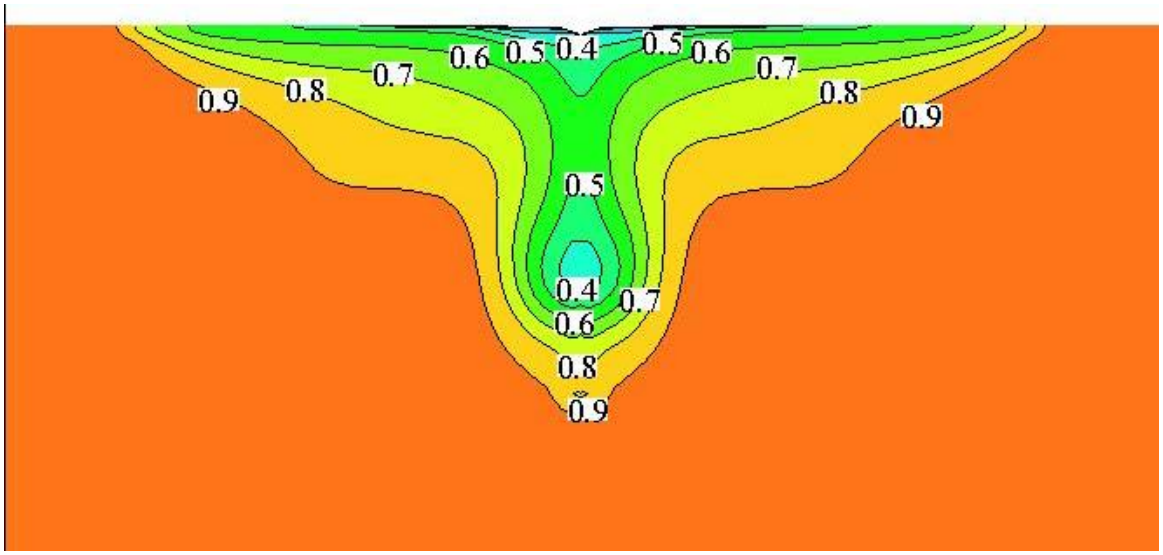

Figure 41d – Slice at 1.0288

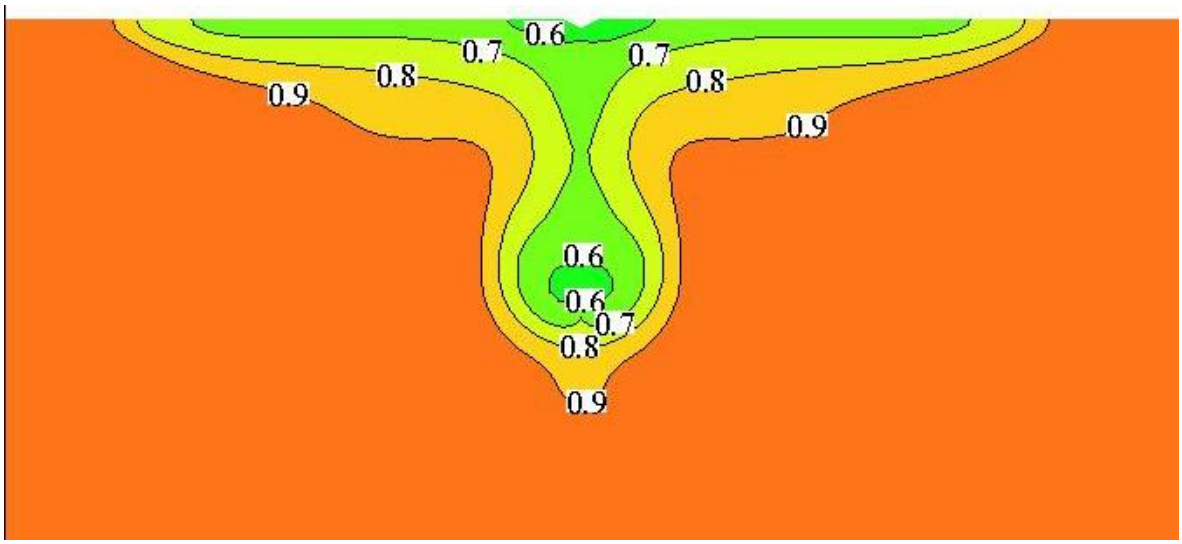

Figure 41e – Slice at 1.1

7.2.2 Presure Distribution

Comparing with the Hull+Propeller case there is no negative pressure at the propeller upstream in this case – Figure 42, Figure 43 and Figure 44. The low presure which is sidewards from the propeller upstream is due to the acceleration of the flow which is due to the bilges and the aft shape of the stern. Upstream the propeller, there is slightly higher pressure which is result of the lowered velocity due to the hulls shape.

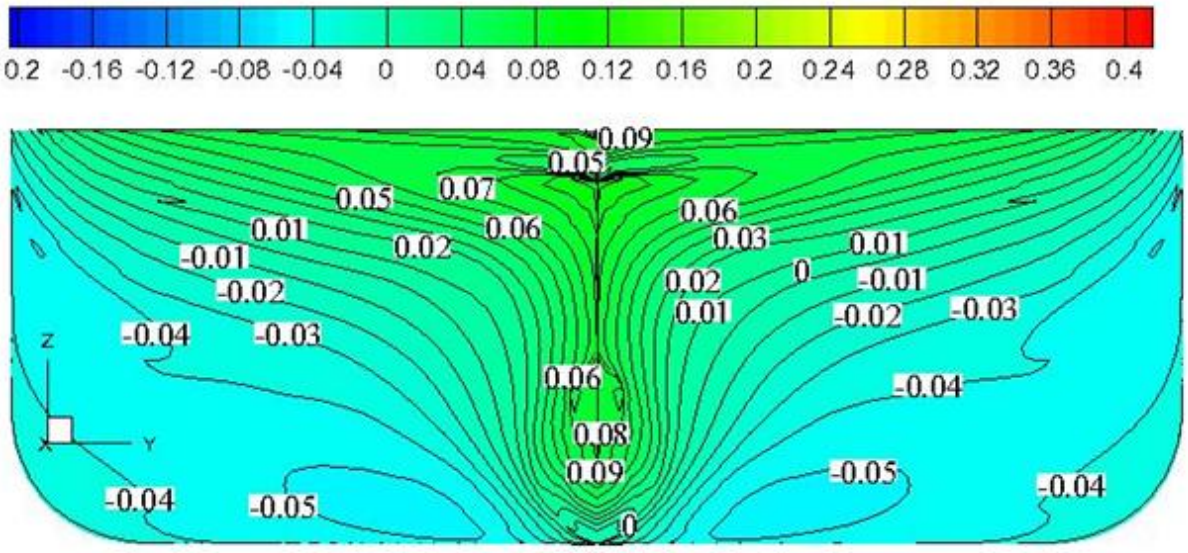

Figure 42 – Pressure distribution on the aft body

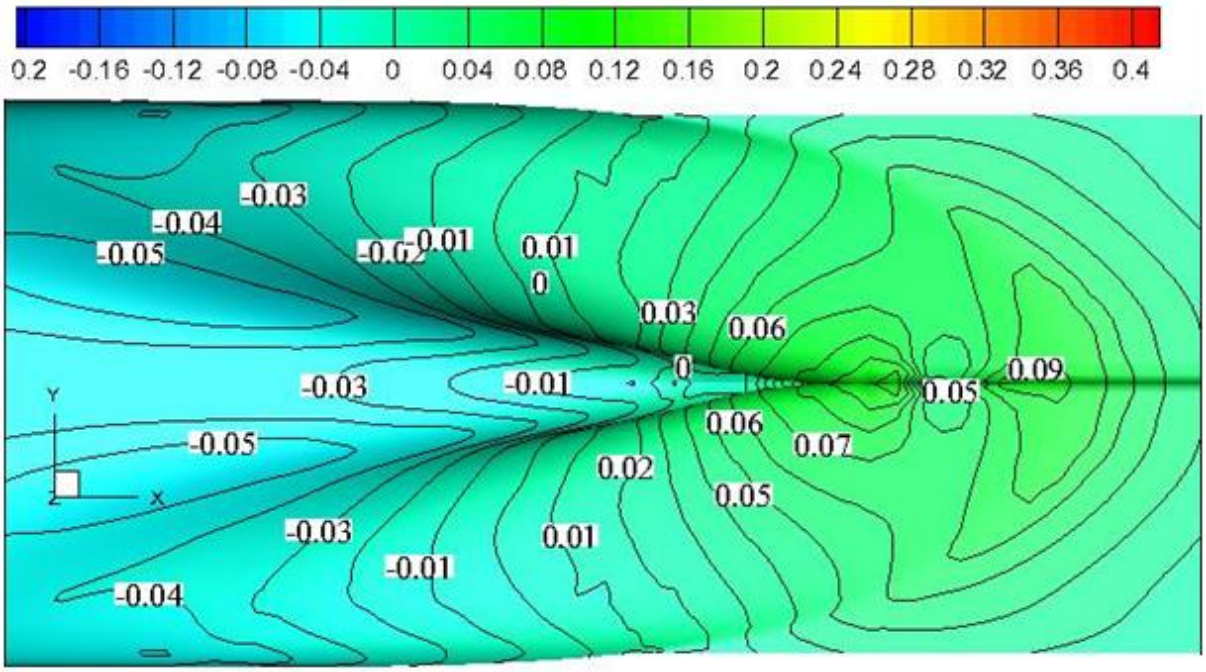

Figure 43 – Pressure distribution on the aft body – bottom view

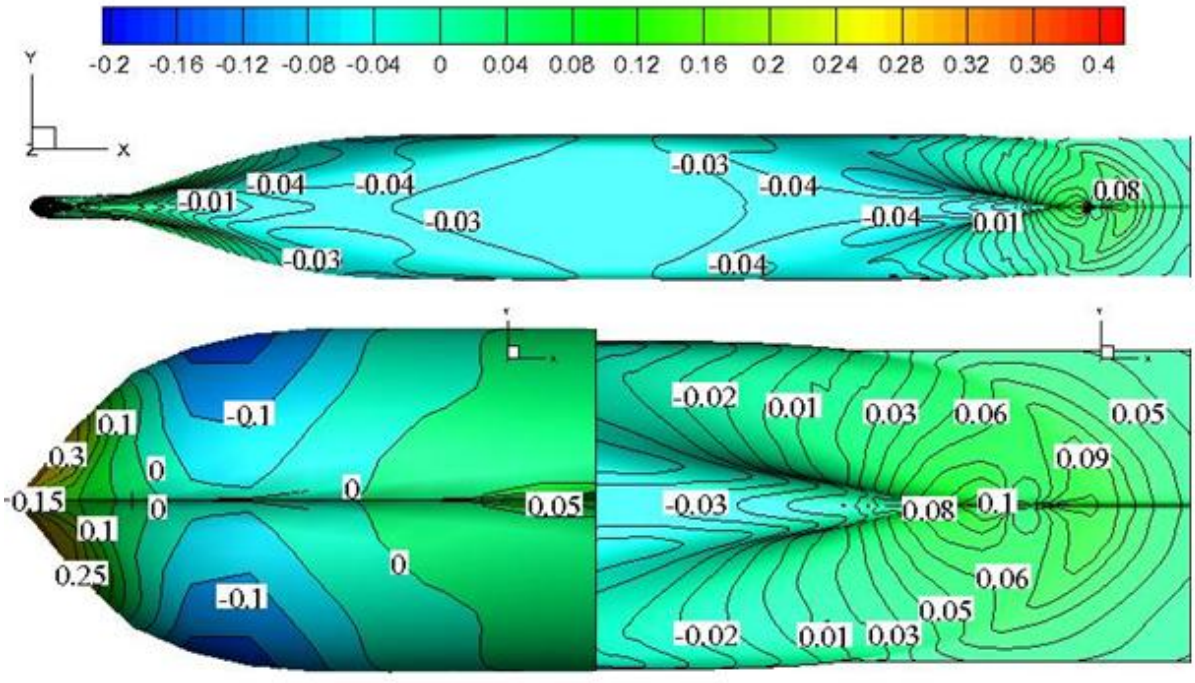

Figure 44 – Pressure distribution on the entire hull – bottom view

7.2.3 Bended Rudder

Computations for bended rudder were performed in order to see the pressure distribution in small and bigger angles. The flow which goes donwstream towards the rudder is accelarated by the propeller. The pressure distribution on the rudder under the angle of attack of the flow coming from the propeller is non symetric according the centre line. Figures 45 and 46 are presenting the pressure distribution on the rudder with varying rudder angle from -30˚ to 30˚ with 10˚ step. There is a low pressure area on the apper part of the rudder whic is due to the rotation of the sleap stream.

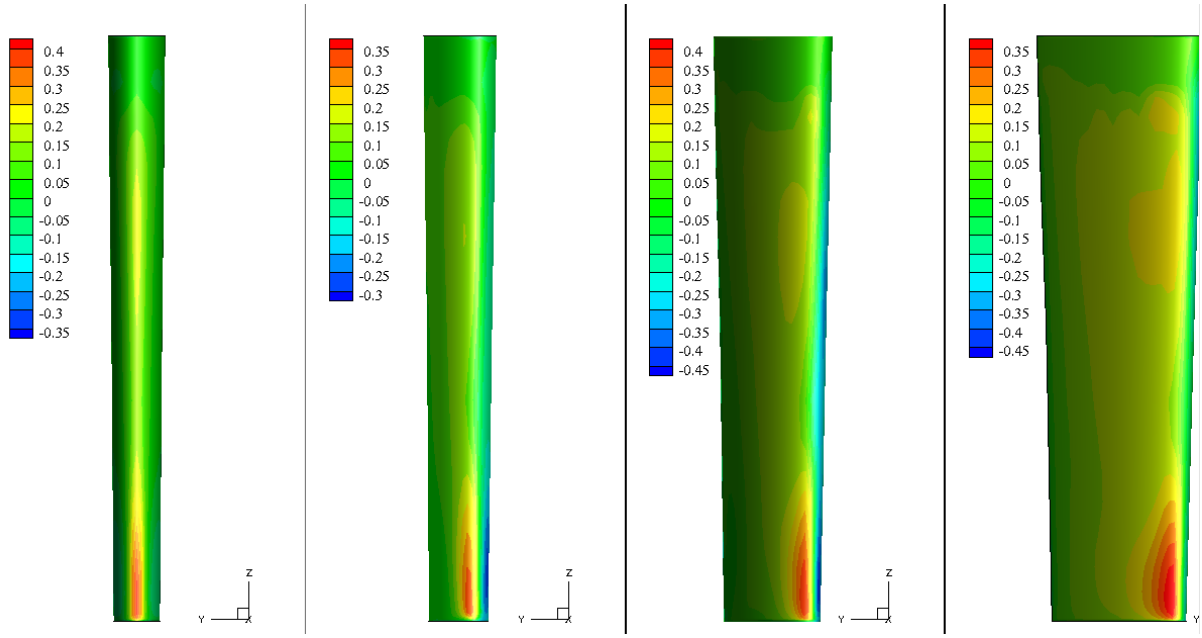

Figure 45 – Pressure distribution on the bended rudder for 4 different degrees of incidence: Starting from left to right: 0, -10, -20, -30 degrees.

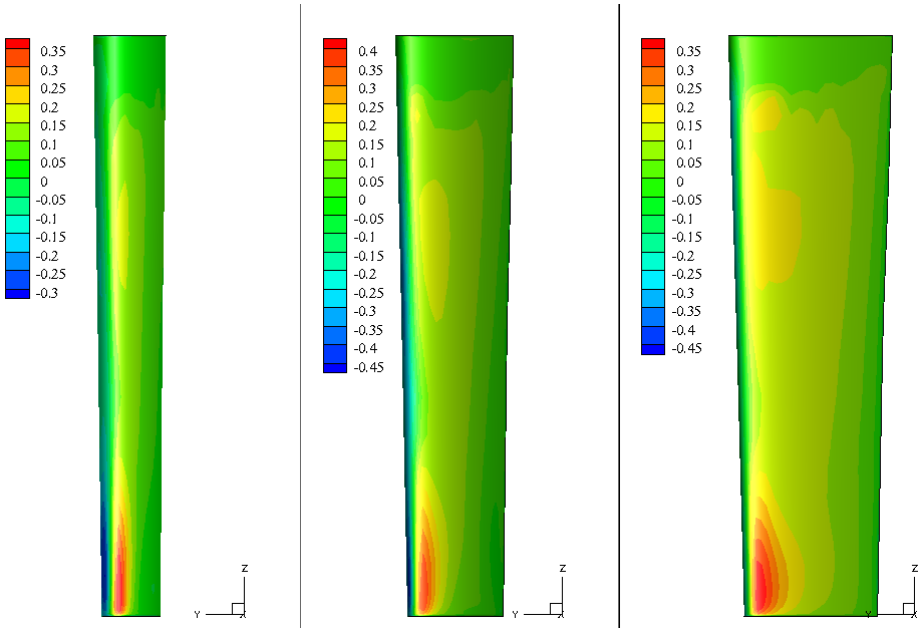

Figure 46 – Pressure distribution on the bended rudder for 4 different degrees of incidence: Starting from left to right: 10, 20, 30 degrees.

The pressure generated by the propeller slip stream on the rudder is bigger for negative incidence than for the positive incidence. This could be explained by the right handed propeller which accelerates the flow grately on the Star board side.

Forces and moments acting on the hull and on the rudder were computed as well. - Figure 47 for the hull and Figure 48 for the rudder. Studying of the hydrodinamic forces and moments is very important for predicting the maneuvering performance of the ship as well as designing appropriate rudder engine. The variation of the hydrodynamic forces and moments was recorded for rudder angle from -30˚ to 30˚ with 10˚ step.

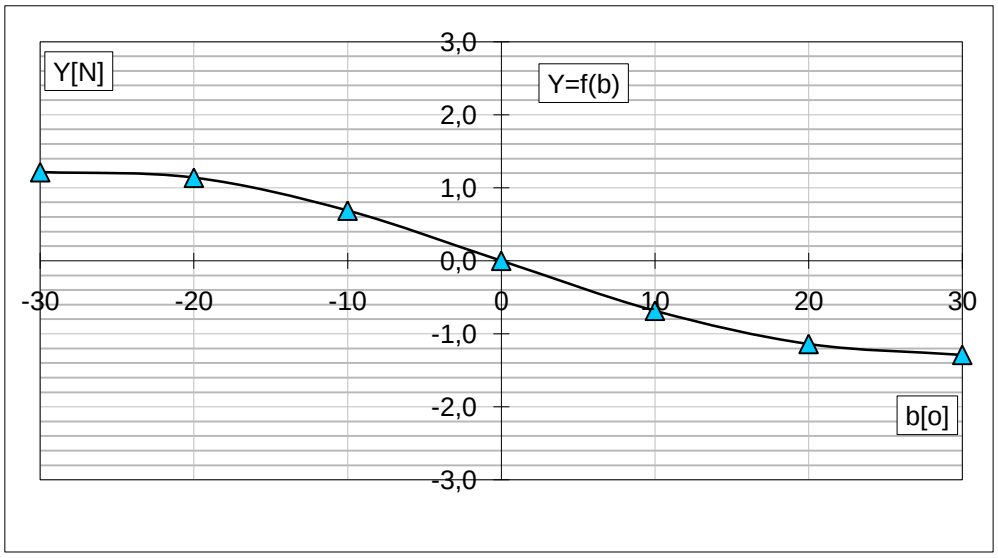

Figure 47a - Forces acting on the hull

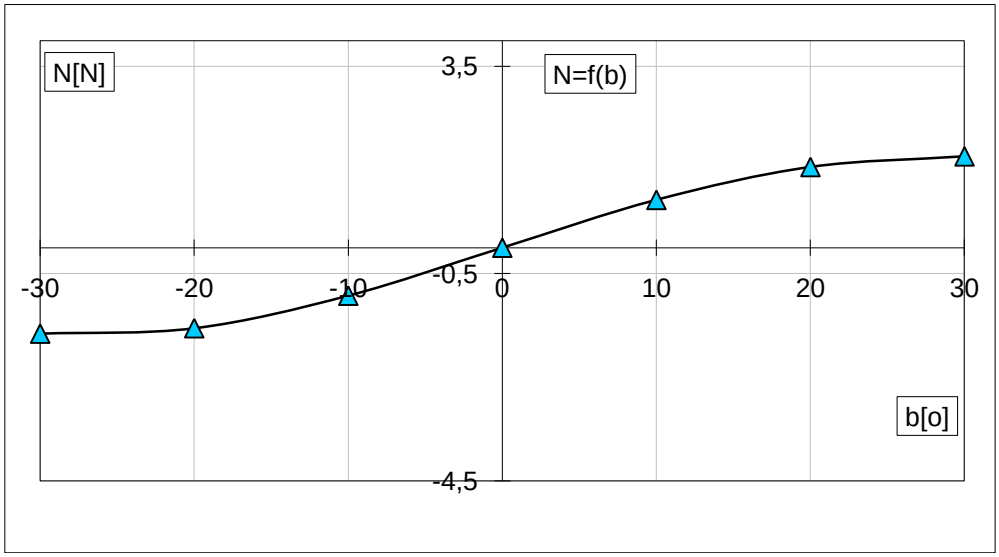

Figure 47b - Moments acting on the hull

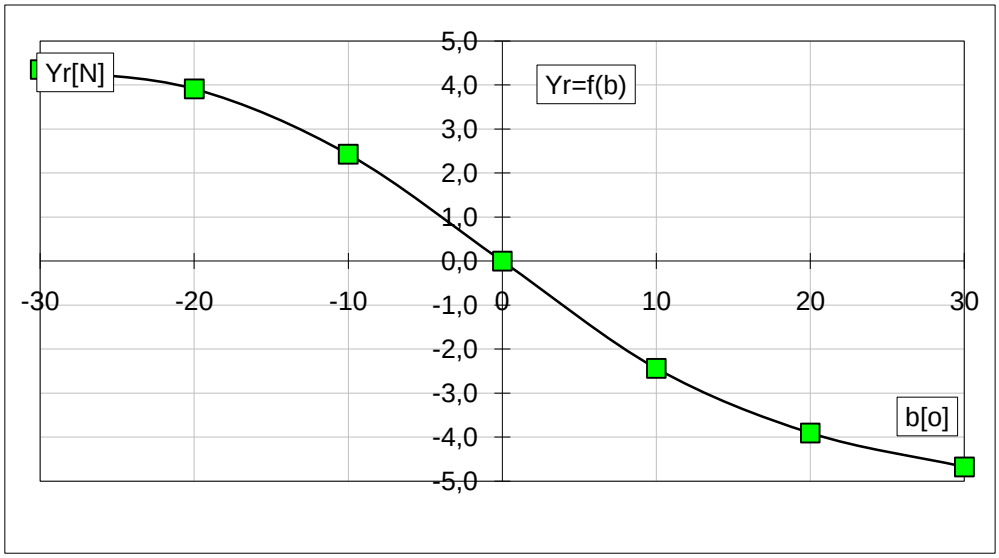

Figure 48a - Forces acting on the ridderl

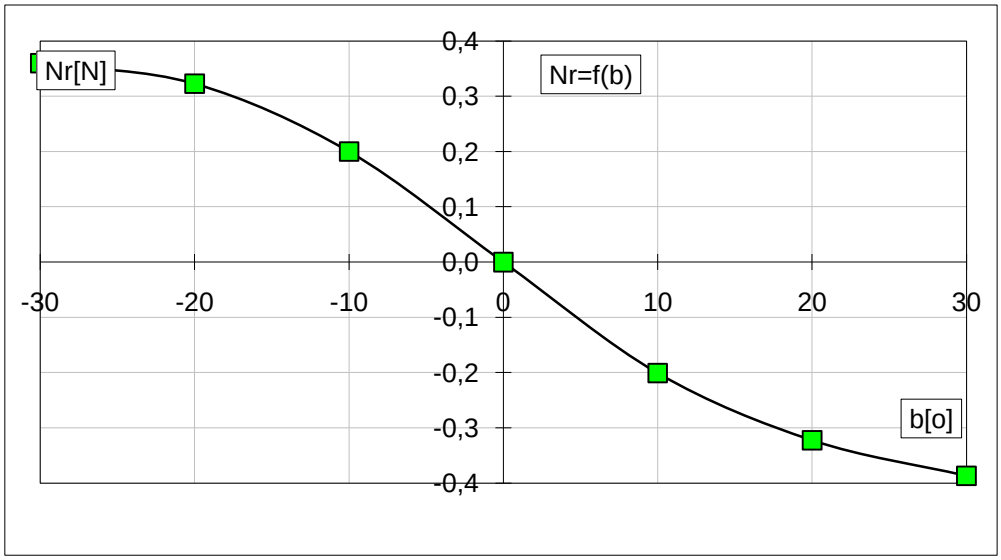

Figure 48b - Moments acting on the rudder

8. HULL WITH RUDDER AND PROPELLER

All single cases so far have been performed for understanding the main influence of each component (hull, propeller, and rudder). In the presence of the whole ensemble there is a hydrodynamic interaction which occurs between each component and the flow developed around them is significantly changed. This case is about the hydrodynamic interaction between the hull rudder and propeller – the essential part of the present research.

As regards the hull-propeller-rudder interaction there are two approaches which can be applied in order to the study these interactions and its effects. The first consists of systematic experimental parameter studies of the hydrodynamic forces. However, since the investigation is carried out at the integral level, this approach provides information about how the forces vary, but it does not provide information about what actually causes the interaction. The second approach is a detailed numerical study of the flow pattern. This analysis gives the data which is lacking in the first approach and which can probably help to understand better the complex flow phenomena.

[1]

8.1. Hydrodynamic Study of the Flow Developed Around the Hull with Propeller and Rudder

8.1.1 Axial Velocity Distribution

The whole ensemble (hull, propeller and rudder) leads to a more spectacular picture. At the first two planes there is almost no disturbance of the flow developed around the ship hull. In the third plane there are the same physics explained above in the hull-propeller case. But the last two planes (Figure 49d and 49e) shows how the flow accelerated by the propeller is hitting the rudder and how is this affected by the rudder action.

As explained above for the hull with rudder case, there are higher velocities at the starboard side and lower at the port side. On the starboard side the flow is moving downwards of the propeller axis whereas on the portside side the flow is moving upwards. When hitting the rudder a lower pressure is found on the bottom part of the rudder whereas a higher pressure region is developed on the upper part of the steering device. Figures 49d and 49e reveals how the twisted propeller flow is separated by the rudder. The starboard flow goes down and the port side flow goes up. This effect depends on the orientation of the propeller (left handed or right handed). If the propeller was left handed the two pieces of twisted fluid would have been moving in the opposite direction.

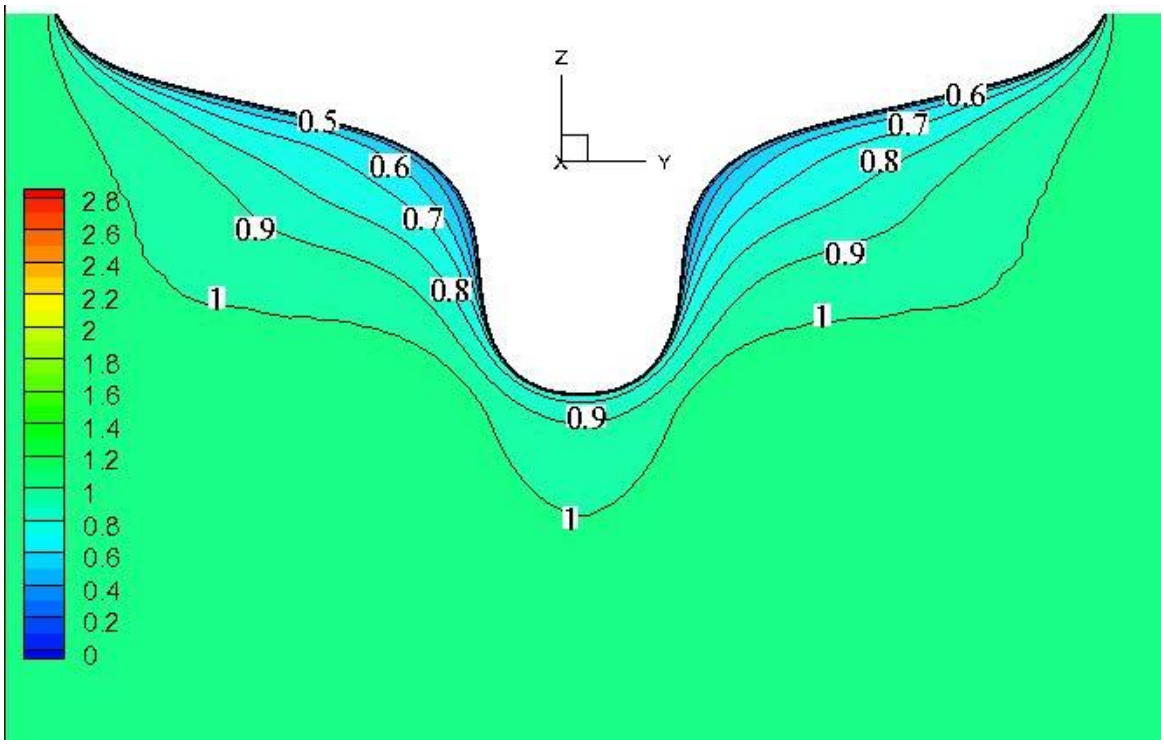

Figure 49a – Slice at 0.9

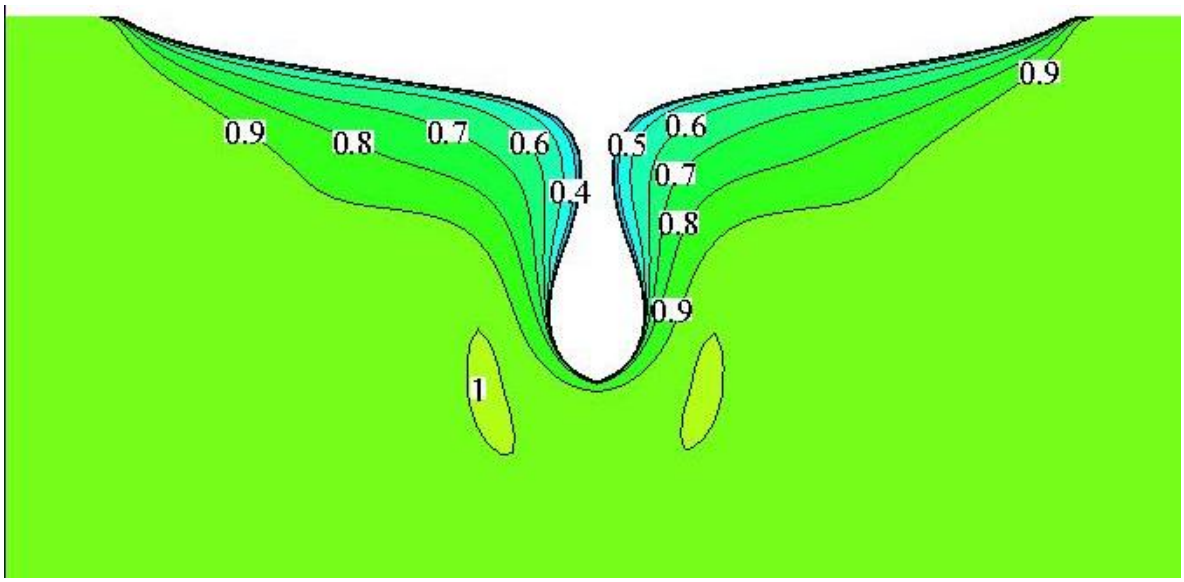

Figure 49b – Slice at 0.95

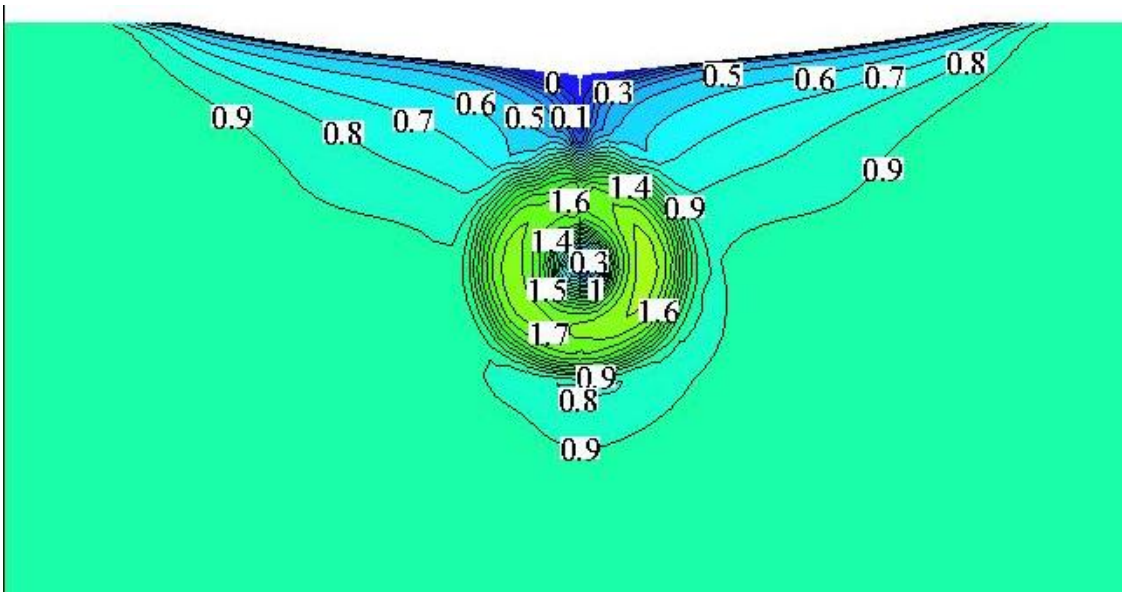

Figure 49c – Slice at 0.9825

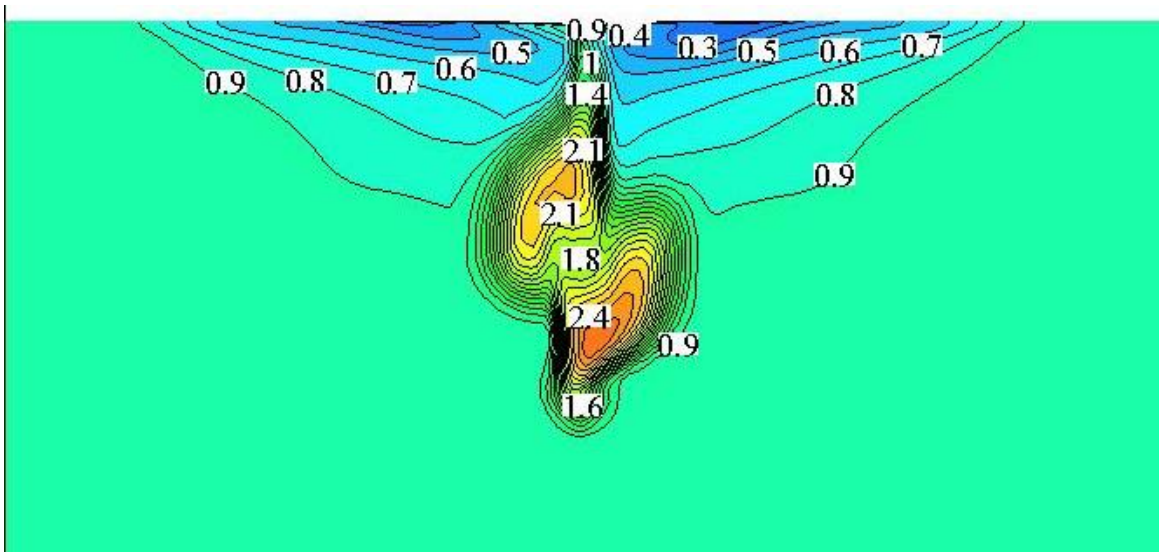

Figure 49d – Slice at 1.0288

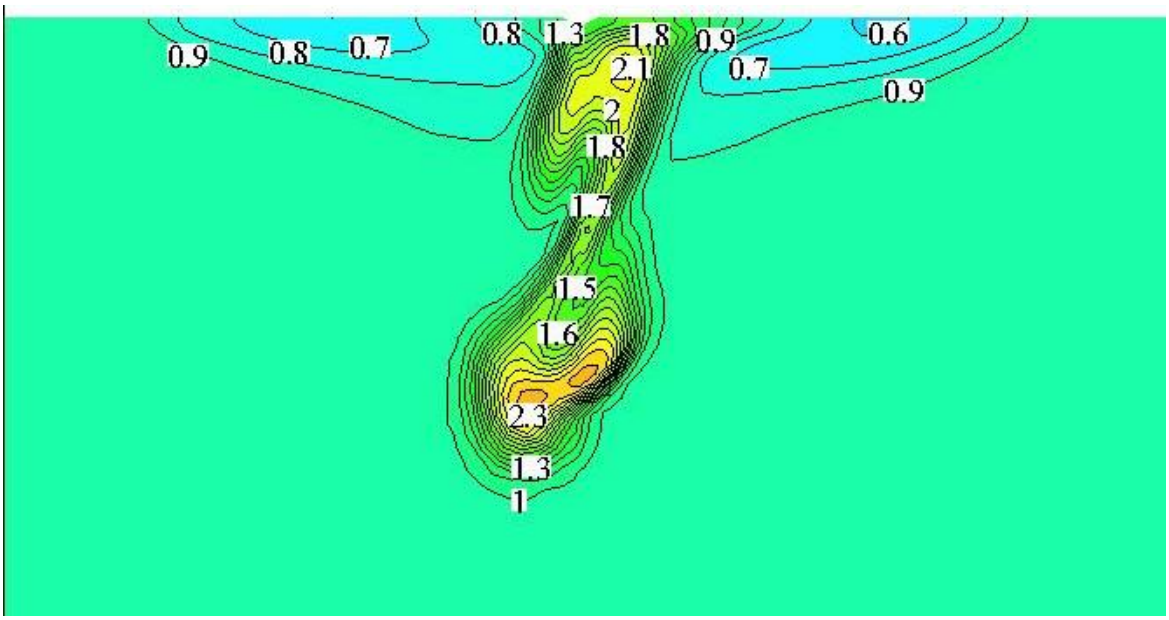

Figure 49e – Slice at 1.1

8.1.2 Pressure Distribution

Comparing to the hull with propeller case, this one shows that the pressure at the suction zone is even lower – Figure 50, Figure 51 and Figure 52. This could be explained due to the presence of the rudder. Due to the shape of the rudder when the flow first hits the leading edge it is decreased, which means that there a local higher pressures, but after passing the leading edge the flow is again accelerated because of the narrowing of the shape – which means that the pressure is decreased. This effect is contributing to the slightly lower pressure on the suction area in front of the propeller.

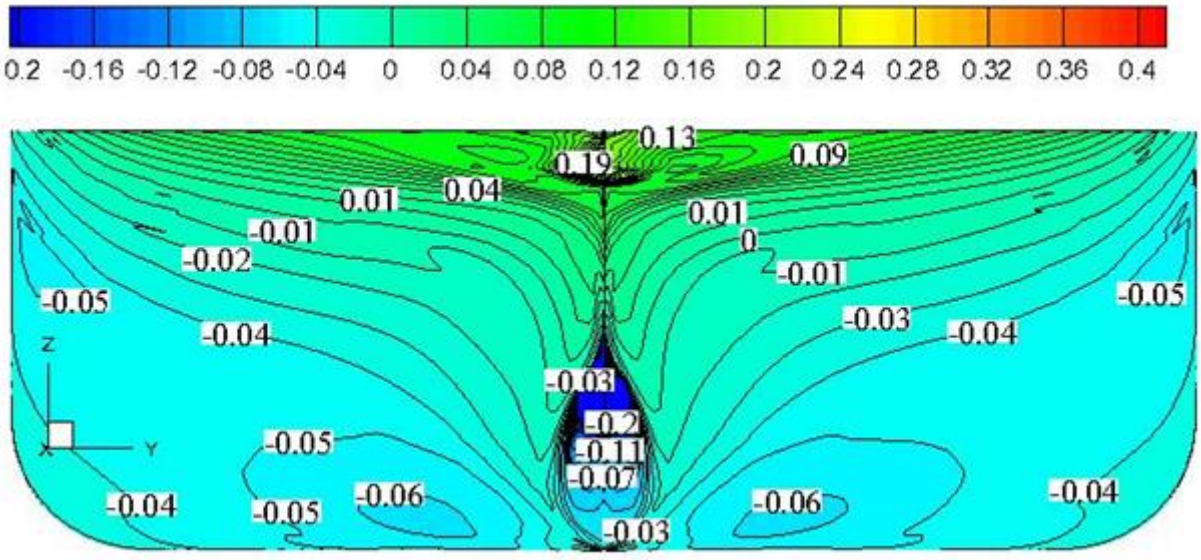

Figure 50 – Pressure distribution on the aft body

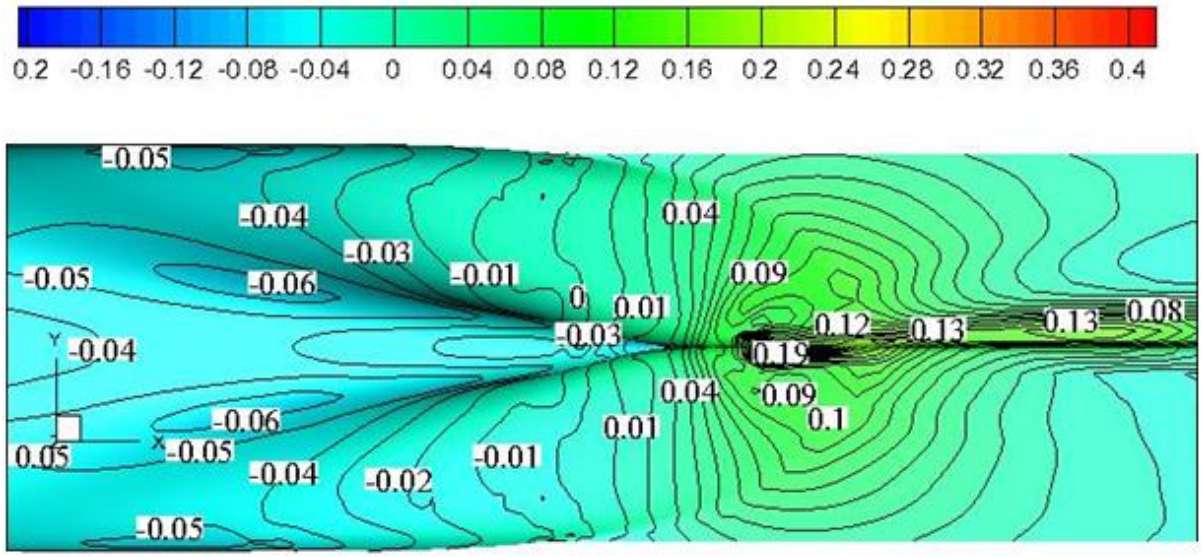

Figure 51 – Pressure distribution on the aft body – bottom view

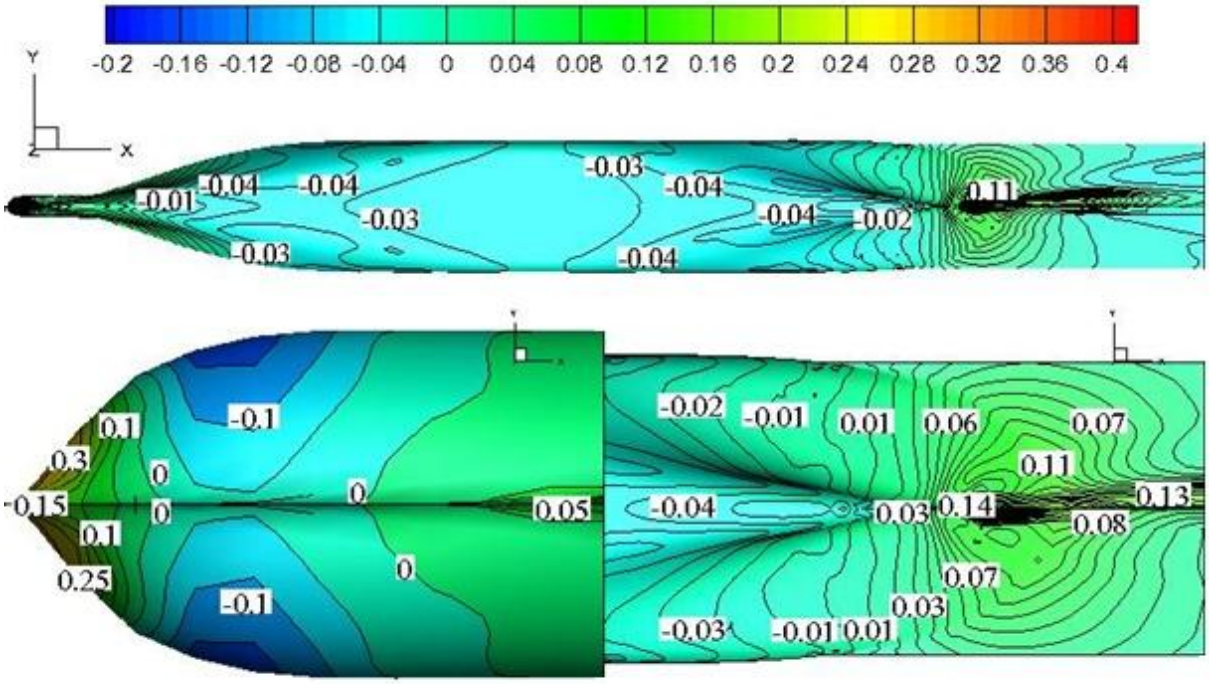

Figure 52 – Pressure distribution on the entire hull – bottom view

CONCLUSIONS

The study of the flow around a modern benchmark container ship model equipped with propeller and rudder was performed. Understanding the features of this flow is very important

for the Naval Architects, even from the early design stages, because it could be used for optimizing the hull shape and consequently the propeller and the rudder. In this way are avoided the bad interactions that can appear between the abovementioned components their performances being improved.

A simplified potential theory method is used to determine the wave resistance and the frictional resistance. RANS code is used in all the viscous computations to determine the hull-propeller-rudder interaction. Lifting line method is considered to model the propeller geometry. Computations are performed for bare hull, propeller open water, self propulsion test, hull with propeller, hull with rudder, hull with bended rudder and in the end for the whole ensemble (hull-propeller-rudder). Excepting the hull-propeller and hull-propeller-rudder cases, the numerical results were compared with experimental data and the error was estimated.

Wave pattern computed by the means of potential flow theory is showing excellent match with the reference result. Axial velocities comparison for the bare hull is in very good agreement with the experimental results. The total resistance computed for the bare hull is slightly bigger for the second and third speed, but for the speed of interest is showing a good agreement with the experiment results, the error is about 4%.

There is a small inconsistency for the Propeller Open Water test comparison between the two approaches but that could be explained by the fact that the method doesn't consider the surface of blade. Even though the Hull-propeller and Hull-Rudder-propeller case were not compared, they are showing really feasible results. Comparison for the Hull-Rudder case with experimental results was done and again the good agreement is for the speed of interest.

As a continuation of the present research, future work could be to include a different drift angle with combinations of different rudder angle. Using optimization software for defining better grid in the beginning could be also considered as a significant contribution for better results.

REFERENCE:

1. "Practical ship hydrodynamics" by Volker Bertram.
2. Computational methods for fluid dynamics "Ferziger J H , Peric M 2001"

3. Ship Flow user manual
4. Measurements of flows around modern commercial ship models. W. J. Kim, S. H. Van, D. H. Kim. Experiments in fluids 31 (2001) – 567-578 © Springer Verlag 2001.
5. Work shop of NMRI
6. "Numerical Grid Generation J.E. Thompson
7. Rudder – Propeller – Hull Interaction: The Results of Some Recent Research In-Service Problems and their Solutions. – First International Symposium on Marine Propulsors smp'09, Trondheim, Norway, June 2009
   Autors: John Carlton, Dejan Radosavljevic, Stewar Whitworth.
8. Rudder, Propeller and Hull Interaction by RANS – Claus D. Simonsen, PhD thesis, May 2000
9. Final Report, Force 187 DCMT – 2009-01-07
   Author(s): Claus Daniel Simonsen and Rasmus Carstens
10. Validation of Calculations of the viscous flow around a ship in oblique motion. The first MARIN-NMRI Workshop in Tokyo (October 25-26, 2004)
    Author – Serge TOXOPEUS.
11. RANS Maneuvering Simulation of Esso Osaka With Rudder and Body-Force Propeller. (June 2005)
    Authors"Claus D. Simonsen and Frederick Stern
12. Numerical Simulation of the flow Around a ship hull, including Interaction effects between hull and propeller. By Roman Gubler.
13. The propulsion Committee. Final Report and recommendations to the 25th ITTC. 2005 and 2008
14. Numerical Simulation of the Self –Propulsion Model test. By Tomasz Bugalski and Pawel Hoffmann, (June 2011)
15. Flow pattern around an appended tanker hull form in simple maneuvering conditions. By Claus D. Simonsen and Fred Stern. (August 2004)
16. Numerical Simulation of the Free-Surface Flow around a Port-Container Ship MARCU O., /master thsesis, dunarea de jos galati, 2010
17. *"Model tests on the KRISO hull for the powering performance assessment"*Marcu, O**.**, Obreja, D. C., 2011, , The Annals of "Dunarea de Jos" University of Galati/ FASCICLE XI – SHIPBUILDING, pp. 17–22.
18. *"Teoria navei"*Obreja, D., , Editura Didactica si Pedagogica, Galati, 2005

ACKNOWLEDGMENTS

This thesis was developed in the frame of the European Master Course in “Integrated Advanced Ship Design” named “EMSHIP” for “European Education in Advanced Ship Design”, Ref.: 159652-1-2009-1-BE-ERA MUNDUS-EMMC.

All the facilities like computer room, towing tank experiments and scientific literature were provided by the University “Dunarea de Jos” in Galati – Romania.

Special thanks to Ph.D. Oana Marcu for her comprehensive cooperation, which significantly contribute until the finalization of the thesis.